Representing Dark Hadrons from Collider to Cosmos

by

Austin Batz

A dissertation accepted and approved in partial fulfillment of the
requirements for the degree of
Doctor of Philosophy
in Physics

Dissertation Committee:
Timothy Cohen, Chair
Graham Kribs, Advisor
Laura Jeanty, Core Member
Boris Botvinnik, Institutional Representative

University of Oregon
Summer 2026

© 2026 Austin Batz
All rights reserved.

DISSERTATION ABSTRACT

Austin Batz

Doctor of Philosophy in Physics

Title: Representing Dark Hadrons from Collider to Cosmos

This dissertation presents analyses of a particular class of dark sectors from two perspectives: the spectrum of possible dark matter candidates and potential signals at colliders that could lead to discovery. First, a calculation of dark baryon electroweak representations and mass spectra is presented. The purpose is to identify the nature of the model's dark matter candidate (the lightest dark baryon) in order to characterize the possibility of discovery via direct detection. The result is that the baryons can exist in a broad variety of representations, but the spectrum commonly includes a gauge singlet. In such "Noble Dark Matter" cases, the dark matter candidate's quantum state is either completely or mostly composed of that singlet, thus limiting the sensitivity of direct detection. Second, two collider signals of the model's dark mesons are discussed. The first is disappearing tracks, which excludes dark mesons with masses below $\sim 1.2\,\text{TeV}$. The second is a scalar resonance decaying to pairs of electroweak bosons, and the constraints can apply to even higher masses, depending on the dark pion decay constant. With future additional data from the High-Luminosity Large Hadron Collider, a significantly expanded parameter space will be probed. The combined results demonstrate a feature of the model under study and confining dark sectors more generally: correlations between signatures in various experiments and search strategies due to the rich spectrum of infrared states.

This dissertation includes previously published co-authored material.

ACKNOWLEDGEMENTS

I want to express my heartfelt gratitude to my family and friends who supported me throughout the highs and lows of my PhD. The humor, late-night conversations, help moving, and mutual advice all made the experience not only educational, but also personally enriching.

I also thank my advisors and other mentors, without whom I would not have access to the dream-fulfilling opportunities I have received. I consider myself extremely fortunate to have met the right people at the right time and place who opened doors that so few others ever walk through.

Thanks as well to the institutions who funded and hosted me. In addition to the University of Oregon Institute for Fundamental Science, this includes the CERN Theory Group that supported my two month-long visits and the Department of Energy's SCGSR program that funded my ten-month fellowship at Lawrence Berkeley National Lab.

Finally, I thank the Caltech theory group for offering me a post-doctoral position. I look forward to the further scientific progress and professional opportunities I will participate in.

TABLE OF CONTENTS

Chapter Page

I INTRODUCTION 11

II NOBLE DARK MATTER: SURPRISING ELUSIVENESS OF DARK BARYONS 16

2.1 Motivation 16

2.2 The Theory 19

2.2.1 $\mathcal{H}$-parity from the Ultraviolet 19

2.2.2 Baryon Representations in the Infrared 20

2.3 Masses in the Heavy Quark Limit 23

2.3.1 Electroweak Contributions in the Quark Model 23

2.3.2 Mass Spectra from the Variational Method 25

2.4 Modifications to the $SU(2)_L$ Running Coupling 27

2.5 Further Details on Hadron Representations 29

2.5.1 Spin and Flavor Representations 30

2.5.2 Finding Hadron Wavefunctions and $SU(2)_L$ Representations . 32

2.6 Further Details on the Mass Calculation 42

2.6.1 The Mass Hamiltonian 43

2.6.2 Quark Mass Splittings 46

2.6.3 Spin-flavor Matrix Elements 48

2.6.4 Spatial Expectation Values 53

2.7 Phenomenology 60

2.7.1 Direct Detection 60

2.7.2 Indirect Detection and Astrophysical Searches 64

2.7.3 Collider Searches 65

Chapter Page

2.8 Discussion 66

III STOPPING DARK MESONS IN THEIR TRACKS WITH LONG-LIVED PARTICLE AND RESONANT SIGNATURES 69

3.1 Bridge 69

3.2 The Model 72

3.2.1 Mesons in the Chiral Effective Theory 73

3.2.2 Dark G-Parity 74

3.2.3 Meson Masses 78

3.3 The 5-plet Anomaly 82

3.3.1 Review of Standard Model Meson Anomalies 82

3.3.2 Uniqueness of the 5-plet Anomaly 84

3.4 Obtaining Flavor Generators 89

3.5 Computing the 5-plet Anomaly 91

3.6 Collider Signals and Constraints 93

3.6.1 Disappearing Tracks: A 3-plet Signature 94

3.6.2 Anomaly-induced Resonances: A 5-plet Signature 98

3.7 Conclusion 103

LIST OF FIGURES

Figure Page

1 Mass $m_{\rm DM}$ of the lightest baryon and overlap of the lightest mass eigenstate $|m_{\rm DM}\rangle$ with the neutral $\mathrm{SU}(2)_L$ 5-plet state $|5\text{-plet}\rangle$ for $(N_c, N_f) = (2,4)$ (**top**) and $(4,3)$ (**bottom**), which are two benchmark models from category II in Sec. 2.2.2. As the dark quark mass m_q increases, DM's overlap with the non-singlet state decreases. DM masses are slightly greater than $N_c m_q$ due to quark self-energy corrections. 27

2 Rough estimates of direct detection cross sections of the lightest dark baryon for $(N_c, N_f) = (2,4)$ and $(4,3)$ with $\Lambda_\chi/m_q = 10^{-2}$ (**top**) and 10^{-6} (**bottom**). We scaled the $\mathrm{SU}(2)_L$ 5-plet cross sections (red dotted line) computed in Ref. [20] using a similar 5-plet WIMP model by $|\langle m_{\rm DM}|5\text{-plet}\rangle|^4$ for each $N_{c,f}$. The suppression of cross sections below the neutrino fog limits the reach of future experiments. 63

3 Feynman diagram corresponding to the anomaly-induced resonant production of the $\hat{\eta}_5$. The $\otimes$ symbols denote insertions of the anomaly operator in Eq. (3.29). The $\hat{\eta}_5$ species are the unique pNGBs of dark chiral symmetry breaking with this operator. Observation of this signal provides sensitivity to UV parameters such as N_c and N_f, which set the strength of the coupling (see Eqs. (3.29) and (3.30)). LHC implications are discussed in Sec. 3.6.2. 86

4 Diagrams representing pair production of the $\hat{\pi}_3$ mesons via Drell-Yan (top) and vector boson fusion (bottom). The VBF processes also get contributions from diagrams with three-point vertices coupling the mesons to vector bosons. Diagrams with production of two neutral mesons via VBF are not pictured, as we do not consider such processes. 95

Figure Page

5 Total LHC production cross sections of the dark meson triplet $\hat{\pi}_3$ pairs we consider. The production rate for exclusively Drell-Yan processes falls much faster as a function of the $\hat{\pi}_3$ mass m_π than the rate of processes that include vector boson fusion. 96

6 The visible cross section for production of disappearing tracks due to decays of the long-lived $\hat{\pi}_3^\pm$ meson. The dashed lines indicate model-independent upper bounds on this cross section based on the ATLAS searches in Refs. [196, 192] and using the re-interpretation methods provided by Ref. [172]. This shows a strong lower bound on the $\hat{\pi}_3$ meson mass m_π of $\sim$1.2 TeV. 97

7 Upper bounds on the cross section to produce various final states from the searches in Refs. [198–206] through resonant production and decay of the scalar $\hat{\eta}$. Solid (dashed) lines correspond to ATLAS (CMS) searches. The ZZ searches used the fully leptonic channel, and the W^+W^-/ZZ searches used the semileptonic channel. In the context of our model, the $\hat{\eta}$ is one of the pNGBs of dark chiral symmetry breaking in the $\mathrm{SU}(2)_L$ 5-plet. Besides the diphoton searches, each of these is specialized to production via VBF. We interpret these upper bounds as lower bounds on $4\pi f_\pi/N_c$ in Fig. 8. 99

8 Lower bounds on the ratio $4\pi f_\pi/N_c$ as a function of the $\hat{\eta}_5$ meson mass m_η using the strongest constraints in Fig. 7 for each diboson final state. The gray contours indicate lower bounds on $4\pi f_\pi/N_c$ for a few values of N_c, below which $m_\eta > 4\pi f_\pi$ and the EFT of mesons breaks down. The region with $m_\eta < 1.2$ TeV is excluded by the disappearing tracks analysis in Sec. 3.6.1. The dotted red contour indicates a projection from a naïve luminosity rescaling of the expected limits of the searches with the strongest constraints on our model for a 3 ab^{-1} dataset. 100

Figure Page

9 Lower bounds on $4\pi f_\pi$ as a function of the $\hat{\eta}_5$ meson mass m_η in the case of $N_c = 4$. Existing and projected resonance constraints due to the 5-plet anomaly, constraints from disappearing tracks due to the dark meson 3-plet $\hat{\pi}_3$, and the meson EFT breakdown where $m_\eta > 4\pi f_\pi$ are shown as in Fig. 8. The disappearing tracks constraint below $4\pi f_\pi = 2.4\,\text{TeV}$ is indicated by a dashed line, where pair production of $\hat{\pi}_3$ mesons with a mass of 1.2 TeV is outside the EFT regime of validity. 101

LIST OF TABLES

Table Page

1 $SU(2)_L$ representations of the lowest-spin dark baryons in the confined phase of the model in Eq. (2.1) for several combinations of number of dark colors N_c and flavors N_f. We define in the text the four categories in the rightmost column describing when singlets and other neutral states appear. 22

2 Order-of-magnitude estimates of $SU(2)_L$ Landau poles Λ_W for various $N_{c,f}$ combinations using Eq. (2.15). Dashes indicate where $SU(2)_L$ remains asymptotically free. Some versions of the theory are safe from sub-Planckian Landau poles, and others require a UV completion at modestly high scales. 29

3 Summary of the pNGBs of dark chiral symmetry breaking, including their representation under $SU(2)_L$, the minimum N_f such that the species exists in the spectrum (Sec. 3.2.1), the charge under the dark G-parity (Sec. 3.2.2), and the dominant decay mode (Secs. 3.2.2 and 3.3.2) for each meson. Decay modes specific to particular components of the $SU(2)_L$ multiplets are specified. Several species decay via cascade, *i.e.* they decay to lighter meson in the same multiplet by radiating an off-shell gauge boson. The higher multiplets decay by hopping down to a lower multiplet with the same G-parity and emitting two gauge bosons. 88

4 Summary of the dark mesons we consider in our collider study. 93

CHAPTER I

INTRODUCTION

The Standard Model (SM) of Particle Physics allows us to predict the interactions between the fundamental particles we have directly observed to a high degree of precision, but is known to be an incomplete description of Nature. One of the most glaring examples of this incompleteness is the lack of a particle that serves as a candidate for dark matter, which we observe in galaxies as a slowly-moving and gravitationally-interacting energy density. This energy density exceeds that of ordinary visible matter, but we do not know its fundamental particle nature. There are many possible candidates spanning a vast range of mass scales. There are also many experimental strategies to search for some non-gravitational interaction between dark matter and SM particles, from direct detection looking for dark matter scattering off of some target material, to indirect detection looking for decays and annihilations of dark matter, to astrophysical searches for other unexplained behavior in the cosmos, to colliders attempting to directly produce either dark matter itself or other related particles in a greater dark sector.

Given the enormous space of possible theories with a dark matter candidate, it helps to have some additional motivation to guide us as to which warrant closer study. Some examples include:

- A solution to some other puzzle that the SM leaves unexplained. A classic example is the Weakly Interacting Massive Particle (WIMP), which is found in supersymmetric theories that explain the unnaturally large hierarchy between the "small" Higgs boson mass and the "large" Planck scale where gravitational effects become unsuppressed.

– Some novel mechanism for discovery that motivates new experimental methods while explaining why existing experiments would not have observed the dark matter candidate.

– Minimality, in the sense that the theory does not require some elaborate network of interactions inserted by hand between a large number of particle species in order to be viable.

– An underlying explanation of the dark matter candidate's stability and suppressed interactions with the SM while maintaining a mechanism to generate its abundance and ideally also some way to discover it with existing or proposed experiments.

The motivations for theories discussed in this dissertation largely fall into the latter two of these categories. These theories are particular examples of confining dark sectors, wherein there is an interaction among a set of new particles that is weak in the ultraviolet (UV, *i.e.* high energies) and strong in the infrared (IR, *i.e.* low energies). The fundamental theory can be very minimal in the UV, containing only a small number of "dark quarks" and "dark gluons" analogous to those that interact via quantum chromodynamics in the SM. In the IR, however, the dark sector particles bind together into a wide variety of bound states (dark hadrons) analogous to protons, neutrons, and mesons in the SM. A common feature of confining dark sectors is that even if the dark quarks have unsuppressed interactions with the SM, some dark hadron species will have highly-suppressed interactions and be stable or very long-lived. The suppression of interactions and decay rates is often explained by an underlying symmetry in the UV.

The particular confining dark sectors studied here involve dark quarks that interact directly with the SM via electroweak interactions. This means that some of them are electrically charged, so they interact with the photon. It is therefore perhaps counter-intuitive that they could constitute dark matter, which is famously dark. Even if the dark quarks form a bound state that is electrically neutral, the photon could plausibly probe its underlying structure, analogously to the magnetic moment of the neutron. Besides the photon, the bound states may also interact with the other electroweak bosons: the W and Z. That is not necessarily a problem, as some WIMPs do so as well, but it would be an additional source of constraints. The subject of Chapter II is an explanation of why the dark matter candidate in some versions of this model in fact has *very* suppressed interactions with the photon, W, and Z, to a degree that goes beyond naïve expectations. The consequence is that direct detection experiments are counter-intuitively insensitive to these candidates, and alternative strategies are needed to discover them in broad regions of parameter space.

Chapter III discusses one such alternative strategy, namely production of other dark sector states in colliders. This strategy exploits the richness of the IR theory, as the existence of neutral dark matter candidates in these particular models implies the existence of other electrically-charged particles that can be directly produced and decay via electroweak interactions. The composite nature of the dark hadrons leads to correlations between signals from different species and exciting opportunities for discovery. Specifically, one of the species is both charged and sufficiently long-lived that it decays after traveling a macroscopic distance inside the detector, leaving a signature known as a disappearing track. Another species can be resonantly produced by the fusion of electroweak bosons,

then decay to pairs of electroweak bosons. Each of these signals is the target of powerful existing searches in experiments at the Large Hadron Collider (LHC), and future searches will expand the range of parameters that may lead to discovery.

A recurring theme throughout the dissertation is representations, which are the mathematical structures that dictate how particles interact with gauge bosons such as the photon, W, and Z. More generally, if some kind of transformation, such as a rotation, is applied to a particle's state, its representation under the corresponding group of transformations determines how the state changes. As a more familiar example, a sphere is in the trivial representation of the group of rotations, as rotations do not change its state at all. A vector does change when it rotates, so it is in a non-trivial representation. Likewise, each gauge boson, which mediates interactions between particles, corresponds to a gauge group, and the representation in which a particle's state transforms under that group is what determines whether and how strongly it interacts with the gauge boson.

The reason this concept is particularly prominent in this dissertation is that when the dark quarks bind together into composite dark hadrons, even if the dark quarks are all in the same representations of their various transformation groups, the dark hadrons may be in many different representations. Determining those representations sometimes requires some effort. A result of the analysis in Chapter II is that the dark matter candidate is often in the trivial representation of the electroweak group, implying it does not interact with the photon, W, or Z at all (up to suppressed interactions that could probe its underlying structure). In Chapter III, the dark hadrons that may be produced in the LHC are in different non-trivial electroweak representations (the focus is the vector **3** and tensor **5** of SU(2)), each of which has completely different experimental signatures. The rich

spectrum of dark hadron representations and correlations of signals between them are part of what makes the class of theories studied in this dissertation, as well as confining dark sectors more generally, so interesting.

Chapters II and III include previously published co-authored material from Refs. [1, 2] with P. Asadi, E. Bernreuther, M. Costa, S. Homiller, and G.D. Kribs.

CHAPTER II

NOBLE DARK MATTER: SURPRISING ELUSIVENESS OF DARK BARYONS

This chapter includes previously published co-authored material from Ref. [1] with P. Asadi and G.D. Kribs. Calculations were performed by A.B. with P.A. providing some cross-checks. All authors contributed to the development of ideas, interpretation of results, and writing of the paper.

2.1 Motivation

The existence of dark matter (DM) is well-established by gravitational observations across various distances, with no non-gravitational signals detected so far, see Ref. [3] for a recent review. On the one hand, such non-gravitational interactions of DM with the Standard Model (SM) are tightly constrained by direct and indirect detection searches. On the other hand, nightmare scenarios of strictly gravitational interactions would not explain the similarity of DM and SM abundances. These observations can be reconciled if a dark sector thermally interacted with the SM in the early universe before undergoing a phase transition that produced SM-singlet relics.

We show that this can occur in a broad class of confining dark sectors. We extend the SM by a sector of dark quarks charged under a confining SU(N_c) that form an N_f-plet of SM SU(2)$_L$ with vanishing hypercharge, see *e.g.* Refs. [4–12] for previous studies of similar theories. The lightest dark baryons in the confined phase are stable and, if neutral, constitute a viable DM candidate. This is a simple DM scenario where the dark sector was in thermal contact with the SM in the early universe (without invoking an additional portal), while the degrees of freedom present today can have very feeble SM interactions, depending on the values of N_c and N_f.

In the deconfined phase of the theory, this model contains ingredients similar to the standard Weakly Interacting Massive Particle (WIMP), with the addition of a dark confining gauge group. In the confined phase of the theory, the dark quarks assemble into dark hadrons, including a WIMP-like dark baryon DM candidate. Similar to a vanilla WIMP model, the dark baryons transform in particular representations of $\mathrm{SU}(2)_L$. Unlike a vanilla WIMP model, we remain agnostic to the mechanism that fixes the DM relic abundance in the early universe, focusing on the prospects of different discovery channels today.

Regardless of N_c and N_f, the DM candidate has suppressed electromagnetic interactions with SM due to $\mathcal{H}$-parity [12]. This symmetry forbids the leading electromagnetic moments of the dark sector's neutral hadrons, which strongly suppresses direct detection signals in our model. Therefore, the leading direct detection signals arise from electroweak loop-induced interactions due to the renormalizable interactions of the dark baryons with the W gauge boson [13–21]. For baryons in the singlet representation of $\mathrm{SU}(2)_L$, these interactions vanish as well.

We study the $\mathrm{SU}(2)_L$ representations of dark baryons for various combinations of N_c and N_f using standard group theory arguments. In the specific case where $N_f = 2$ and N_c is even, the lightest dark baryon is a pure singlet,[1] and the interactions with the SM become highly suppressed.[2] For many other combinations of N_c and N_f, we find that the DM state is composed primarily of a singlet of $\mathrm{SU}(2)_L$ with only a small mixing with non-singlet dark baryons, so the elastic scattering rate relevant to direct detection signals of these models is

[1] By "singlet", we refer specifically to a state transforming in the trivial representation of $\mathrm{SU}(2)_L$. Neutral components of non-trivial $\mathrm{SU}(2)_L$ multiplets are referred to as such.

[2] The leading interaction is the electromagnetic polarizability of the composite singlet.

suppressed by this small mixing. These (approximate) singlet baryons are inert composites of charged constituents, analogous to noble gases, so we have named them Noble Dark Matter.

Despite confining dark sectors being targets of different search strategies, *e.g.* see Refs. [22–25, 4, 26–31, 7, 32–34, 10, 9, 35–50, 21, 51–61], our results imply that even this simplest confining extension of the WIMP paradigm is far more elusive than historically appreciated (see also Ref. [62] for non-confining WIMPs that are notoriously difficult to detect). Confinement in the dark sector naturally gives rise to a rich spectrum of WIMP-like states in the infrared (IR) despite including only one set of dark quarks in the ultraviolet (UV) that transform in a vector-like representation of the electroweak and the dark gauge groups. The effective field theory (EFT) in the IR inherits symmetries from the UV, particularly $\mathcal{H}$-parity, that forbid some interactions between the dark sector and the SM. The UV theory also predicts other mechanisms that suppress interactions between the SM and the dark sector in the IR (*i.e.* singlets with small mixings with other states) that may appear unnatural or contrived from a bottom-up perspective. Earlier simplified model approaches introducing a single (possibly composite) electroweak multiplet have neglected this possibility.

The structure of the paper is as follows: In Sec. 2.2, we introduce our model, review $\mathcal{H}$-parity, and explain baryon $\mathrm{SU}(2)_L$ representations. We compute the lowest-lying baryon mass spectra and mixings of states in different $\mathrm{SU}(2)_L$ representations for two $N_{c,f}$ combinations in Sec. 2.3 using the non-relativistic quark model, including electroweak contributions. We find that the DM candidate in these examples is mostly made of an $\mathrm{SU}(2)_L$ singlet state and discuss in Sec. 2.7 the resulting suppression of (in)direct detection signals, motivating searches at

current and future high-energy colliders. We conclude in Sec. 2.8. In Sec. 2.4, we study the effect of the new fields on the running of $\mathrm{SU}(2)_L$ gauge coupling. Further details on group theory arguments relevant for determining the $\mathrm{SU}(2)_L$ representations and wavefunctions of dark baryons are provided in Sec. 2.5. We also discuss details of a variation method used in determining the baryon mass spectrum in Sec. 2.6.

2.2 The Theory

2.2.1 $\mathcal{H}$-parity from the Ultraviolet. We propose a theory of dark matter that arises from a new strongly-coupled confining gauge sector with the Lagrangian

$$\mathcal{L}_{\rm dark} = -\frac{1}{4} G^{\mu\nu\, a} G^a_{\mu\nu} + \overline{\mathbf{Q}} \left(i \not{D} - m_0 \right) \mathbf{Q} \,, \tag{2.1}$$

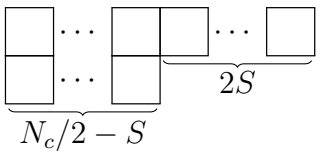
where $G^a_{\mu\nu}$ is the field strength of the dark $\mathrm{SU}(N_c)$ with confinement scale Λ_χ and coupling α_χ, and $\mathbf{Q}$ is a vector-like dark quark with bare mass m_0 that transforms as a fundamental of $\mathrm{SU}(N_c)$ and an N_f-plet of $\mathrm{SU}(2)_L$.[3] In the confined phase of the theory, dark quarks bind into mesons and baryons. Since $\mathcal{L}_{\rm dark}$ includes no hypercharge interactions, each quark or hadron in the dark sector has an electric charge equal to its weak isospin.

The lightest baryon in the confined phase is stabilized by a $\mathrm{U}(1)_{\rm baryon}$ in the standard way. If this baryon is neutral, it can be a viable DM candidate. As shown in Ref. [12], electromagnetic moments of the neutral dark baryons are strongly suppressed because they are eigenstates of the $\mathcal{H}$-parity transformation (where the electroweak gauge fields are charge-conjugated and $\mathbf{Q} \to e^{i\pi J_y} \mathbf{Q}$, with J_y the second

[3] The added matter content can spoil the asymptotic freedom of $\mathrm{SU}(2)_L$. See Sec. 2.4 for a discussion of Landau poles.

generator of $\mathrm{SU}(2)_L$). In the upcoming sections, we discuss the baryons' $\mathrm{SU}(2)_L$ representations and mass spectrum, as well as the phenomenological implications of our findings. The vanishing of baryon electromagnetic moments and the spectrum of $\mathrm{SU}(2)_L$ representations have a strong impact on possible experimental signatures.

2.2.2 Baryon Representations in the Infrared. In the confined phase of the theory, hadron states can be organized into multiplets transforming in irreducible representations of $\mathrm{SU}(2)_L$. Baryon wavefunctions can be thought of as multi-particle states of identical fermions tracking each particle's position, dark color, flavor, and spin. For symmetric spatial states and anti-symmetric ($\mathrm{SU}(N_c)$-singlet) color states, the required constituent exchange symmetry of baryon spin-flavor wavefunctions restricts baryon states to those in specific flavor representations of $\mathrm{SU}(N_f)$. In particular, the allowed flavor representations of $\mathrm{SU}(N_f)$ have a corresponding $\mathrm{SU}(2)_{\mathrm{spin}}$ representation with an identical Young tableau. These tableaux have the form



(2.2)

for spin-S baryons because N_c dark quarks are combined to make a color-singlet baryon, and the tableau for a spin-S representation of $\mathrm{SU}(2)_{\mathrm{spin}}$ has at most two boxes in each column and $2S$ columns with one box. See Sec. 2.5.1 for more details.

Enumerating the dark baryons' $\mathrm{SU}(2)_L$ representations amounts to decomposing the $\mathrm{SU}(N_f)$ representation in Eq. (2.2) into representations of its

gauged SU(2) subgroup. We explain the derivation of these decompositions and hadron spin-flavor wavefunctions in Sec. 2.5.2.

In the electroweak-broken phase, states in different $\mathrm{SU}(2)_L$ representations can mix. However, neutral baryons in adjacent odd representations have opposite charges under $\mathcal{H}$-parity [12], which forbids their mixing. For example, consider an electroweak 3-plet and 5-plet. They transform under $\mathcal{H}$ as

$$\text{3-plet} = \begin{pmatrix} 3^+ \\ 3^0 \\ 3^- \end{pmatrix} \overset{\mathcal{H}}{\to} \begin{pmatrix} 3^- \\ -3^0 \\ 3^+ \end{pmatrix}, \tag{2.3}$$

$$\text{5-plet} = \begin{pmatrix} 5^{++} \\ 5^+ \\ 5^0 \\ 5^- \\ 5^{--} \end{pmatrix} \overset{\mathcal{H}}{\to} \begin{pmatrix} 5^{--} \\ -5^- \\ 5^0 \\ -5^+ \\ 5^{++} \end{pmatrix}, \tag{2.4}$$

i.e. the neutral components of odd $\mathrm{SU}(2)_L$ multiplets are eigenstates of $\mathcal{H}$ with alternating eigenvalues ± 1. Therefore, a singlet baryon can mix with the neutral components of 5-plets, 9-plets, *etc.* ($\mathcal{H}$-parity even), while it cannot mix with neutral components of 3-plets, 7-plets, *etc.* ($\mathcal{H}$-parity odd). This argument does not apply to the charged baryons in our model because they are not eigenstates of $\mathcal{H}$.

In Table 1, we show the $\mathrm{SU}(2)_L$ representations of all lowest-spin and spatially symmetric baryons for each set of $N_{c,f} = 2, \ldots, 5$.Note the appearance

$(N_c,\, N_f)$	Baryon $\mathrm{SU}(2)_L$ Representations	Category
(2,2)	$\mathbf{1}$	I
(2,3)	$\mathbf{3}$	III
(2,4)	$\mathbf{5} \oplus \mathbf{1}$	II
(2,5)	$\mathbf{7} \oplus \mathbf{3}$	III
(3,2)	$\mathbf{2}$	IV
(3,3)	$\mathbf{5} \oplus \mathbf{3}$	III
(3,4)	$\mathbf{8} \oplus \mathbf{6} \oplus \mathbf{4} \oplus \mathbf{2}$	IV
(3,5)	$\mathbf{11} \oplus \mathbf{9} \oplus \mathbf{7} \oplus \mathbf{5} \oplus \mathbf{5} \oplus \mathbf{3}$	III
(4,2)	$\mathbf{1}$	I
(4,3)	$\mathbf{5} \oplus \mathbf{1}$	II
(4,4)	$\mathbf{9} \oplus \mathbf{5} \oplus \mathbf{5} \oplus \mathbf{1}$	II
(4,5)	$\mathbf{13} \oplus \mathbf{9} \oplus \mathbf{9} \oplus \mathbf{7} \oplus \mathbf{5} \oplus \mathbf{5} \oplus \mathbf{1} \oplus \mathbf{1}$	II
(5,2)	$\mathbf{2}$	IV
(5,3)	$\mathbf{7} \oplus \mathbf{5} \oplus \mathbf{3}$	III
(5,4)	$\mathbf{12} \oplus \mathbf{10} \oplus \mathbf{8} \oplus \mathbf{8} \oplus \mathbf{6} \oplus \mathbf{6} \oplus \mathbf{4} \oplus \mathbf{4} \oplus \mathbf{2}$	IV
(5,5)	$\mathbf{17} \oplus \mathbf{15} \oplus \mathbf{13} \oplus \mathbf{13} \oplus \mathbf{11} \oplus \mathbf{11} \oplus \mathbf{11} \oplus \mathbf{9} \oplus \mathbf{9} \oplus \mathbf{9} \oplus \mathbf{9} \oplus \mathbf{7} \oplus \mathbf{7} \oplus \mathbf{7} \oplus \mathbf{5} \oplus \mathbf{5} \oplus \mathbf{5} \oplus \mathbf{5} \oplus \mathbf{3} \oplus \mathbf{3} \oplus \mathbf{1}$	II

Table 1. $\mathrm{SU}(2)_L$ representations of the lowest-spin dark baryons in the confined phase of the model in Eq. (2.1) for several combinations of number of dark colors N_c and flavors N_f. We define in the text the four categories in the rightmost column describing when singlets and other neutral states appear.

of $\mathrm{SU}(2)_L$ singlets, as states composed of singlets will have important implications for dark matter interactions, as we will see. We can classify the theory space into four categories:

I. When N_c is even and $N_f = 2$, the lowest-spin baryon spectrum includes only a singlet of $\mathrm{SU}(2)_L$, as one can infer from Eq. (2.2).

II. One or more singlets are accompanied by non-trivial odd representations of $\mathrm{SU}(2)_L$. The lightest state in the spectrum can be a mixture of the singlet and other neutral states.

III. There are no singlets, and instead only non-trivial odd representations of $\mathrm{SU}(2)_L$. The lightest baryon may be neutral, but it must transform non-trivially under $\mathrm{SU}(2)_L$.

IV. When N_c is odd and N_f is even, the baryons are in even representations of $\mathrm{SU}(2)_L$, so none of them are neutral.

We discuss the phenomenology of prospective DM candidates corresponding to each category in Sec. 2.7. As we will explain, categories I and II are particularly interesting to us.

2.3 Masses in the Heavy Quark Limit

Our DM candidate is the lightest mass eigenstate in the dark baryon spectrum. To identify which baryon state is the lightest, we use the non-relativistic quark model in the heavy quark limit, where hadrons are well-approximated as weakly-coupled bound states of their valence quarks [63–65]. We discuss the mass Hamiltonian in this limit and our approximation of its ground state using the variational method. We focus on the models with $(N_c, N_f) = (2, 4)$ and $(4, 3)$, as these are the simplest cases in category II defined in Sec. 2.2.2 (where the baryon spectra include singlets among neutral states in non-trivial $\mathrm{SU}(2)_L$ multiplets).

2.3.1 Electroweak Contributions in the Quark Model.

Including leading-order $\mathrm{SU}(N_c)$ and electroweak effects, the spatially-symmetric baryon mass is given by the operator (derived in Sec. 2.6.1) [66]

$$M = \sum_i \left(m_i + \frac{\langle p_i^2 \rangle}{2m_i} \right) + \sum_{i<j} \left\langle V_{ij}^{\chi} + V_{ij}^{\mathrm{EM}} + V_{ij}^{Z} + V_{ij}^{W} \right\rangle + \mathcal{O}(p_{i,j}^3/m_q^3), \tag{2.5}$$

$$
\begin{aligned}
\langle V_{ij}^{\chi}\rangle &= -\alpha_\chi \frac{N_c+1}{2N_c}\,\mathcal{V}(0) + \mathcal{O}(\alpha_\chi^2),\\
\langle V_{ij}^{\mathrm{EM}}\rangle &= \alpha_{\mathrm{EM}} Q_i Q_j \mathcal{V}(0) + \mathcal{O}(\alpha_{\mathrm{EM}}^2),\\
\langle V_{ij}^{Z}\rangle &= \alpha_W \cos^2\theta_W Q_i Q_j \mathcal{V}(m_Z) + \mathcal{O}(\alpha_W^2),\\
\langle V_{ij}^{W}\rangle &= \frac{\alpha_W}{2}\left(J_+^i J_-^j + J_-^i J_+^j\right)\mathcal{V}(m_W) + \mathcal{O}(\alpha_W^2),\\
\mathcal{V}(m_V) &= a_1 + \frac{1}{4m_q^2}\left(1+\frac{8}{3}\boldsymbol{S}_i\cdot\boldsymbol{S}_j\right)(m_V^2 a_1 - 4\pi\delta)\\
&\quad + \frac{m_V}{8m_q^2}\left(m_V^2 a_0 - 6m_V a_1 + 4a_2\right)\\
&\quad - \frac{1}{4m_q^2}\left(m_V^2 c_1 - 4m_V c_2 - 2b + m_V d_2 - 2d_3\right),
\end{aligned}
$$

where sums are over constituents in the i^{th} position of the spin-flavor wavefunction with masses m_i, momenta $\boldsymbol{p}_i$, spins $\boldsymbol{S}_i$, and charges Q_i. The inter-quark potential has terms from exchange of a dark gluon (V_{ij}^{χ}), photon (V_{ij}^{EM}), and weak bosons ($V_{ij}^{W,Z}$). The electromagnetic and $\mathrm{SU}(2)_L$ couplings α_{EM} and α_W appear, as well as the Weinberg angle θ_W. $J_\pm^i$ are $\mathrm{SU}(2)_L$ ladder operators acting on the i^{th} constituent (see Sec. 2.5.2 for explicit forms). Expectation values $\langle\cdot\rangle$ in Eq. (2.5) are taken with respect to spatial wavefunctions, so M is an operator that acts on baryon spin-flavor states. The mass m_q is the common tree-level mass of the quarks, which is distinct from m_i due to self-energy corrections inducing quark mass splittings (see Sec. 2.6.2). The function $\mathcal{V}$ depends on the vector boson mass m_V and various spatial expectation values, written in the position basis as

$$
\begin{aligned}
a_n &= \left\langle r^{-n} e^{-m_V r}\right\rangle,\\
b &= \left\langle r^{-1} e^{-m_V r}\,\boldsymbol{\nabla}_i\cdot\boldsymbol{\nabla}_j\right\rangle,\\
c_n &= \left\langle r^{-n} e^{-m_V r}\boldsymbol{r}\cdot(\boldsymbol{\nabla}_i - \boldsymbol{\nabla}_j)\right\rangle,\\
d_n &= \left\langle r^{-n} e^{-m_V r}\boldsymbol{r}\cdot(\boldsymbol{r}\cdot\boldsymbol{\nabla}_i)\boldsymbol{\nabla}_j\right\rangle,
\end{aligned}
\tag{2.6}
$$

$$\delta = \left\langle \delta^{(3)}(\boldsymbol{r}) \right\rangle ,$$

with $\boldsymbol{r} = \boldsymbol{r}_i - \boldsymbol{r}_j$ the inter-quark separation and $\boldsymbol{\nabla}_i$ the gradient with respect to $\boldsymbol{r}_i$. The potential is a generalization of the well-known Fermi-Breit potential (used in Ref. [63] for the electromagnetic and strong potentials in the SM) to include effects of the W and Z masses $m_{W,Z}$.

The W and Z potentials include contact terms (with the δ factor) that are unsuppressed in the limit $m_q/m_V \to 0$. These terms are essential for M to be consistent with gauge invariance in the limit $m_{W,Z} \to 0$, as explained in Sec. 2.6.3. Also, new terms arise in the finite-$m_{W,Z}$ regime that are not present in the usual Fermi-Breit potential for massless vector boson exchange [66]. We must account for both of these effects to accurately capture the mass splittings induced by differences among baryon spin-flavor matrix elements of operators with $Q_i Q_j$ and $J^i_\pm J^j_\mp$.

There are two physically-relevant bases in which we express baryon states: the $\mathrm{SU}(2)_L$ basis and the mass basis. In the $\mathrm{SU}(2)_L$ basis, each state is a component of a multiplet that transforms in a well-defined irreducible representation of $\mathrm{SU}(2)_L$. We express the mass operator in Eq. (2.5) in the $\mathrm{SU}(2)_L$ basis, then diagonalize it to transform to the mass basis. In this way, we can express a baryon mass eigenstate as a linear combination of states with well-defined SM interactions.

2.3.2 Mass Spectra from the Variational Method. To estimate the spatial expectation values in Eq. (2.6), we use the variational method with the following template spatial wavefunction:

$$\psi = \left(1 + k_1 \sum_{i<j} |\boldsymbol{r}_i - \boldsymbol{r}_j|\right) e^{-k \sum_{i<j} |\boldsymbol{r}_i - \boldsymbol{r}_j|} , \tag{2.7}$$

where k and k_1 are optimization parameters with respect to which we minimize mass eigenvalues. The function is symmetric in the exchange of constituents, as we are interested in the lowest-lying (s-wave) hadrons. Similar template functions were used in Ref. [8], and an overall exponential suppression is typical in other weakly-bound states such as atoms. Further details on how we compute the spatial expectation values are in Sec. 2.6.4.

We show the masses of the lightest neutral baryons and their overlaps with the $\mathrm{SU}(2)_L$ 5-plet states in Fig. 1 for $(N_c, N_f) = (2, 4)$ and $(4, 3)$. In the full parameter space shown, the lightest baryons are neutral and therefore may be viable DM candidates. The numerous terms in Eq. (2.5), each with different dependence on m_q and Λ_χ, give rise to non-trivial features in the mixing contours.

We verified that our calculation satisfies various consistency checks. For example, the quark-level calculation should reproduce expectations from hadron-level self-energy corrections. In particular, charged hadrons should typically be heavier than neutral hadrons, and hadron states in $\mathrm{SU}(2)_L$ representations with larger Casimir factors should have a larger overlap with heavier mass eigenstates. Indeed, we find that the lightest baryon is neutral in the full parameter space shown, and the 5-plet has larger overlap with heavier mass eigenstates than the singlet. The heavier neutral mass eigenstate can be heavier than the singly-charged state in the small-m_q region due to quark mass splittings or differences in electroweak matrix elements. See Sec. 2.6.3 for elaboration.

In our numerical evaluation of the mass spectrum, we verified that in the limit of $m_q, \Lambda_\chi \gg m_{W,Z}$, the mixing between the singlet and the neutral component of the 5-plet vanish, as expected. In the large-m_q regime, we find the mass splittings between the heavier neutral and singly-charged baryons to be

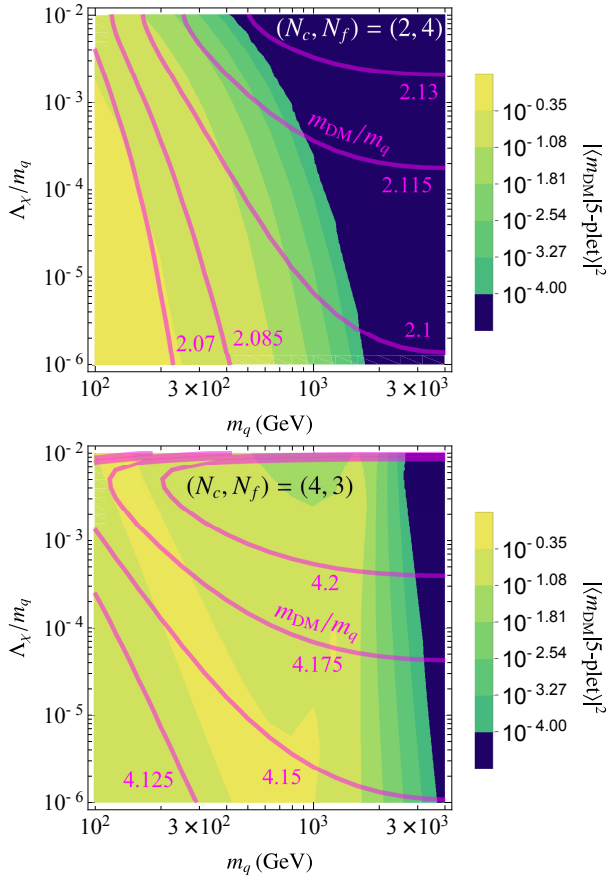


Figure 1. Mass $m_{\rm DM}$ of the lightest baryon and overlap of the lightest mass eigenstate $|m_{\rm DM}\rangle$ with the neutral $\mathrm{SU}(2)_L$ 5-plet state $|5\text{-plet}\rangle$ for $(N_c, N_f) = (2, 4)$ (**top**) and $(4, 3)$ (**bottom**), which are two benchmark models from category II in Sec. 2.2.2. As the dark quark mass m_q increases, DM's overlap with the non-singlet state decreases. DM masses are slightly greater than $N_c m_q$ due to quark self-energy corrections.

$\mathcal{O}(10^2)$ MeV, which is very close to the 166 MeV expectation for the mass splitting of any heavy singly-charged and neutral component of an $\mathrm{SU}(2)_L$ multiplet [67].

2.4 Modifications to the $\mathrm{SU}(2)_L$ Running Coupling

The dark quark fields we introduce in Eq. (2.1) modify the β-function of α_W at scales above m_q. At sufficiently large N_c and N_f, the appearance of Landau poles necessitates a UV completion at a scale below where the coupling diverges [68]. At one loop and for renormalization scale $\mu > m_q$ [69],

$$\frac{1}{\alpha_W(\mu)} = \frac{1}{\alpha_W(m_q)} - \frac{\beta_0}{2\pi}\ln\frac{\mu}{m_q} \tag{2.8}$$

$$\simeq \frac{1}{\alpha_W(m_Z)} - \frac{\beta_{\rm SM}}{2\pi}\ln\frac{m_q}{m_Z} - \frac{\beta_0}{2\pi}\ln\frac{\mu}{m_q}\,, \tag{2.9}$$

with

$$\beta_0 = \beta_{\rm SM} + \frac{4}{3}T_R N_c \tag{2.10}$$

$$\beta_{\rm SM} = -\frac{19}{6} \tag{2.11}$$

$$\mathrm{Tr}(J_a J_b) = T_R\,\delta_{ab},\ \ a,b\in\{x,y,z\} \tag{2.12}$$

$$T_R = \frac{N_f(N_f^2-1)}{12}\,. \tag{2.13}$$

One obtains Eq. (2.9) from Eq. (2.8) by running α_W from $\mu = m_Z$ to $\mu = m_q$ with the SM field content.

The N_f^3 scaling of T_R quickly spoils the asymptotic freedom of $\mathrm{SU}(2)_L$, as the β-function is negative only if $N_f = 2$ and $N_c \leq 4$. Otherwise, there is a UV Landau pole Λ_W where $1/\alpha_W(\Lambda_W) = 0$. Solving Eq. (2.9) for Λ_W,

$$\Lambda_W = m_q\left(\frac{m_Z}{m_q}\right)^{\beta_{\rm SM}/\beta_0}\exp\left(\frac{2\pi}{\beta_0\,\alpha_W(m_Z)}\right) \tag{2.14}$$

$$= m_q\left(\frac{m_Z}{m_q}\right)^{\frac{-57}{-57+2N_cN_f(N_f^2-1)}}\exp\left(\frac{36\pi}{(-57+2N_cN_f(N_f^2-1))\,\alpha_W(m_Z)}\right)\,. \tag{2.15}$$

As shown in Table 2, one quickly encounters sub-Planckian Landau poles ($\Lambda_W < M_{\rm Pl} \sim 10^{19}\,\mathrm{GeV}$) for modest values of $N_{c,f}$. It was already noted in Ref. [12] that our model requires a UV completion below the Planck scale (perhaps even below the Grand Unification scale) to facilitate meson decays before Big Bang Nucleosynthesis, but the Landau poles imply that a UV completion is needed at

$(N_c,\, N_f)$	Λ_W (GeV) for $m_q = 1\,\mathrm{TeV}$	Λ_W (GeV) for $m_q = 1\,\mathrm{PeV}$
(2,2)	—	—
(2,3)	10^{42}	10^{49}
(2,4)	10^{11}	10^{15}
(2,5)	10^{6}	10^{10}
(3,2)	—	—
(3,3)	10^{20}	10^{25}
(3,4)	10^{8}	10^{11}
(3,5)	10^{5}	10^{8}
(4,2)	—	—
(4,3)	10^{14}	10^{18}
(4,4)	10^{6}	10^{10}
(4,5)	10^{4}	10^{8}
(5,2)	10^{508}	10^{568}
(5,3)	10^{11}	10^{15}
(5,4)	10^{6}	10^{9}
(5,5)	10^{4}	10^{7}

Table 2. Order-of-magnitude estimates of $\mathrm{SU}(2)_L$ Landau poles Λ_W for various $N_{c,f}$ combinations using Eq. (2.15). Dashes indicate where $\mathrm{SU}(2)_L$ remains asymptotically free. Some versions of the theory are safe from sub-Planckian Landau poles, and others require a UV completion at modestly high scales.

an even lower scale for some N_c,N_f. When Λ_W/m_q is not very large (say $\lesssim 10^3$), one must carefully consider the effects of higher-dimensional operators induced by the UV completion. These effects can include baryon number violation, $\mathcal{H}$-parity violation, and large two-loop corrections to the SM $\mathrm{SU}(3)_{\mathrm{color}}$ and $\mathrm{U}(1)_Y$ couplings. This pathology is particularly pronounced for $N_f \geq 5$, where Λ_W/m_q can be $\mathcal{O}(10)$.

2.5 Further Details on Hadron Representations

Our conclusions about the phenomenology of the confining dark sector we present in Sec. 2.2 depend on the possible $\mathrm{SU}(2)_L$ representations of the

dark baryons, so we require a systematic approach to enumerate them for any combination of N_c and N_f. Future analyses of collider signals and cosmology would also benefit from understanding the meson spectrum and representations.

2.5.1 Spin and Flavor Representations. We employ the quark model [63–65], wherein hadron states are products of color, flavor, spin, and spatial wavefunctions. Baryon states with identical fermionic constituents must be totally anti-symmetric under particle exchange. Meson constituents transform in conjugate representations of their symmetry groups, so a multi-particle meson state does not consist of identical particles and therefore need not have definite exchange symmetry. Since we are most interested in the lightest hadrons, we restrict our analysis to states with vanishing orbital angular momentum and symmetric spatial wavefunctions, and we emphasize the lowest-spin states.

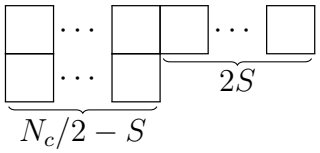
Under the assumption of confinement, hadron states transform in the singlet representation of SU(N_c), which implies baryon color wavefunctions are totally anti-symmetric in exchange of their N_c constituents. With our additional assumption of even spatial wavefunctions, the combined spin-flavor states of the baryons in our model must be totally symmetric in particle exchange. Therefore, baryons with spin-1/2 constituents have spin-flavor states belonging to the symmetric representation of SU($2N_f$) with the Young tableau

$$\underbrace{\square\cdots\square}_{N_c} \tag{2.16}$$

$$\text{dimension} = \frac{(2N_f - 1 + N_c)!}{N_c!\,(2N_f - 1)!}\,.$$

The group is $\mathrm{SU}(2N_f)$ since for each of the N_f possible flavors, there are two possible spin states. The dimension of this representation counts the number of baryon spin-flavor states, including all spin degrees of freedom. However, since we want to understand the hadrons' $\mathrm{SU}(2)_L$ representations, and $\mathrm{SU}(2)_L$ is a subgroup of the $\mathrm{SU}(N_f)$ flavor symmetry (analogous to SM isospin), it is useful to consider the hadron states' flavor representations in $\mathrm{SU}(N_f)$ separately from their spin representations in $\mathrm{SU}(2)_{\mathrm{spin}}$.

In order for a baryon's combined spin-flavor representation to be totally symmetric, its representations in $\mathrm{SU}(N_f)$ and $\mathrm{SU}(2)_{\mathrm{spin}}$ *must have identical exchange symmetries*. Therefore, those representations must have identical Young tableaux when written out with all N_c boxes. The tableaux for $\mathrm{SU}(2)_{\mathrm{spin}}$ representations have at most two boxes in each column, so the same is true for the relevant $\mathrm{SU}(N_f)$ representations. Thus, spin-S baryon states belong to the flavor representation of $\mathrm{SU}(N_f)$ with the tableau[4]



(2.17)

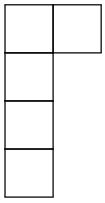
$$\text{dimension} = \frac{(2S+1)(N_f+N_c/2+S-1)!\,(N_f+N_c/2-S-2)!}{(N_f-1)!\,(N_f-2)!\,(N_c/2+S+1)!\,(N_c/2-S)!}\,,$$

and the dimension of this representation counts the number of spin-S baryons, see also Ref. [8] for similar results. Unlike the expression in Eq. (2.16), this counting

[4] A spin-S representation of $\mathrm{SU}(2)_{\mathrm{spin}}$ has a row of $2S$ boxes in its Young tableau after contraction.

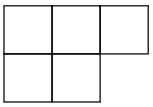
does not include all values of $S_z = -S, \ldots, S$ for the various $|S\, S_z\rangle$ baryon spin states.

As an example of applying Eq. (2.17), consider the model with $N_c = 5$ and $N_f = 4$. Naïvely, a candidate flavor representation of SU(4) for spin-1/2 baryons would be



(2.18)

which can be contracted to the fundamental representation of SU(4). This may seem to suggest that baryon states can be constructed in the flavor representation in Eq. (2.18) and the fundamental representation of $\mathrm{SU}(2)_{\mathrm{spin}}$. This is, however, not true because there is no representation of $\mathrm{SU}(2)_{\mathrm{spin}}$ with the Young tableau in Eq. (2.18). Any spin configuration with $S = 1/2$ has different particle exchange symmetries than any flavor configuration in the above representation, so the combined spin-flavor representation would not be totally symmetric. The only flavor representation with spin-1/2 baryons in this model would be



(2.19)

which is a valid tableau for an $\mathrm{SU}(2)_{\mathrm{spin}}$ representation that can be contracted to the fundamental representation. This is a dimension-60 representation of the SU(4) flavor group. In Sec. 2.5.2, we describe how to construct baryon spin-flavor wavefunctions using the symmetry of the full $\mathrm{SU}(2N_f)$ representation.

2.5.2 Finding Hadron Wavefunctions and $\mathrm{SU}(2)_L$ Representations.

Now that we have the flavor representations in $\mathrm{SU}(N_f)$, we can formally understand why the baryon states are in specific $\mathrm{SU}(2)_L$ multiplets. Recall that $\mathrm{SU}(2)_L$ is a subgroup of $\mathrm{SU}(N_f)$. For $\mathcal{H}$-parity symmetric models,

we are interested in the embedding of $\mathrm{SU}(2)_L$ in $\mathrm{SU}(N_f)$ where one identifies the N_f-dimensional irreducible representation of $\mathrm{SU}(2)_L$ with the fundamental representation of $\mathrm{SU}(N_f)$. One can express the flavor representation in Eq. (2.17) as a direct sum of irreducible $\mathrm{SU}(2)_L$ representations corresponding to this embedding. This is the decomposition shown in Table 1 for several combinations of N_c and N_f and the lowest-spin baryons.

We have an algorithm for finding all hadron spin-flavor wavefunctions with a particular spin state, organizing the states into $\mathrm{SU}(2)_L$ multiplets, and using the wavefunctions to compute the matrix elements needed for the mass calculation. For concreteness, we define a spin-flavor eigenstate as a simultaneous eigenstate of the spin operators S^2 and S_z as well as all flavor number operators (*i.e.* a spin-flavor eigenstate has definite quark flavor content). We likewise define an $\mathrm{SU}(2)_L$ eigenstate as a simultaneous eigenstate of the quadratic Casimir operator J^2 and the third generator J_z of $\mathrm{SU}(2)_L$. The eigenvalues of J_z are electric charges Q (as the dark sector particles have vanishing hypercharge), and the eigenvalues of J^2 are $J(J+1)$. The spectrum of J quantum numbers indicates the decomposition of the $\mathrm{SU}(N_f)$ representation in Eq. (2.17) into representations of $\mathrm{SU}(2)_L$, and each eigenstate of J^2 belongs to a $(2J+1)$-plet of $\mathrm{SU}(2)_L$. Enumerating all of these states requires finding all appropriately symmetrized combinations of flavor and spin configurations, then expressing these in a basis that simultaneously diagonalizes S^2, S_z, J^2, and J_z. Our algorithm finds these states for either mesons or baryons, and we specify the differences in those cases below.

A schematic description of our algorithm is

1. Find a complete basis of constituent spin configurations for the desired hadron spin state.

2. Find a complete basis of flavor configurations for the hadrons with the "middlest" electric charge ($Q = 1/2$ when N_c is odd and N_f is even and $Q = 0$ otherwise).

3. Combine the spin and flavor eigenstates to obtain a complete basis of spin-flavor eigenstates with this charge. For baryons, symmetrize the states and eliminate linear dependence and overlap of the symmetrized states.

4. Transform the basis of spin-flavor eigenstates to a basis that diagonalizes J^2 of $\mathrm{SU}(2)_L$. Deduce the spectrum of hadron $\mathrm{SU}(2)_L$ multiplets from the eigenvalues of J^2.

5. Apply the $\mathrm{SU}(2)_L$ ladder operators to the eigenstates of J^2 with the middlest charge to find all other $\mathrm{SU}(2)_L$ eigenstates in each multiplet.

We elaborate on each step below, including examples. We start with the middlest electric charge because all $\mathrm{SU}(2)_L$ multiplets contain a state with this charge. One could alternatively start with the highest charge and repeatedly lower it to construct the multiplets. However, that approach is more complicated because there may be additional states with the lower charge that one would have to find. For example, in the $(N_c, N_f) = (5, 3)$ model, if one started with the $Q = 3$ state in the baryon 7-plet and lowered it to the $Q = 2$ state, one would need to find the $Q = 2$ state in the 5-plet, then do the same again for the $Q = 1$ states in the 5-plet and triplet. By contrast, by finding all the $Q = 0$ states and raising/lowering them to fill out the multiplets, one needs to find all states with a particular charge only once.

One must first specify the desired $|S\, S_z\rangle$ hadron spin state. One can then find a complete, orthonormal basis of constituent spin configurations for that state.

For mesons with spin-1/2 constituents, this basis is the well-known spin singlet or triplet state, so we emphasize the baryon case. One can start with the highest-spin baryon state $\left|S = \frac{N_c}{2}\ S_z = \frac{N_c}{2}\right\rangle$ and repeatedly apply the lowering operator S_- until the state has the desired S_z. One now has a spin state in the multiplet corresponding to the totally symmetric $\mathrm{SU}(2)_{\mathrm{spin}}$ representation with dimension $N_c + 1$. Therefore, the state is composed of all basis state spin configurations with the desired S_z. One can use this basis to diagonalize the operator S^2 and isolate the eigenstates with the desired $S(S+1)$ eigenvalues. One now has a complete, orthonormal basis of constituent spin configurations with the desired hadron spin state.

As an illustrative example, consider the baryon spectrum in the model with $(N_c, N_f) = (4, 3)$. The flavor representations of the required form in Eq. (2.17) are



(2.20)

corresponding to spin-0, spin-1, and spin-2 baryons, respectively. Suppose we desire baryons in the spin state $|S = 0\ S_z = 0\rangle$. One applies S_- to the highest-spin state $|\uparrow\uparrow\uparrow\uparrow\rangle$ to find the basis of six states with $S_z = 0$, each with two spin-up and two spin-down quarks. After diagonalizing S^2, one finds two states with $S = 0$. A (non-unique) orthonormal basis in which to write these states is

$$|s_1\rangle = \frac{1}{\sqrt{12}}\left(2|\uparrow\uparrow\downarrow\downarrow\rangle + 2|\downarrow\downarrow\uparrow\uparrow\rangle - |\uparrow\downarrow\uparrow\downarrow\rangle - |\downarrow\uparrow\downarrow\uparrow\rangle - |\uparrow\downarrow\downarrow\uparrow\rangle - |\downarrow\uparrow\uparrow\downarrow\rangle\right) \tag{2.21}$$

$$|s_2\rangle = \frac{1}{2}\left(|\uparrow\downarrow\uparrow\downarrow\rangle - |\downarrow\uparrow\uparrow\downarrow\rangle + |\downarrow\uparrow\downarrow\uparrow\rangle - |\uparrow\downarrow\downarrow\uparrow\rangle\right). \tag{2.22}$$

Note that $|s_1\rangle$ is symmetric in exchanges of the first pair and last pair of particles, and $|s_2\rangle$ is anti-symmetric in these exchanges.

Next, one needs a complete, orthonormal basis of flavor configurations with the middlest charge, either $Q = 1/2$ or $Q = 0$. This can be done similarly to the spin configurations above. Starting with the highest-charge flavor state, one can generate the symmetric $\mathrm{SU}(2)_L$ multiplet by repeatedly applying J_-, and the resulting state is a combination of all flavor configurations with the desired charge. Labeling quark flavors by their charge and labeling anti-quark flavors with charge $-Q$ as $\overline{Q}$, the $SU(2)_L$ generators act on baryon and meson flavor states as

$$J_z \left|Q_1, \ldots, Q_{N_c}\right\rangle = \sum_{i=1}^{N_c} Q_i \ \left|Q_1, \ldots, Q_{N_c}\right\rangle , \tag{2.23}$$

$$J_\pm \left|Q_1, \ldots, Q_{N_c}\right\rangle = \sum_{i=1}^{N_c} \sqrt{\frac{N_f^2-1}{4} - Q_i(Q_i \pm 1)} \ \left|Q_1, \ldots, Q_i \pm 1, \ldots, Q_{N_c}\right\rangle , \tag{2.24}$$

$$J_z \left|Q_1, \overline{Q}_2\right\rangle = (Q_1 - Q_2) \left|Q_1, \overline{Q}_2\right\rangle , \tag{2.25}$$

$$J_\pm \left|Q_1, \overline{Q}_2\right\rangle = \sqrt{\frac{N_f^2-1}{4} - Q_1(Q_1 \pm 1)} \ \left|Q_1 \pm 1, \overline{Q}_2\right\rangle \tag{2.26}$$

$$- \sqrt{\frac{N_f^2-1}{4} - Q_2(Q_2 \mp 1)} \ \left|Q_1, \overline{Q_2 \mp 1}\right\rangle . \tag{2.27}$$

We work in the convention with

$$J_\pm = J_x \pm i J_y , \tag{2.28}$$

$$J^2 = J_z^2 + \frac{1}{2}\left(J_+ J_- + J_- J_+\right) , \tag{2.29}$$

where J_x and J_y are the first and second generators of $\mathrm{SU}(2)_L$, respectively.

In the example of the $(4, 3)$ model, we can label the quark flavors as $+, 0, -$, corresponding to positive, zero, and negative electric charges, respectively. The highest-charge state is $|+ + + +\rangle$. After applying J_-, one finds the $Q = 0$ flavor configurations

$$|f_1\rangle = |0000\rangle \tag{2.30}$$

$$|f_2\rangle = |--++\rangle \tag{2.31}$$

$$|f_3\rangle = |-\ 00\ +\rangle, \tag{2.32}$$

plus permutations. Note that $|f_1\rangle$ has more exchange symmetries than $|f_2\rangle$, which has more than $|f_3\rangle$.

Now that one has bases for the spin and flavor configurations, one can find the combined spin-flavor states. For meson states, these are simply the tensor products of each flavor configuration with the spin configuration identified above. However, baryon spin-flavor states must be symmetrized. To find all the needed baryon states, one can start by finding the tensor product state of each flavor configuration with each spin configuration. For each of these tensor product states, written with each particle $p_1, \ldots, p_{N_c}$ having some flavor and spin assignment, one then finds the symmetrized state

$$\sum_{\sigma \in \text{perms}(N_c)} \left| p_{\sigma(1)}, \ldots, p_{\sigma(N_c)} \right\rangle, \tag{2.33}$$

where perms(N_c) is the set of all permutations of N_c elements. Any valid baryon spin-flavor eigenstate must be some symmetrized product of a flavor content with a spin configuration, so the set of all states obtained using Eq. (2.33) is an over-complete set from which a complete basis of baryon spin-flavor eigenstates can be extracted. One can iteratively construct an orthogonal basis $\{|b_1\rangle, \ldots, |b_n\rangle\}$ of states that are linear combinations of non-orthogonal states in the set $\{|v_1\rangle, \ldots, |v_n\rangle\}$ using the Gram-Schmidt process. One sets $|b_1\rangle = |v_1\rangle$, then $|b_n\rangle$ is constructed using the previously found $n-1$ states as

$$|b_n\rangle = |v_n\rangle - \sum_{i=1}^{n-1} \frac{\langle b_i|v_n\rangle}{\langle b_i|b_i\rangle}|b_i\rangle. \tag{2.34}$$

Since the original set of symmetrized baryon states is over-complete, some of the states constructed in this way will have zero norm, and such states can be discarded. One now has a complete, orthogonal basis of meson or baryon spin-flavor eigenstates with the desired spin and the middlest charge.

In the $(4, 3)$ model, symmetrizing the tensor product of the $|f_1\rangle$ flavor configuration with either spin configuration results in the state with zero norm. This is unsurprising, as $|f_1\rangle$ is totally symmetric in particle exchange, while neither spin configuration is totally symmetric. This case is analogous to the lack of a spin-1/2 baryon with three up quarks in the SM.

Finding the product of $|f_2\rangle$ with either spin state and symmetrizing gives the neutral baryon spin-flavor eigenstate

$$|\mathcal{B}_1^0\rangle = \frac{1}{\sqrt{72}}|--++\rangle \otimes (2|\uparrow\uparrow\downarrow\downarrow\rangle + 2|\downarrow\downarrow\uparrow\uparrow\rangle \tag{2.35}$$

$$- |\uparrow\downarrow\uparrow\downarrow\rangle - |\downarrow\uparrow\downarrow\uparrow\rangle - |\uparrow\downarrow\downarrow\uparrow\rangle - |\downarrow\uparrow\uparrow\downarrow\rangle) + \text{perms}, \tag{2.36}$$

where "perms" denotes particle permutations that do not return the same configuration. Doing the same with $|f_3\rangle$ results in

$$|\mathcal{B}_2^0\rangle = \frac{1}{12}|-00+\rangle \otimes (|\uparrow\uparrow\downarrow\downarrow\rangle + |\downarrow\downarrow\uparrow\uparrow\rangle \tag{2.37}$$

$$+ |\uparrow\downarrow\uparrow\downarrow\rangle + |\downarrow\uparrow\downarrow\uparrow\rangle - 2|\uparrow\downarrow\downarrow\uparrow\rangle - 2|\downarrow\uparrow\uparrow\downarrow\rangle) + \text{perms}. \tag{2.38}$$

These form a complete basis of neutral baryons with the desired spin, but our algorithm prescribes also finding the symmetrized baryon states generated by the permuted flavor configurations not shown above to ensure all baryons are found.

The Gram-Schmidt process eliminates the redundancy from pairing flavor and spin states that provide linearly dependent symmetrized baryon states.

One can determine the spectrum of hadron $\mathrm{SU}(2)_L$ multiplets by using the basis of spin-flavor eigenstates to diagonalize the J^2 operator. These multiplets provide the decomposition of the $\mathrm{SU}(N_f)$ flavor representation into irreducible representations of $\mathrm{SU}(2)_L$. Some eigenvalues of J^2 may be degenerate (*e.g.* the scalar singlets for $(N_c, N_f) = (4, 5)$), in which case there is not a unique way to write the $\mathrm{SU}(2)_L$ eigenstates as linear combinations of spin-flavor eigenstates.

Finally, one can repeatedly apply the $J_\pm$ operators to the $\mathrm{SU}(2)_L$ eigenstates with the middlest charge to obtain the spin-flavor wavefunctions for all entries of each multiplet. One now has the full spectrum of lowest-lying hadron spin-flavor states with the desired spin, organized by $\mathrm{SU}(2)_L$ representation and charge.

For the $(4, 3)$ model, using the states in Eqs. (2.35) and (2.37) to diagonalize J^2 shows that the linear combination

$$|\mathcal{J}_0^0\rangle = -\frac{1}{\sqrt{3}}\,|\mathcal{B}_1^0\rangle + \sqrt{\frac{2}{3}}\,|\mathcal{B}_2^0\rangle \tag{2.39}$$

is an $\mathrm{SU}(2)_L$ singlet, and acting with $J_\pm$ on the orthogonal combination generates the $\mathrm{SU}(2)_L$ 5-plet

$$\begin{pmatrix} |\mathcal{J}_2^{++}\rangle \\ |\mathcal{J}_2^{+}\rangle \\ |\mathcal{J}_2^{0}\rangle \\ |\mathcal{J}_2^{-}\rangle \\ |\mathcal{J}_2^{--}\rangle \end{pmatrix} = \begin{pmatrix} |\mathcal{B}^{++}\rangle \\ |\mathcal{B}^{+}\rangle \\ \sqrt{\frac{2}{3}}\,|\mathcal{B}_1^0\rangle + \frac{1}{\sqrt{3}}\,|\mathcal{B}_2^0\rangle \\ |\mathcal{B}^{-}\rangle \\ |\mathcal{B}^{--}\rangle \end{pmatrix}, \tag{2.40}$$

where

$$|\mathcal{B}^{++}\rangle = \frac{1}{\sqrt{72}}|00++\rangle \otimes (2|\uparrow\uparrow\downarrow\downarrow\rangle + 2|\downarrow\downarrow\uparrow\uparrow\rangle - |\uparrow\downarrow\uparrow\downarrow\rangle \tag{2.41}$$

$$- |\downarrow\uparrow\downarrow\uparrow\rangle - |\uparrow\downarrow\downarrow\uparrow\rangle - |\downarrow\uparrow\uparrow\downarrow\rangle) + \text{perms} \tag{2.42}$$

$$|\mathcal{B}^{+}\rangle = \frac{1}{12}|-0++\rangle \otimes (2|\uparrow\uparrow\downarrow\downarrow\rangle + 2|\downarrow\downarrow\uparrow\uparrow\rangle - |\uparrow\downarrow\uparrow\downarrow\rangle \tag{2.43}$$

$$- |\downarrow\uparrow\downarrow\uparrow\rangle - |\uparrow\downarrow\downarrow\uparrow\rangle - |\downarrow\uparrow\uparrow\downarrow\rangle) + \text{perms}, \tag{2.44}$$

and the negatively-charged states $|\mathcal{B}^{-}\rangle$ and $|\mathcal{B}^{--}\rangle$ can be found by negating the flavors of the positively-charged states. In the above notation, states labeled with $\mathcal{B}$ are spin-flavor eigenstates. States labeled with $\mathcal{J}$ are $\mathrm{SU}(2)_L$ eigenstates whose subscripts denote the J quantum numbers corresponding to the $J(J+1)$ eigenvalues of J^2. The presence of the singlet and 5-plet shows that for the relevant embedding, the SU(3) flavor representation decomposes to $\mathrm{SU}(2)_L$ representations as

$$\mathrm{SU}(3) \supset \mathrm{SU}(2)_L \tag{2.45}$$

$$\square\square \to \mathbf{5} \oplus \mathbf{1}\,,$$

as stated in Table 1.

Our other main example in Sec. 2.3.2 is the $(N_c, N_f) = (2, 4)$ model, for which we briefly walk through the baryon wavefunction derivation here. The SU(4) flavor representations are

$$\square \qquad\qquad \square\square \tag{2.46}$$

for spin-0 and spin-1 baryons, respectively. We again specify the $|S=0\ S_z=0\rangle$ spin state, for which the only spin configuration is the well-known anti-symmetric two-body spin-singlet state. The flavor configurations with $Q=0$ are

$$\left|-\frac{3}{2}\ +\frac{3}{2}\right\rangle, \qquad \left|+\frac{3}{2}\ -\frac{3}{2}\right\rangle, \qquad \left|-\frac{1}{2}\ +\frac{1}{2}\right\rangle, \qquad \left|+\frac{1}{2}\ -\frac{1}{2}\right\rangle. \tag{2.47}$$

When paired with the allowed spin configuration and symmetrized, these generate the baryon spin-flavor eigenstates

$$|\mathrm{B}_1^0\rangle = \frac{1}{2}\left(\left|-\frac{3}{2}\ +\frac{3}{2}\right\rangle - \left|+\frac{3}{2}\ -\frac{3}{2}\right\rangle\right)\otimes\left(|\uparrow\downarrow\rangle - |\downarrow\uparrow\rangle\right), \tag{2.48}$$

$$|\mathrm{B}_2^0\rangle = \frac{1}{2}\left(\left|-\frac{1}{2}\ +\frac{1}{2}\right\rangle - \left|+\frac{1}{2}\ -\frac{1}{2}\right\rangle\right)\otimes\left(|\uparrow\downarrow\rangle - |\downarrow\uparrow\rangle\right), \tag{2.49}$$

which, when written in the basis that diagonalizes J^2 and acted on with $J_\pm$, provide the $\mathrm{SU}(2)_L$ singlet

$$|\mathrm{J}_0^0\rangle = \frac{1}{\sqrt{2}}\left(|\mathrm{B}_1^0\rangle - |\mathrm{B}_2^0\rangle\right) \tag{2.50}$$

and 5-plet

$$\begin{pmatrix} |\mathrm{J}_2^{++}\rangle \\ |\mathrm{J}_2^{+}\rangle \\ |\mathrm{J}_2^{0}\rangle \\ |\mathrm{J}_2^{-}\rangle \\ |\mathrm{J}_2^{--}\rangle \end{pmatrix} = \begin{pmatrix} |\mathrm{B}^{++}\rangle \\ |\mathrm{B}^{+}\rangle \\ \frac{1}{\sqrt{2}}\left(|\mathrm{B}_1^0\rangle + |\mathrm{B}_2^0\rangle\right) \\ |\mathrm{B}^{-}\rangle \\ |\mathrm{B}^{--}\rangle \end{pmatrix}, \tag{2.51}$$

where

$$|\mathrm{B}^{++}\rangle = \frac{1}{2}\left(\left|+\frac{1}{2}\ +\frac{3}{2}\right\rangle - \left|+\frac{3}{2}\ +\frac{1}{2}\right\rangle\right)\otimes\left(|\uparrow\downarrow\rangle - |\downarrow\uparrow\rangle\right) \tag{2.52}$$

$$|\mathrm{B}^{+}\rangle = \frac{1}{2}\left(\left|-\frac{1}{2}\ +\frac{3}{2}\right\rangle - \left|+\frac{3}{2}\ -\frac{1}{2}\right\rangle\right)\otimes\left(|\uparrow\downarrow\rangle - |\downarrow\uparrow\rangle\right), \tag{2.53}$$

and so on for the negatively-charged states. These multiplets indicate the decomposition

$$\mathrm{SU}(4) \supset \mathrm{SU}(2)_L \tag{2.54}$$
$$\square\!\!\square \rightarrow \mathbf{5}\oplus\mathbf{1}\,,$$

for our embedding of $\mathrm{SU}(2)_L$ in flavor SU(4). The only reason why we chose both benchmark models to have the same $\mathrm{SU}(2)_L$ multiplets is because the singlet and 5-plet combination is the simplest case where there is a singlet in the spectrum and mixing of neutral states in different representations.

In the electroweak-symmetric phase of the SM, gauge invariance guarantees that each 5-plet baryon state in Eq. (2.40) is a mass eigenstate with exactly the same mass, and likewise for the states in Eq. (2.51). Then, the singlets in Eqs. (2.39) and (2.50) are mass eigenstates with different masses. In the electroweak-broken phase, charge differences cause the masses of states in the 5-plets to split apart, and the neutral $\mathrm{SU}(2)_L$ eigenstates will no longer be mass eigenstates. Sec. 2.6 details the mass calculation and implications of these observations.

2.6 Further Details on the Mass Calculation

In the limit where the dark quark mass m_q is significantly larger than the dark sector confinement scale Λ_χ, mesons and baryons are well-approximated as weakly-coupled bound states of non-relativistic constituents. In Ref. [63], this

quark model picture is applied to the SM, where the physical quark masses are less than the confinement scale, and non-perturbative effects give large contributions to hadron masses. Nonetheless, this approach predicts SM hadron mass splittings fairly well using non-perturbative dressed quark masses. In the heavy quark limit of our model, we treat non-perturbative and relativistic effects as negligible, so we expect the quark model prediction to be a valid approximation of hadron masses (not only their splittings) using physical quark masses. We cannot reliably compute the hadron masses when m_q is not significantly greater than Λ_χ, but our qualitative conclusions concerning relative mass splittings and mixings likely still hold as these are driven by perturbative electroweak effects.

2.6.1 The Mass Hamiltonian. The mass operator in Eq. (2.5) comes from the Hamiltonian

$$H = H_{\text{free}} + \sum_{i<j} V_{ij} \,, \tag{2.55}$$

where V_{ij} is the inter-quark potential, and H_{free} is the free Hamiltonian

$$H_{\text{free}} = \sum_i \left(m_i + \frac{p_i^2}{2m_i} \right) , \tag{2.56}$$

in the non-relativistic approximation. At first order in the gauge couplings, the inter-quark potential comes from exchange of a single gauge boson. For massless gauge bosons (*i.e.* the photon and dark gluons) and at first order in the non-relativistic expansion in p^2/m_q^2, this potential is the Fermi-Breit potential familiar from the Hydrogen atom in non-relativistic quantum mechanics.

In addition to the dark sector coupling, the dark gluon potential in Eq. (2.5) includes a color factor $-(N_c+1)/(2N_c)$ from contractions of SU(N_c) generators in

the fundamental representation with anti-symmetric baryon color wavefunctions. For mesons, this factor should be replaced with $-(N_c^2-1)/(2N_c)$, where the sign is from fermion statistics, and the N_c-dependence is from contracting $\mathrm{SU}(N_c)$ generators with color-singlet wavefunctions. In the SM with $N_c = 3$, these color factors reproduce the $-2/3$ for baryons and $-4/3$ for mesons found in Ref. [63].

In the electroweak-symmetric limit, the photon and Z contributions in Eq. (2.5) sum to the contribution of the third $\mathrm{SU}(2)_L$ gauge boson, the W^3, since $\alpha_{\mathrm{EM}} + \alpha_W \cos^2\theta_W = \alpha_W$. The raising and lowering operators in Eq. (2.5) allow the W boson to mix hadron states with different flavor content, which is why the spin-flavor eigenstates described in Sec. 2.5 are not in general equivalent to $\mathrm{SU}(2)_L$ eigenstates or mass eigenstates. In the $m_q, \Lambda_\chi \gg m_W$ limit, electroweak symmetry breaking is "small" in the dark sector, and mass eigenstates should be nearly identical to $\mathrm{SU}(2)_L$ eigenstates as shown in Fig. 1. In the $m_q, \Lambda_\chi \ll m_W$ limit where one can integrate out the W, spin-flavor eigenstates should be nearly identical to mass eigenstates as their mixing due to the W is suppressed. We indeed see this behavior in Fig. 1, as the overlaps of the mass eigenstates with the $\mathrm{SU}(2)_L$ eigenstates approach the overlaps of the spin-flavor eigenstates with the $\mathrm{SU}(2)_L$ eigenstates as m_q becomes small.

In order to incorporate finite-mass effects of the W and Z, we require a generalization of the Fermi-Breit potential whose 0^{th} order term in the non-relativistic expansion is the Yukawa potential rather than the Coulomb potential. Ref. [66] derived that, up to color factors and couplings, the inter-quark potential is

$$V_{ij} = V_0(r) \tag{2.57}$$

$$+ \left(\frac{1}{8m_i^2} + \frac{1}{8m_j^2}\right) \nabla^2 V_0(r) \tag{2.58}$$

$$+\left[\left(\frac{1}{2m_i^2}+\frac{1}{m_i m_j}\right)\boldsymbol{S}_i+\left(\frac{1}{2m_j^2}+\frac{1}{m_i m_j}\right)\boldsymbol{S}_j\right]\cdot\boldsymbol{\ell}\,\frac{V_0'(r)}{r} \tag{2.59}$$

$$+\frac{1}{m_i m_j}\left[\frac{2}{3}\boldsymbol{S}_i\cdot\boldsymbol{S}_j\nabla^2 V_0(r)\right. \tag{2.60}$$

$$\left.+\left((\boldsymbol{S}_i\cdot\hat{r})(\boldsymbol{S}_j\cdot\hat{r})-\frac{1}{3}\boldsymbol{S}_i\cdot\boldsymbol{S}_j\right)\left(V_0''(r)-\frac{V_0'(r)}{r}\right)\right] \tag{2.61}$$

$$-\frac{1}{8m_i m_j}\left(\{\boldsymbol{p}_i\cdot\boldsymbol{p}_j,V_0(r)\}+2p_i^\alpha V_0(r)p_j^\alpha\right) \tag{2.62}$$

$$-\frac{1}{4m_i m_j}\left(\left\{p_i^\alpha p_j^\beta,\hat{r}^\alpha\hat{r}^\beta W(r)\right\}+2p_i^\alpha\hat{r}^\alpha\hat{r}^\beta W(r)p_j^\beta\right) \tag{2.63}$$

at $\mathcal{O}(p^2/m^2)$, where $V_0(r)$ is the potential at 0^{th} order in the non-relativistic expansion, $W(r)=-rV_0'(r)/2$, $\boldsymbol{\ell}$ is the angular momentum operator, $\hat{r}$ is the unit vector in the direction of the inter-quark separation $\boldsymbol{r}=\boldsymbol{r}_i-\boldsymbol{r}_j$, and α,β are Cartesian indices.[5] One may recognize Eqs. (2.58) and (2.59) as the fine-structure correction and Eqs. (2.60) and (2.61) as the hyperfine-structure correction.

For hadrons with symmetric spatial wavefunctions, the spin-orbit coupling in Eq. (2.59) and tensor force contribution in Eq. (2.61) do not contribute, since $\boldsymbol{\ell}$ has odd parity and $\langle(\hat{r}\cdot\boldsymbol{S}_i)(\hat{r}\cdot\boldsymbol{S}_j)\rangle\to\langle\boldsymbol{S}_i\cdot\boldsymbol{S}_j\rangle/3$ [72]. The remaining contributions are $V_0(r)$, the Darwin term in Eq. (2.58), the spin-spin coupling in Eq. (2.60), and the orbit-orbit coupling in Eqs. (2.62) and (2.63). Using $V_0(r)=e^{-m_V r}/r$ for the Yukawa potential, expanding out the momentum operators in terms of gradients, taking the expectation value with respect to a symmetric spatial wavefunction, setting $m_{i,j}=m_q$, and re-inserting coupling coefficients, one recovers Eq. (2.5).

The contact terms that arise from the spin-spin coupling and Darwin terms are not suppressed by the mass of the exchanged boson. It is unclear how

[5] In standard derivations of the Fermi-Breit potential (*e.g.* Refs. [70, 71]), the ordering of position and momentum operators is not handled carefully, so applying the same calculations to massive boson exchange does not ensure a Hermitian potential. When transforming the potential from momentum space to position space, one must keep initial and final momentum operators written on opposite sides of position operators so that p_{initial} acts on $|p_{\text{initial}}\rangle$ and p_{final} acts on $\langle p_{\text{final}}|$.

important the contact terms from W and Z exchange are to the quark model calculation in the SM, which has additional complications of chiral couplings (which Eq. (2.57) does not accommodate) and non-trivial relativistic and non-perturbative corrections. In our model, these contact terms are indispensable for correctly predicting which baryons species is lightest, particularly when $m_W \ll m_q$.

2.6.2 Quark Mass Splittings. Invariance of the Lagrangian under $\mathrm{SU}(2)_L$ requires that the tree-level quark masses in our model must be degenerate. Spontaneous breaking of electroweak symmetry breaks that degeneracy at one loop due to self-energy corrections.

In the mass Hamiltonian, we work to leading order in the gauge couplings, so corrections to m_q in the inter-quark potential are higher-order. In the free Hamiltonian, however, the one-loop correction to m_q is at the same order in perturbation theory as the inter-quark potential. We therefore use

$$m_i = m_q - \Sigma_i^{\text{1-loop}}(m_q) + \mathcal{O}(\alpha^2)\,, \tag{2.64}$$

where $\Sigma_i^{\text{1-loop}}(m_q)$ is the one-loop self-energy of the i^{th} quark evaluated at $\not{p} = m_q$, and $\mathcal{O}(\alpha^2)$ represents corrections at higher order in the gauge couplings [73]. Then, the free Hamiltonian has the form

$$H_{\text{free}} = \sum_i \left(m_q + \frac{p_i^2}{2m_q} + \left(\frac{p_i^2}{2m_q^2} - 1 \right) \Sigma_i^{\text{1-loop}}(m_q) \right) + \mathcal{O}(\alpha^2)\,. \tag{2.65}$$

This correction can cause our predictions for baryon masses to be greater than $N_c m_q$, even when the expectation value of the inter-quark potential is negative.

The self-energy is given by

$$\Sigma_i^{\text{1-loop}}(m_q) = -\frac{m_q}{2\pi}\left[\left(\alpha_{\text{EM}}Q_i^2 + \frac{N_c^2-1}{2N_c}\alpha_\chi\right) f(0) + \alpha_W \cos^2(\theta_W) Q_i^2 \, f(m_Z/m_q)\right. \tag{2.66}$$

$$\left. + \, \alpha_W \left(\frac{N_f^2-1}{4} - Q_i^2\right) f(m_W/m_q)\right],$$

where

$$f(r) = \frac{1}{2}\left(4 + 3\ln\left(\frac{\mu^2}{m_q^2}\right) - r^4 \ln r + r^2\right. \tag{2.67}$$

$$\left. -\frac{r}{2}\sqrt{r^2-4}\left(r^2+2\right)\ln\left(\frac{r^2-2-r\sqrt{r^2-4}}{2}\right)\right), \tag{2.68}$$

with μ the renormalization scale, using Feynman gauge and the $\overline{\text{MS}}$ scheme.[6] We define the tree-level mass to equal m_q at the scale m_q and therefore evaluate the self-energy and running couplings therein at $\mu = m_q$. One should interpret the Q_i^2 factors as operators acting on spin-flavor wavefunctions. Note that in the electroweak-symmetric limit, the terms in Eq. (2.66) with Q_i^2 cancel, and the remaining $(N_f^2-1)/4$ prefactor on the electroweak contribution is the Casimir invariant C_2 defined by $J^a_{ik}J^a_{kj} = C_2\delta_{ij}$ for the N_f-dimensional representation of $\text{SU}(2)_L$. This factor is the $\text{SU}(2)_L$ analog of the $(N_c^2-1)/(2N_c)$ color factor that appears in the dark gluon contribution [74].

So far, our discussion of the mass calculation has been in the effective field theory of quarks rather than the effective field theory of hadrons. In the theory of hadrons, mass splittings derive from the same topologies of electroweak loop diagrams as in the quark theory. In the limit where W and Z cannot resolve the

[6] For the loops with massless gauge bosons, an apparent infrared divergence can be regulated by introducing a gauge boson mass and taking the limit of that mass going to zero. Despite the logarithms, $f(r)$ has a well-defined $r \to 0^+$ limit.

structure of the hadron, *i.e.* when $1/m_{W,Z}$ is much greater than the hadron's characteristic size scale, we expect the quark model calculation of hadron mass splittings to approximately match onto the mass splittings computed in the effective field theory of hadrons. As computed in Ref. [67], for vector-like fermions or scalars much heavier than $m_{W,Z}$ with zero hypercharge in some multiplet of $\mathrm{SU}(2)_L$, the mass splitting between the $Q = 1$ and $Q = 0$ components of the multiplet is

$$M_{Q=1} - M_{Q=0} \simeq \alpha_W m_W \sin(\theta_W/2) \simeq 166\,\mathrm{MeV}. \tag{2.69}$$

In the limit $m_q, \Lambda_\chi \gg m_W$, our prediction for the splitting between singly-charged and neutral hadrons in the same $\mathrm{SU}(2)_L$ multiplet approximately reproduces this result. This serves as a check on our calculation.

2.6.3 Spin-flavor Matrix Elements. The charge, spin, and ladder operators in Eq. (2.5) act on the spin-flavor wavefunctions found in Sec. 2.5.2. Here, we discuss the actions of these operators on $\mathrm{SU}(2)_L$ eigenstates in the $(N_c, N_f) = (4, 3)$ and $(2, 4)$ models. We use the following notation for these spin-flavor operators as matrices acting on baryon states:

$$\langle \mathcal{J}^0 | Q_i Q_j | \mathcal{J}^0 \rangle \equiv \begin{pmatrix} \langle \mathcal{J}_0^0 | \\ \\ \langle \mathcal{J}_2^0 | \end{pmatrix} \left(\sum_{i<j} Q_i Q_j \right) \begin{pmatrix} |\mathcal{J}_0^0\rangle & |\mathcal{J}_2^0\rangle \end{pmatrix}, \tag{2.70}$$

and so on for other operators and $\mathrm{SU}(2)_L$ eigenstates. We abbreviate $(J_+^i J_-^j + J_-^i J_+^j)/2$ as $J_\pm^i J_\mp^j$. As discussed in Sec. 2.6.2, we will need the $\sum_i Q_i^2$ operator in addition to the operators appearing in the inter-quark potential. When acting on

hadron states that are not spin-flavor eigenstates, the operators Q_iQ_j, $Q_iQ_j\boldsymbol{S}_i\cdot\boldsymbol{S}_j$, and Q_i^2 have off-diagonal matrix elements.

In the $(4,3)$ model, the required matrix elements are

$$\langle\mathcal{J}^0|Q_iQ_j|\mathcal{J}^0\rangle=\begin{pmatrix}-4/3 & \sqrt{2}/3\\ \sqrt{2}/3 & -5/3\end{pmatrix} \tag{2.71}$$

$$\langle\mathcal{J}^0|Q_iQ_j\boldsymbol{S}_i\cdot\boldsymbol{S}_j|\mathcal{J}^0\rangle=\begin{pmatrix}2/3 & -11/\sqrt{72}\\ -11/\sqrt{72} & 19/12\end{pmatrix} \tag{2.72}$$

$$\langle\mathcal{J}^0|J_\pm^iJ_\mp^j|\mathcal{J}^0\rangle=\begin{pmatrix}-8/3 & -\sqrt{2}/3\\ -\sqrt{2}/3 & 2/3\end{pmatrix} \tag{2.73}$$

$$\langle\mathcal{J}^0|J_\pm^iJ_\mp^j\boldsymbol{S}_i\cdot\boldsymbol{S}_j|\mathcal{J}^0\rangle=\begin{pmatrix}4/3 & 11/\sqrt{72}\\ 11/\sqrt{72} & 7/6\end{pmatrix} \tag{2.74}$$

$$\langle\mathcal{J}^0|Q_i^2|\mathcal{J}^0\rangle=\begin{pmatrix}8/3 & -\sqrt{8}/3\\ -\sqrt{8}/3 & 10/3\end{pmatrix} \tag{2.75}$$

$$\langle\mathcal{J}^0|\boldsymbol{S}_i\cdot\boldsymbol{S}_j|\mathcal{J}^0\rangle=\begin{pmatrix}-3/2 & 0\\ 0 & -3/2\end{pmatrix} \tag{2.76}$$

$$\langle\mathcal{J}^+|Q_iQ_j|\mathcal{J}^+\rangle=-1 \qquad \langle\mathcal{J}^+|Q_iQ_j\boldsymbol{S}_i\cdot\boldsymbol{S}_j|\mathcal{J}^+\rangle=5/4 \tag{2.77}$$

$$\langle \mathcal{J}^+|J^i_\pm J^j_\mp|\mathcal{J}^+\rangle = 0 \qquad \langle \mathcal{J}^+|J^i_\pm J^j_\mp \boldsymbol{S}_i\cdot\boldsymbol{S}_j|\mathcal{J}^+\rangle = 3/2 \tag{2.78}$$

$$\langle \mathcal{J}^+|Q_i^2|\mathcal{J}^+\rangle = 3 \qquad \langle \mathcal{J}^+|\boldsymbol{S}_i\cdot\boldsymbol{S}_j|\mathcal{J}^+\rangle = -3/2 \tag{2.79}$$

$$\langle \mathcal{J}^{++}|Q_iQ_j|\mathcal{J}^{++}\rangle = 1 \qquad \langle \mathcal{J}^{++}|Q_iQ_j\boldsymbol{S}_i\cdot\boldsymbol{S}_j|\mathcal{J}^{++}\rangle = 1/4 \tag{2.80}$$

$$\langle \mathcal{J}^{++}|J^i_\pm J^j_\mp|\mathcal{J}^{++}\rangle = -2 \qquad \langle \mathcal{J}^{++}|J^i_\pm J^j_\mp \boldsymbol{S}_i\cdot\boldsymbol{S}_j|\mathcal{J}^{++}\rangle = 5/2 \tag{2.81}$$

$$\langle \mathcal{J}^{++}|Q_i^2|\mathcal{J}^{++}\rangle = 2 \qquad \langle \mathcal{J}^{++}|\boldsymbol{S}_i\cdot\boldsymbol{S}_j|\mathcal{J}^{++}\rangle = -3/2 \tag{2.82}$$

The negatively-charged baryons have the same matrix elements as the corresponding positively-charged baryons.

One can see that these matrix elements are consistent with gauge invariance in the electroweak-symmetric phase. The charge operators encode the contribution of the third $\mathrm{SU}(2)_L$ force carrier, the W^3, and the ladder operators encode the contributions of the W^1 and W^2. When $m_{W,Z} = 0$, the off-diagonal elements in Eqs. (2.72) and (2.74) cancel between the $W^{1,2}$ and W^3 contributions, and this cancellation occurs independently for the operators with and without spin. Therefore, the neutral $\mathrm{SU}(2)_L$ eigenstates are mass eigenstates in this limit, as required. Moreover, observing the second diagonal entries for the neutral baryon matrices (corresponding to the neutral component of the baryon 5-plet) and the matrix elements for the charged baryons, the sum of the $W^{1,2}$ and W^3 contributions is identical for each 5-plet baryon. This is again true for the operators with and

without spin independently. Therefore, the baryon 5-plet is exactly mass-degenerate in the symmetric phase, as required by gauge invariance. These observations are an important check on the validity of our approach and are true regardless of the spatial expectation value computation.

In the $(2,4)$ model,

$$\langle \mathrm{J}^0|Q_iQ_j|\mathrm{J}^0\rangle = \begin{pmatrix} -5/4 & 1 \\ 1 & -5/4 \end{pmatrix} \qquad \langle \mathrm{J}^0|Q_iQ_j\boldsymbol{S}_i\cdot\boldsymbol{S}_j|\mathrm{J}^0\rangle = \begin{pmatrix} 15/16 & -3/4 \\ -3/4 & 15/16 \end{pmatrix} \tag{2.83}$$

$$\langle \mathrm{J}^0|J^i_\pm J^j_\mp|\mathrm{J}^0\rangle = \begin{pmatrix} -5/2 & -1 \\ -1 & 1/2 \end{pmatrix} \qquad \langle \mathrm{J}^0|J^i_\pm J^j_\mp\boldsymbol{S}_i\cdot\boldsymbol{S}_j|\mathrm{J}^0\rangle = \begin{pmatrix} 15/8 & 3/4 \\ 3/4 & -3/8 \end{pmatrix} \tag{2.84}$$

$$\langle \mathrm{J}^0|Q_i^2|\mathrm{J}^0\rangle = \begin{pmatrix} 5/2 & -2 \\ -2 & 5/2 \end{pmatrix} \qquad \langle \mathrm{J}^0|\boldsymbol{S}_i\cdot\boldsymbol{S}_j|\mathrm{J}^0\rangle = \begin{pmatrix} -3/4 & 0 \\ 0 & -3/4 \end{pmatrix} \tag{2.85}$$

$$\langle \mathrm{J}^+|Q_iQ_j|\mathrm{J}^+\rangle = -3/4 \qquad \langle \mathrm{J}^+|Q_iQ_j\boldsymbol{S}_i\cdot\boldsymbol{S}_j|\mathrm{J}^+\rangle = 9/16 \tag{2.86}$$

$$\langle \mathrm{J}^+|J^i_\pm J^j_\mp|\mathrm{J}^+\rangle = 0 \qquad \langle \mathrm{J}^+|J^i_\pm J^j_\mp\boldsymbol{S}_i\cdot\boldsymbol{S}_j|\mathrm{J}^+\rangle = 0 \tag{2.87}$$

$$\langle \mathrm{J}^+|Q_i^2|\mathrm{J}^+\rangle = 5/2 \qquad \langle \mathrm{J}^+|\boldsymbol{S}_i\cdot\boldsymbol{S}_j|\mathrm{J}^+\rangle = -3/4 \tag{2.88}$$

$$\langle \mathrm{J}^{++}|Q_iQ_j|\mathrm{J}^{++}\rangle = 3/4 \qquad \langle \mathrm{J}^{++}|Q_iQ_j\boldsymbol{S}_i\cdot\boldsymbol{S}_j|\mathrm{J}^{++}\rangle = -9/16 \tag{2.89}$$

$$\langle \mathrm{J}^{++}|J^i_\pm J^j_\mp|\mathrm{J}^{++}\rangle = -3/2 \qquad \langle \mathrm{J}^{++}|J^i_\pm J^j_\mp\boldsymbol{S}_i\cdot\boldsymbol{S}_j|\mathrm{J}^{++}\rangle = 9/8 \tag{2.90}$$

$$\langle \mathrm{J}^{++}|Q_i^2|\mathrm{J}^{++}\rangle = 5/2 \qquad\qquad \langle \mathrm{J}^{++}|\boldsymbol{S}_i \cdot \boldsymbol{S}_j|\mathrm{J}^{++}\rangle = -3/4 \tag{2.91}$$

The same observations of the $W^{1,2}$ and W^3 contributions as above show that these matrix elements are also consistent with gauge invariance.

The above matrix elements provide some insight into the expected hierarchy of baryon masses. In the limit $m_q \ll m_W$, the $W^\pm$ can be integrated out, and the spin-flavor eigenstates become approximate mass eigenstates. A neutral spin-flavor eigenstate can have a larger $\sum_i Q_i^2$ than a charged spin-flavor eigenstate. Then, baryon mass splittings can be dominated by quark mass splittings, and a charged baryon can be lighter than a neutral baryon.

Even when quark mass splitting do not dominate baryon mass splittings, differences in these matrix elements can cause charged states to be lighter than neutral states when $m_q \lesssim m_W$. Note for example the Q_iQ_j and $J^i_\pm J^j_\mp$ matrix elements in the (2,4) model. The $W^\pm$ contributions to the potential cancel for the singly-charged states and not for the neutral states. So when m_W is non-negligible and the electroweak inter-quark potentials are dominated by the photon, the potential is deeper for the singly-charged state than the heavier of the neutral states.

In the limit $m_q \gg m_W$, electroweak symmetry appears approximately restored in the dark sector, so the Q_i^2 contributions to the quark mass splittings nearly cancel, and the 5-plet baryons are approximately mass-degenerate. Then, in the effective field theory of baryons rather than quarks, electroweak self-energy corrections to baryons in a $(2J+1)$-plet are proportional to the Casimir factor $J(J+1)$. Baryons in the 5-plets therefore receive larger self-energy corrections, so they are generically expected to be heavier than the singlet baryons in the large m_q limit.

As noted in Sec. 2.2.2, neutral states in adjacent odd $\mathrm{SU}(2)_L$ representations (*i.e.* representations whose dimensions are odd and differ by two) are forbidden from mixing because they are eigenstates of the $\mathcal{H}$-parity transformation with opposite charges. In such cases, the lack of mixing is manifest in the mass calculation because the off-diagonal spin-flavor matrix elements that would mix these states vanish exactly.

2.6.4 Spatial Expectation Values. We use the variational method to estimate the spatial expectation values in the inter-quark potential with the template wavefunction in Eq. (2.7). We minimize baryon masses with respect to the k and k_1 parameters, thereby placing a bound on the ground state of the Hamiltonian. We are free to use any normalizable template function with appropriate boundary conditions, and the closer the ansatz is to the true solution of the Schrödinger equation, the better the estimate of the ground state. We chose a slight generalization of an exponentially-suppressed function, which is a typical qualitative form of bound state wavefunctions such as the ground state of the Hydrogen atom.

Expectation values of operators $\mathcal{O}$ acting on baryon spatial states can be computed in the standard way

$$\langle \mathcal{O} \rangle = \frac{\int \mathrm{d}^3 r_1 \cdots \mathrm{d}^3 r_{N_c} \psi^* \mathcal{O} \psi}{\int \mathrm{d}^3 r_1 \cdots \mathrm{d}^3 r_{N_c} \psi^* \psi} \,. \tag{2.92}$$

However, integrating over all positions gives a volume factor in the numerator and denominator. The integrands are translationally invariant, so it is practical to choose an origin $\mathbf{r}_0$ (analogous to fixing the proton at the origin in the Hydrogen atom) and enforcing it with a delta function.

$$\langle \mathcal{O} \rangle = \frac{\int \mathrm{d}^3 r_1 \cdots \mathrm{d}^3 r_{N_c} \psi^* \mathcal{O} \psi \; \delta^{(3)}(\mathbf{r}_0)}{\int \mathrm{d}^3 r_1 \cdots \mathrm{d}^3 r_{N_c} \psi^* \psi \; \delta^{(3)}(\mathbf{r}_0)} \,. \tag{2.93}$$

The choice of origin is arbitrary, but it is convenient to choose $\boldsymbol{r}_0 = \boldsymbol{r}_{N_c}$. The required expectation values include those listed in Eq. (2.6), as well as the $\langle p_i^2 \rangle$ factor in the free Hamiltonian.

The spatial integrals in Eq. (2.93) become increasingly challenging as N_c becomes large. For the two-body wavefunction (relevant for $N_c = 2$ baryons and all mesons), we analytically find

$$a_0 = \frac{8(4k^2 + 12k_1^2 + 6k_1 m_V + m_V^2 + 12kk_1 + 4km_V)}{(k^2 + 3kk_1 + 3k_1^2)(m_V/k + 2)^5} \tag{2.94}$$

$$a_1 = \frac{4k(4k^2 + 6k_1^2 + 4k_1 m_V + m_V^2 + 8kk_1 + 4km_V)}{(k^2 + 3kk_1 + 3k_1^2)(m_V/k + 2)^4} \tag{2.95}$$

$$a_2 = \frac{4k^2(4k^2 + 2k_1^2 + 2k_1 m_V + m_V^2 + 4kk_1 + 4km_V)}{(k^2 + 3kk_1 + 3k_1^2)(m_V/k + 2)^3} \tag{2.96}$$

$$b = \frac{4k(12k^4 + 20k^3 m_V - 6kk_1 m_V^2 + 2km_V^3 - 2k_1^2 m_V^2 - 2k_1 m_V^3)}{(k^2 + 3kk_1 + 3k_1^2)(m_V/k + 2)^4} \tag{2.97}$$

$$+ \frac{4k(2k^2 k_1^2 - 4k^2 k_1 m_V + 11k^2 m_V^2)}{(k^2 + 3kk_1 + 3k_1^2)(m_V/k + 2)^4} \tag{2.98}$$

$$c_1 = -\frac{16(4k^3 + 8k^2 k_1 + 4k^2 m_V - 3k_1^2 m_V - k_1 m_V^2 + 6kk_1^2 + 2kk_1 m_V + km_V^2)}{(k^2 + 3kk_1 + 3k_1^2)(m_V/k + 2)^5} \tag{2.99}$$

$$c_2 = -\frac{8k(4k^3 + 4k^2 k_1 + 4k^2 m_V - 2k_1^2 m_V - k_1 m_V^2 + 2kk_1^2 + km_V^2)}{(k^2 + 3kk_1 + 3k_1^2)(m_V/k + 2)^4} \tag{2.100}$$

$$d_2 = -\frac{8k(4k^3 - 2kk_1 m_V + km_V^2 + 4k^2 k_1 + 4k^2 m_V - 6k_1^2 m_V - 2k_1 m_V^2)}{(k^2 + 3kk_1 + 3k_1^2)(m_V/k + 2)^5} \tag{2.101}$$

$$d_3 = -\frac{4k^2(4k^3 + 4k^2 m_V - 4k_1^2 m_V - 2k_1 m_V^2 - 2kk_1^2 - 4kk_1 m_V + km_V^2)}{(k^2 + 3kk_1 + 3k_1^2)(m_V/k + 2)^4} \tag{2.102}$$

$$\delta = \frac{k^5}{\pi(k^2 + 3kk_1 + 3k_1^2)} \tag{2.103}$$

$$\langle p_i^2 \rangle = \frac{k^2(k^2 + kk_1 + k_1^2)}{k^2 + 3kk_1 + 3k_1^2} \,. \tag{2.104}$$

Note that the denominators above contain identical normalization factors, and integrals whose integrands are quadratic in ψ must be quadratic in k_1. For greater than two bodies, we resort to numerical computation. For the expectation values that do not depend on m_V, the dimensionful scale k can be factored out of the integrand, and one can perform a scale-free numerical integral for the terms constant, linear, and quadratic in k_1.

For the expectation values that do depend on m_V, factoring out k from the integrand leaves a dependence on the ratio m_V/k. With some insight from the integrals we can perform analytically, we can make an ansatz for how the integrals depend on m_V/k. Each matrix element we have computed analytically (some of which are feasible with three bodies) organizes itself into a sum of Laurent series in m_V/k with particular pole structures. The poles are at $m_V/k = -2$ for two bodies and $m_V/k = -4$ for three bodies. While unphysical, this analytic structure at negative values of m_V/k helps us predict forms of the integrals for baryons with larger N_c. To understand why these poles appear, consider the integrand for computing a_0 with $k_1 = 0$ for three bodies

$$a_0 = \left\langle e^{-m_V|\boldsymbol{r}_1-\boldsymbol{r}_3|} \right\rangle \propto \int \mathrm{d}^3r_1\mathrm{d}^3r_2\mathrm{d}^3r_3 \; e^{-m_V|\boldsymbol{r}_1-\boldsymbol{r}_3|}|\psi|^2\delta^{(3)}(\boldsymbol{r}_3) \tag{2.105}$$

$$\propto \int \mathrm{d}^3u_1\mathrm{d}^3u_2 \; e^{-(m_V/k)u_1-2(|\boldsymbol{u}_1-\boldsymbol{u}_2|+u_1+u_2)}\,, \tag{2.106}$$

where $\boldsymbol{u}_i = k\boldsymbol{r}_i$ is a dimensionless spatial variable. This integral is singular when the argument of the exponent has non-negative real part. If one evaluates the $\boldsymbol{u}_1$ integral while holding $\boldsymbol{u}_2$ fixed, the m_V-independent part of the exponent scales like $-4u_1$, and there is a singularity in the limit $m_V/k \to -4$. This argument provides some intuition as to why the poles in the analytical solutions appear at specific

values of m_V/k. Moreover, we can extend this intuition to N_c bodies, for which the m_V-independent part of the exponent scales like $-2(N_c-1)u_1$ holding the other variables constant, so we expect a pole in the above expectation values at $m_V/k = -2(N_c-1)$.

For $N_c > 3$, the integrals may acquire additional poles at negative values of m_V/k that are further from zero than $-2(N_c-1)$. This is because there are more complicated integration trajectories that give rise to a singularity. For $N_c = 4$, consider

$$a_0 \propto \int \mathrm{d}^3u_1 \mathrm{d}^3u_2 \mathrm{d}^3u_3 \; e^{-(m_V/k)u_1 - 2(|\boldsymbol{u}_1-\boldsymbol{u}_2|+|\boldsymbol{u}_1-\boldsymbol{u}_3|+|\boldsymbol{u}_2-\boldsymbol{u}_3|+u_1+u_2+u_3)} \tag{2.107}$$

when $k_1 = 0$. Holding $\boldsymbol{u}_3$ fixed and integrating along the trajectory with $\boldsymbol{u}_2 = \boldsymbol{u}_1$, the m_V-independent part of the exponent scales like $-8u_1$, which suggests a pole at $m_V/k = -8$ in addition to the pole at $m_V/k = -6$ identified above. By contrast, for the $N_c = 3$ case, integrating along the trajectory $\boldsymbol{u}_2 = \boldsymbol{u}_1$ suggests a pole at $m_V/k = -4$ (identical to the pole found above), so there is no reason to expect more than one pole in the three-body integrals. Likewise, integrating along the $\boldsymbol{u}_3 = \boldsymbol{u}_2 = \boldsymbol{u}_1$ trajectory in the four-body integral suggests the same pole at $m_V/k = -6$ as identified above. When $N_c > 4$, even more poles may appear, but these become more negative and therefore have more suppressed contributions for physically relevant values of m_V/k as N_c increases.

In our analysis with $N_c = 4$, we estimate the m_V-dependence of the spatial expectation values by numerically integrating with many values of m_V and performing fits to sums of Laurent series with strictly negative powers centered at each of the two expected poles

$$\langle \mathcal{O} \rangle = \sum_{n=n_{\min}}^{n_{\max}} \sum_{x \in \text{poles}} \frac{f_{n,x}}{(m_V/k - x)^n} \,, \tag{2.108}$$

where $f_{n,x}$ are fit coefficients. We do this for terms constant, linear, and quadratic in k_1 independently. To decide which terms to include in the Laurent series (set by $n_{\min}$ and $n_{\max}$ in Eq. (2.108)), we again take inspiration from the two- and three-body analytical integrals. In particular, we conjecture that in the large-m_V limit, where the series in Eq. (2.108) is dominated by terms with $n = n_{\min}$, any particular spatial matrix element decreases in magnitude with respect to m_V equally quickly for all values of N_c. For example, $a_0 \sim 1/m_V^3$ for large m_V when $N_c \in \{2, 3\}$, so we assume this is true for all N_c. This conjecture fixes $n_{\min}$ and is sensible because if the decrease in m_V were slower, the contribution of the term to the potential in Eq. (2.5) may *increase* with m_V, which is clearly unphysical. To fix $n_{\max}$, we observe that when N_c increases by one, there is an additional radial integral in the expectation value computation, which contributes an additional factor of r_i^2. These two powers of r_i lead to two additional powers of m_V in the denominator, so we conjecture

$$n_{\max} = 2(N_c - 2) + n_{\max}^{N_c=2} \,, \tag{2.109}$$

where $n_{\max}^{N_c=2}$ is the two-body value of $n_{\max}$. We find good numerical agreement with this approach.

We can check for self-consistency in our estimates of these integrals by noting that some of the spatial expectation values are inter-related by derivatives:

$$a_0 = -\frac{\partial\, a_1}{\partial\, m_V} \qquad\qquad a_1 = -\frac{\partial\, a_2}{\partial\, m_V} \tag{2.110}$$

$$c_1 = -\frac{\partial\, c_2}{\partial\, m_V} \qquad\qquad d_2 = -\frac{\partial\, d_3}{\partial\, m_V}\,. \tag{2.111}$$

We found that our estimates of a_n and c_n agreed well with these relations. For d_3 with $N_c = 4$, we encountered difficulties in the convergence of the numerical integrals, so we found our estimate of d_3 by anti-differentiating our estimate of d_2. Note that these derivatives are consistent with our conjectures for $n_{\rm min}$ and $n_{\rm max}$.

We can now express the hadron mass operator as a matrix acting on the space of hadron $\mathrm{SU}(2)_L$ eigenstates that depends on k and k_1. For the variational method, we estimate the ground state by minimizing the mass with respect to k and k_1. One remaining question is the renormalization scale μ at which to evaluate the running couplings that appear in the inter-quark potential. To answer this question, we identify the characteristic hadron length scale (the "Bohr radius") as $1/k$, as this sets the exponential decay rate of the spatial wavefunction in Eq. (2.7). We therefore identify the hadron's characteristic energy scale as k and evaluate the running couplings at $\mu = k$. We use the one-loop renormalization group evolution of α_χ in the effective field theory with the dark quarks integrated out [75]

$$\alpha_\chi(\mu) = \frac{6\pi}{11 N_c \ln(\mu/\Lambda_\chi)}\,. \tag{2.112}$$

We also run α_W and $\alpha_{\rm EM}$ at one loop in the effective field theory without the Higgs or top quark when $\mu < m_Z$ and with the full SM when $\mu > m_Z$ (neglecting threshold effects) [69]. The running of α_W and $\alpha_{\rm EM}$ has a very small impact.

If one tries to minimize the mass with respect to k while using $\mu = k$ in the running couplings, Eq. (2.112) shows that one encounters unphysical large logarithms that disrupt the minimization procedure. We therefore implement an

iterative minimization approach. We start with an initial hypothesis for the inverse Bohr radius of $k \simeq \alpha_\chi(k)\, m_q$, which is solved by

$$k \simeq \frac{6\pi\, m_q}{11 N_c\, \mathcal{W}\!\left(\frac{6\pi\, m_q}{11 N_c \Lambda_\chi}\right)}, \tag{2.113}$$

where $\mathcal{W}$ is the principal branch of the Lambert W function (also known as the product logarithm) [76]. We evaluate the couplings in the inter-quark potential with μ equal to this hypothesized k, minimize with respect to the k and k_1 that appear in the spatial expectation values, use the value of k corresponding to that minimum as the new hypothesis for μ, then repeat the minimization in this way until the minimized mass converges. This procedure ensures the couplings are evaluated at the inverse Bohr radius while avoiding large logarithms in their renormalization group evolution.

Performing the minimization procedure described in above is straightforward for hadron states that are not mixed by the mass operator (*e.g.* the charged states in the $(2, 4)$ and $(4, 3)$ models). These are simultaneous $\mathrm{SU}(2)_L$ and mass eigenstates, and each will have its own optimal k and k_1. However, there is an ambiguity in the minimization calculation when the mass operator has off-diagonal elements. Consider the 2×2 mass matrix in the basis of the neutral $\mathrm{SU}(2)_L$ eigenstates in the $(2, 4)$ or $(4, 3)$ model. Each matrix element is a function of k and k_1, as is each mass eigenvalue and the mixing angle between the $\mathrm{SU}(2)_L$ eigenstates. If we simply minimized each mass eigenvalue with respect to its own k and k_1 individually, each value of the optimization parameters corresponds to a distinct set of eigenvectors. If the mass eigenstates are evaluated with different values of k and k_1, those states are not orthogonal. In other words, the mixing angle is ill-defined if there are different values of k and k_1 used for the two mass eigenvalues.

We resolve this ambiguity by performing the minimization in multiple ways. We start by minimizing the lesser mass eigenvalue and using the optimal k and k_1 values to find the greater mass eigenvalue and mass eigenstates. We then do the reverse, minimizing the greater eigenvalue and using the corresponding optimization parameters to evaluate the lesser eigenvalue and eigenstates. The differences between the masses and mixing angles computed using each method represents uncertainties in the calculation. This uncertainty in the DM mass is around 0.1% for the $(2, 4)$ model and 0.001% for the $(4, 3)$ model. The resulting uncertainty in $|\langle m_{\rm DM}|\text{5-plet}\rangle|^2$ is $\mathcal{O}(10\%)$, which shifts the steep drop-off shown in Fig. 1 by less than half an order-of-magnitude in m_q.

2.7 Phenomenology

In this section, we discuss the phenomenology of our Noble Dark Matter in different contexts. In particular, we highlight their elusiveness in direct detection experiments, while also commenting on possible collider and astrophysical signatures.

2.7.1 Direct Detection. As first described in Ref. [12], $\mathcal{H}$-parity forbids leading electromagnetic moments of neutral hadrons in our model for all $N_{c,f}$ values, and thus significantly reduces the cross section of $\mathcal{H}$-parity-symmetric DM with the SM. Therefore, as with WIMPs, electroweak loop-induced interactions become the dominant source of direct detection signal [13–21]. The strength of these interactions strongly depends on the lightest baryon's representation under $\mathrm{SU}(2)_L$, giving rise to different phenomenology in each of the four categories defined in Sec. 2.2.2. Below, we discuss the direct detection signal of each category.

I. DM is a pure $\mathrm{SU}(2)_L$ singlet,[7] so it does not have renormalizable interactions with electroweak gauge bosons. This is nearly a direct detection nightmare scenario.[8]

II. DM can be a mixture of the singlet and other neutral states, as shown in Fig. 1 for $(N_c, N_f) = (2, 4)$ and $(4, 3)$. Electroweak loop-induced signals are suppressed by this mixing, as explored below.

III. DM can be a mixture of neutral states in different non-trivial $\mathrm{SU}(2)_L$ multiplets, and their interfering electroweak loop-induced interactions would need to be calculated carefully. In the special case where there is only one multiplet, or if the mixing of the lightest state with neutral states in other multiplets is forbidden by $\mathcal{H}$-parity,[9] then DM has well-defined non-trivial interactions with the W (similar to the standard WIMP).

IV. When there are no neutral baryons, there is no viable single-baryon DM candidate. We do not discuss this category further in this work.

To constrain categories II and III with direct detection experiments, one should first identify the lightest mass eigenstate, verify it is neutral, and compute its composition of states in each $\mathrm{SU}(2)_L$ representation. In the heavy quark limit, this can be carried out with the variational method we proposed in Sec. 2.3.

[7] For the specific case of $N_{c,f} = 2$, it is shown that bound states of dark baryons can be stable and constitute a fraction of DM [51, 77].

[8] The leading direct detection signal becomes polarizability, to which foreseeable experiments are insensitive for DM masses $> \mathcal{O}(100)\,\mathrm{GeV}$ [12].

[9] An example of this case is $(N_c, N_f) = (3, 3)$ (studied in Ref. [12]). The lowest-spin baryon spectrum contains only a 3-plet and 5-plet (adjacent odd representations), so $\mathcal{H}$-parity forbids the mixing of the neutral components.

In Fig. 2, we illustrate the effect of mixings in category II by estimating the direct detection cross sections for benchmark models $(N_c, N_f) = (2, 4)$ and $(4, 3)$, with $\Lambda_\chi/m_q = 10^{-2}$ and 10^{-6}. We use cross sections computed in Ref. [20] for a pure 5-plet WIMP, scaling the pure 5-plet cross sections by the overlap of the $|5\text{-plet}\rangle$ state with the lightest mass eigenstate $|m_{\rm DM}\rangle$. The uncertainty bands in Fig. 2 are inherited from uncertainties in the calculation of Ref. [20] due to *e.g.* non-perturbative nuclear matrix elements. At sufficiently small masses, the DM candidate may be excluded by existing [78] or projected [79] constraints, or by future experiments probing down to the neutrino fog. As expected from Fig. 1, for sufficiently high DM masses (*i.e.* where $\mathrm{SU}(2)_L$ appears unbroken) the cross section drops rapidly as the mixing between the DM and the 5-plet states approaches zero. For the parameters shown in the figure, the cross sections are suppressed below the neutrino fog for $m_{\rm DM} \gtrsim \mathcal{O}(0.1 - 1)\,\mathrm{TeV}$, requiring new techniques for probing heavier DM masses in future direct detection experiments, see *e.g.* Refs. [80, 81].[10]

The effect of uncertainties in the cross section is most evident in the $(4, 3)$ model with $\Lambda_\chi/m_q = 10^{-6}$. In this case, Fig. 2 suggests the reach of future experiments that can probe down to the neutrino fog can vary from below 300 GeV to $\sim$ 5 TeV, depending on the uncertainties. This large range of possibilities warrants a more precise calculation of the cross sections applicable to a wider range of DM masses in future work.

As noted in Ref. [12], the dimension-7 polarizability operators of our dark baryons are not forbidden by $\mathcal{H}$-parity and can give rise to scattering in direct detection experiments, even when DM is a singlet of $\mathrm{SU}(2)_L$. The cross section from these operators suffers from large uncertainties [86, 87] and is at

[10] In these benchmark models, we also find that the mass splittings of our lightest baryons are far above the $\sim 100\,\mathrm{keV}$ threshold required for inelastic direct detection signals [82, 43, 44, 83–85].

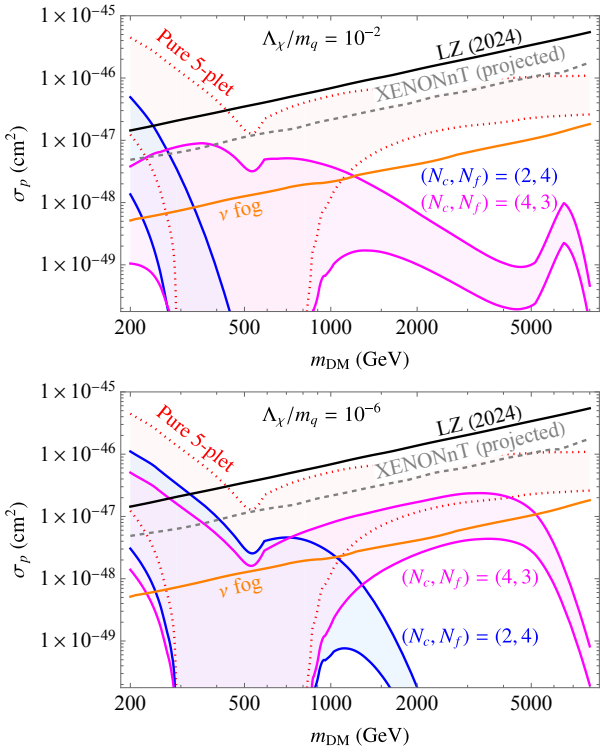


Figure 2. Rough estimates of direct detection cross sections of the lightest dark baryon for $(N_c, N_f) = (2, 4)$ and $(4, 3)$ with $\Lambda_\chi/m_q = 10^{-2}$ (**top**) and 10^{-6} (**bottom**). We scaled the $\mathrm{SU}(2)_L$ 5-plet cross sections (red dotted line) computed in Ref. [20] using a similar 5-plet WIMP model by $|\langle m_{\rm DM}|\text{5-plet}\rangle|^4$ for each $N_{c,f}$. The suppression of cross sections below the neutrino fog limits the reach of future experiments.

best detectable in the current experiments for DM masses below a few hundred GeV. Future searches will not improve current bounds owing to the rapid drop in the cross section as a function of DM mass ($\sigma \propto 1/m_{\rm DM}^6$). We have also checked numerically that in the large DM mass limit, the electroweak loop-induced interactions scale as $\sigma \propto 1/m_{\rm DM}^4$. Therefore, the polarizability interaction is subdominant despite the small mixing.

We expect in general that other DM candidates in category II will be mostly comprised of singlet states with similarly small mixings of states in

larger representations as in the two examples above. Therefore, we call the DM candidates in categories I and II Noble Dark Matter.

2.7.2 Indirect Detection and Astrophysical Searches. As for indirect detection, note that in the heavy quark limit, for the DM masses shown in Fig. 2, the symmetric dark baryon abundance is completely depleted during a 1^{st} order confinement phase transition by the squeezeout mechanism [88–90]. Thus, when the phase transition is of the 1^{st} order, which is anticipated to occur for $N_c > 2$ and $\Lambda_\chi/m_q \lesssim 10^{-2}$ [91–97], we would need to augment the model to generate an asymmetric DM abundance today.

Even in the asymmetric limit, DM can accumulate in the center of stars. This can occur if the DM has a large enough interaction with SM such that it can lose its kinetic energy and slow down to below the escape velocity of the object. This accumulation can result in an implosion of the star via formation of a dense core that eventually collapses into a black hole [98–111]. There remains some debate in the literature as to the applicability of these bounds in certain DM ranges or self-interaction rates [112–115], thus a detailed study of this signal in our model remains an interesting future direction.

It is also argued that in models where there is more than one stable dark particle (whether baryons or nuclei), dark nucleosynthesis processes can give rise to detectable indirect detection signals, even in the asymmetric DM limit [51]. While lattice studies have established the existence of stable nuclei for the case of $N_{c,f} = 2$ [77], further studies on other combinations of N_f and N_c would be needed to determine the relevance of dark nucleosynthesis in these theories. Such dark nucleosynthesis processes are enhanced if the DM interacts enough with SM to be captured in the core of different celestial bodies.

In the case where a symmetric abundance could arise, such as by going to larger values of Λ_χ/m_q or for $N_c = 2$ where the phase transition is of 2$^{\text{nd}}$ order, other indirect detection signals can exist for the model as well. For models in category II, there can be direct annihilation of dark baryons to the SM, but the rate is suppressed by the mixing with non-singlet representations as in direct detection. The leading indirect detection signal arises from dark baryons annihilating to dark sector glueballs and/or rearranging into mesons. These daughter hadrons may further decay to the SM. In particular, as many of these mesons can be long-lived [5], this annihilation signal may be detectable in celestial-body focused searches [116]. A thorough study of all these indirect detection signals, in either the symmetric or asymmetric abundance limit, is left for future work.

2.7.3 Collider Searches. Sufficiently high-energy collisions could produce mesons, baryons, or glueballs of the dark sector. Glueballs are the lightest hadrons when $\Lambda_\chi \ll m_q$, but they could only be produced (at one loop) via highly-suppressed dimension-8 operators unless we introduced an additional portal [25, 27]. If $\Lambda_\chi \lesssim$ few GeV, the Z boson can decay to dark glueballs through a quark loop to three dark gluons. Future colliders may be able to probe this contribution to the invisible width of the Z. See Refs. [117–119] for invisible Z decay studies at future colliders.

If kinematically accessible, dark mesons and baryons can be produced in colliders via electroweak processes. For example, charged hadrons can be pair-produced, and neutral vector hadrons can mix with the SM photon or Z before decaying [4, 10]. Mesons (being lighter than baryons for $N_c > 2$) would dominate signals, potentially including *e.g.* missing energy plus initial state radiation [120],

heavy stable charged particles, displaced vertices, disappearing tracks [121–125], semi-visible jets [31, 126], emerging jets [30], tumblers [127], and quirks [24]. For the relevant mass ranges in Fig. 2, the center-of-mass energy of hard scattering processes in foreseeable colliders would be insufficient to produce the large dark hadron multiplicities required for soft bombs (SUEPs) [33, 39]. See Refs. [128–130] for reviews.

These signals depend on the lifetimes of mesons, which can span a large range due to an accidental symmetry [5]. If these signals can be tagged efficiently, and if the energy of hard interactions that produce dark quarks and gluons is large enough relative to the dark hadron masses such that a parton shower and jet formation take place within the dark sector, then energy-energy correlators could be used to probe the dark confining phase transition [131–133]. We leave a comprehensive study of all these collider signals for future work.

2.8 Discussion

We studied a sector with dark quarks transforming under a confining $\mathrm{SU}(N_c)$ as well as an N_f-plet of $\mathrm{SU}(2)_L$. We described a systematic way to determine dark baryon $\mathrm{SU}(2)_L$ representations using Eq. (2.2) and showed that for various N_c,N_f combinations, there are one or more $\mathrm{SU}(2)_L$ singlets in the lowest-spin baryon spectrum, see Table 1. Using the non-relativistic quark model, we develop a variational method for calculating the baryon mass spectrum in the heavy quark limit, including the electroweak contributions in the inter-quark potential.

We found that the lightest baryons in these models are neutral and mostly overlap with the singlet states. For $m_q \gtrsim \mathcal{O}(1)$ TeV, the mixing of the DM candidate with the non-singlet state is significantly suppressed, as illustrated

in Fig. 1. Thus, while the dark sector is in thermal contact with the SM in the early universe, the DM candidate in the hadronic phase has strongly suppressed interactions with SM today.

Our Noble Dark Matter candidates are highly elusive in direct detection searches because their leading electromagnetic moments are forbidden by $\mathcal{H}$-parity [12], and electroweak loop-induced signals are suppressed when the DM candidates are (approximate) $\mathrm{SU}(2)_L$ singlets. It is remarkable that symmetries of the simple UV theory considered in this paper lead to a low energy effective theory of dark matter with such highly suppressed interactions.

We focused on the $(N_c, N_f) = (2, 4)$ and $(4, 3)$ baryon spectra because they have two neutral states (which are permitted to mix by $\mathcal{H}$-parity), one of which is a singlet. The lowest-spin spectra of other $N_{c,f}$ combinations can contain only a singlet (category I from Table 1), a singlet with more complicated mixing (category II), or no singlet with a nonetheless viable DM candidate (category III). Each of these possibilities warrants further investigation, and we have presented methods to estimate the mass spectra and mixings of states in different $\mathrm{SU}(2)_L$ representations in the heavy quark limit. In the $m_q < \Lambda_\chi$ regime, the calculation is complicated by relativistic and non-perturbative corrections, but we expect our qualitative conclusions based on perturbative electroweak effects to hold true. In particular, states in each $\mathrm{SU}(2)_L$ representation become approximate mass eigenstates for $m_q \gg m_W$, states in larger representations of $\mathrm{SU}(2)_L$ tend to be heavier, and charged states tend to be heavier than neutral states.

There are various generalizations of the model in Eq. (2.1) that could alter the phenomenology. Adding additional quark generations, scalar quarks, or quarks in different $\mathrm{SU}(N_c)$ representations would complicate the hadron spectrum while

preserving $\mathcal{H}$-parity. One could also add additional portals (such as a Higgs portal) to facilitate production and decay of dark hadrons, including glueballs.

It is interesting to compare and contrast our model to theories with elementary WIMPs. It is well known that DM composed of the neutral component of a single non-trivial $\mathrm{SU}(2)_L$ multiplet (such as Wino) has a large indirect detection signal [134–137] and is widely considered to be ruled out. In our composite realization, electroweak multiplets can naturally mix with singlet states. This implies that considering only individual electroweak multiplets in isolation may prematurely dismiss WIMP-like dark matter. Combinations of multiple WIMPs could have been considered in the context of an EFT of elementary states, but the mass hierarchy and mixings would be free parameters. We have seen that the IR description of a composite realization of electroweak multiplets provides the mass spectrum and the mixings as calculable outcomes of a simple UV theory. Therefore, there is a much larger theory space of WIMP-like dark matter with multiple states and associated mixings.

There are of course distinctions between elementary WIMPs and the composite WIMP-like states that we encounter in Noble Dark Matter. For instance, in addition to the baryon states, there is also a set of meson states that are expected to be lighter than the baryons. The meson states are anticipated to have important implications for indirect detection (annihilation of dark baryons to dark mesons) as well as collider signals. We reserve a more thorough analysis of the rich phenomenology for future work.

CHAPTER III

STOPPING DARK MESONS IN THEIR TRACKS WITH LONG-LIVED PARTICLE AND RESONANT SIGNATURES

This chapter includes previously published co-authored material from Ref. [2] with P. Asadi, E. Bernreuther, M. Costa, S. Homiller, and G.D. Kribs. A.B. performed the calculations. All authors contributed to the development of ideas, interpretation of results, and writing of the paper.

3.1 Bridge

While new physics is required to explain dark matter, the Standard Model (SM) has maintained remarkable consistency with various kinds of experiments over many years. Many searches for new physics have focused on minimal extensions of the SM and have placed stringent bounds on them. This motivates exploring directions beyond the most minimal models. At the same time, simple models with concrete predictions serve as useful benchmarks to target in experimental searches. Confining dark sectors can simultaneously provide this non-minimality and simplicity. In such models, the SM is extended by a non-abelian gauge interaction with dark quarks in the ultraviolet (UV) that bind into dark hadrons in the infrared (IR). The UV theory may contain only a few degrees of freedom while the IR theory consists of a rich spectrum of states with a variety of possible interactions with the SM.

New confining sectors have motivated numerous dedicated searches at the Large Hadron Collider (LHC) [138–147], as well as reinterpretations of other searches [148, 10, 50, 149, 150]. Depending on the dark quark masses, confinement scale, number of flavors, number of colors, and the portal to the SM, these models can give rise to various intriguing signatures. Examples include

long-lived particles [4, 151, 28, 30, 121, 152–154, 41], novel shower patterns [22, 23, 31, 47, 33, 126, 8, 155, 156, 37–39, 157, 158], and exotic phenomena such as quirks [24, 34, 35]. See Refs. [128] and [159] for reviews. Of particular importance to this work is the variety of potential dark hadron production mechanisms. New particles with electroweak interactions can of course be pair-produced at sufficiently high energies via Drell-Yan (DY) and vector boson fusion (VBF), but other possibilities including vector mesons mixing with gauge bosons [4, 10] and single production of pion-like states through chiral anomalies [47] exist as well. As we will show, correlations between the rates of these processes can even shed light on details of the UV theory.

We study collider signals of models with a confining dark sector that include vector-like dark quarks in the N_f-dimensional representation of SM $\mathrm{SU}(2)_L$, in addition to being charged under the new $\mathrm{SU}(N_c)$. See Refs. [4–8, 148, 9–11] for similar models. It was recently discovered [12] that this model has a natural $\mathbb{Z}_2$ symmetry, known as $\mathcal{H}$-parity, that forbids the leading electromagnetic moments of the neutral dark hadrons. This observation on its own significantly relaxes naïvely stringent direct detection constraints on the dark baryons as dark matter candidates. It was additionally pointed out in Chapter II that the lightest dark baryons are pure or approximate SM singlets for many combinations of N_c and N_f, which even further suppresses direct detection signals of these so-called Noble Dark Matter candidates. The counter-intuitive implication is that while the dark quarks are electrically charged, the dark sector may be more readily discovered at colliders than other types of experiment. This is the possibility we investigate in this paper. Even beyond the underlying dark matter motivations, we will explore

various interesting features of collider phenomenology that arise in the presence of heavy dark hadrons whose constituents are in an arbitrary $\mathrm{SU}(2)_L$ representation.

We consider the regime where the mass of the dark quarks is significantly *below* the dark sector confinement scale. This allows us to exploit our knowledge of SM quantum chromodynamics (QCD) and work in an effective field theory (EFT) of dark mesons. We focus on the limit where the pseudo-Nambu–Goldstone bosons (pNGBs) of chiral symmetry breaking in the dark sector are the only dark hadrons that are kinematically accessible in experiments at the LHC.

We analyze two under-explored signals of these confining dark sectors. The first is disappearing tracks from long-lived dark mesons, and the second is resonant diboson production from singly produced dark meson decays. These signatures allow us to reinterpret existing LHC searches to constrain our model parameters. Moreover, the model is an excellent benchmark for future searches targeting the same final states.

For all $N_f \geq 2$, there is an $\mathrm{SU}(2)_L$ 3-plet of pNGBs denoted by $\hat{\pi}_3$. For dark hadron mass scales within the regime we consider (*i.e.* above the scale of electroweak symmetry breaking), there is a $\sim 170\,\mathrm{MeV}$ mass splitting between the charged and neutral components of the $\hat{\pi}_3$ [67]. These mesons are forbidden from decaying directly to the SM by a $\mathbb{Z}_2$ known as G-parity (which is related to $\mathcal{H}$-parity and an analogous $\mathbb{Z}_2$ in the SM, as explained in Sec. 3.2.2) [5]. The dark G-parity has such importance that we denote G-odd pNGBs by $\hat{\pi}$ and G-even pNGBs by $\hat{\eta}$, loosely following an analogy to SM mesons. The charged components of the $\hat{\pi}_3$ (denoted $\hat{\pi}_3^\pm$) decay to the neutral component $\hat{\pi}_3^0$ by emitting an SM pion, and the small phase space for this process causes the $\hat{\pi}_3^\pm$ to be long-lived. The $\hat{\pi}_3^\pm$ are therefore targets for long-lived particle (LLP) searches with signals very similar to

those of charginos [160, 161]. When the charged meson decays inside a detector's inner tracker and the soft pion is not reconstructed, this leaves a signature known as a disappearing track. In Sec. 3.6.1, we use disappearing track searches to derive a lower bound on this meson's mass.

We also study the single production of specific meson species. If $N_f \geq 3$, there is an $\mathrm{SU}(2)_L$ 5-plet of pNGBs (denoted by $\hat{\eta}_5$) in the spectrum that is *unique* in that it is the only representation of dark mesons that has an anomaly with $\mathrm{SU}(2)_L$. As explained in Sec. 3.3, this is analogous to the SM neutral pion's anomaly with quantum electrodynamics (QED). This anomaly allows the $\hat{\eta}_5$ to be resonantly produced via VBF before decaying to a pair of electroweak bosons. The rate for this process depends on N_f and f_π/N_c, where f_π is the dark pion decay constant. Thus, measuring these anomaly-induced collider signals would reveal details of the UV model. Similar examples of bound state resonances have been considered in Refs. [162–165]. We use searches for scalar resonances decaying to diboson final states to place constraints on f_π/N_c in Sec. 3.6.2.

3.2 The Model

We study dark mesons arising from a new strongly-coupled confining gauge sector with the Lagrangian

$$\mathcal{L}_{\text{dark}} = -\frac{1}{4} G^{\mu\nu\,a} G^a_{\mu\nu} + \overline{\mathbf{Q}} \left(i \not{D} - m_0 \right) \mathbf{Q} \,, \tag{3.1}$$

where $G^a_{\mu\nu}$ is the field strength of the dark $\mathrm{SU}(N_c)$, and $\mathbf{Q}$ is a vector-like dark quark with mass m_0 that transforms as a fundamental of $\mathrm{SU}(N_c)$ and an N_f-plet of $\mathrm{SU}(2)_L$ with $N_f \geq 2$. Since the quarks transform in the N_f-dimensional representation of $\mathrm{SU}(2)_L$, one can think of $\mathrm{SU}(2)_L$ as a gauged subgroup of an $\mathrm{SU}(N_f)$ flavor symmetry. Gauge invariance requires the flavor multiplet to have

degenerate mass at tree level. The quarks have vanishing hypercharge, so each dark sector particle has an electric charge equal to its weak isospin. At low energies, these quarks bind into dark mesons and baryons.

As pointed out in Ref. [12], this model has a $\mathbb{Z}_2$ symmetry known as $\mathcal{H}$-parity, under which the fields transform as

$$\mathbf{Q} \xrightarrow{\mathcal{H}} e^{i\pi J_y}\mathbf{Q}, \qquad W_\mu^i \xrightarrow{\mathcal{H}} \mathcal{C}W_\mu^i\mathcal{C}, \qquad B_\mu \xrightarrow{\mathcal{H}} \mathcal{C}B_\mu\mathcal{C}, \tag{3.2}$$

where J_y is the second generator of $\mathrm{SU}(2)_L$, W_μ^i is the mediator of $\mathrm{SU}(2)_L$, B_μ is the mediator of $\mathrm{U}(1)_Y$, and $\mathcal{C}$ denotes charge conjugation. The neutral dark quarks and hadrons in odd representations of $\mathrm{SU}(2)_L$ are eigenstates of $\mathcal{H}$ with eigenvalue ± 1, whereas $\mathcal{H}$ maps charged states to opposite-charge states (up to a sign). $\mathcal{H}$-parity has great importance for the dark matter phenomenology of the dark baryons, as explored in Ref. [12] and Chapter II.

While mesons also transform under $\mathcal{H}$-parity, there is a slightly different $\mathbb{Z}_2$ known as G-parity [5] that has direct implications for meson phenomenology. As we explain in Sec. 3.2.2, G-parity selection rules imply large hierarchies between the meson lifetimes.

3.2.1 Mesons in the Chiral Effective Theory. This work focuses on the light quark limit, where the dark quark mass is significantly smaller than the dark sector confinement scale. In this limit, we can use an effective theory of dark mesons — the chiral Lagrangian — and trade the UV parameters of the quark mass and confinement scale for the IR parameters of the lightest dark meson mass m_π and the dark pion decay constant f_π.

Since our regime is similar to that of the light mesons in QCD, we can borrow much intuition from the SM. The $\mathrm{U}(N_f)_L \times \mathrm{U}(N_f)_R$ flavor symmetry in the

massless limit of Eq. (3.1) is spontaneously broken during confinement by the quark condensate $\langle \overline{\mathbf{Q}}\,\mathbf{Q} \rangle$ to its diagonal SU(N_f) subgroup, plus a U(1) associated with a dark baryon number. There are $N_f^2 - 1$ light pseudo-scalar pNGBs in addition to a heavy flavor-singlet $\hat{\eta}'$ that is the would-be pNBG of the anomalous axial U(1). Explicit breaking of $\mathrm{U}(N_f)_L \times \mathrm{U}(N_f)_R$ by the quark masses and gauging its $\mathrm{SU}(2)_L$ subgroup gives mass to the pNGBs, as further explained in Sec. 3.2.3.

Each meson species transforms in some representation of $\mathrm{SU}(2)_L$ that determines its interactions with the SM. A meson flavor state is a superposition of states with a quark flavor and an anti-quark flavor. Both the quark and the anti-quark are in the self-conjugate representation $\mathbf{N_f}$ of $\mathrm{SU}(2)_L$, so the mesons are organized into the irreducible representations in

$$\mathbf{N_f} \otimes \mathbf{N_f} = \bigoplus_{m=1}^{N_f} (\mathbf{2m-1}) = \mathbf{1} \oplus \mathbf{3} \oplus \mathbf{5} \oplus \cdots \oplus (\mathbf{2N_f - 1}). \tag{3.3}$$

For the lowest-lying pseudo-scalar mesons, we can identify the $\mathbf{3}, \mathbf{5}$, *etc.* as the representations of the pNGBs and the flavor-singlet $\mathbf{1}$ as the would-be pNGB $\hat{\eta}'$. Note in particular that there is always a 3-plet $\hat{\pi}_3$ (since $N_f \geq 2$), and there is a 5-plet $\hat{\eta}_5$ for all $N_f \geq 3$. In the rest of this work, we explore the interesting features that arise for each of these meson representations and the consequences for phenomenology.

3.2.2 Dark G-Parity. This model has a $\mathbb{Z}_2$ symmetry known as G-parity [5] that has important implications for the dark mesons and has an analogy in the SM [166, 167]. Let us first review the SM case. The isospin group $\mathrm{SU}(2)_I$, which acts on u and d quarks, is a subgroup of the SU(3) flavor symmetry that acts on u, d, and s quarks.[1] Besides the would-be pNGB SM η', there is an SU(3) octet

[1] $\mathrm{SU}(2)_I$ is embedded in flavor SU(3) in the SM differently from how $\mathrm{SU}(2)_L$ is embedded in SU(N_f) in the dark sector. In our model, the fundamental of SU(N_f) is identified with the $\mathbf{N_f}$ of $\mathrm{SU}(2)_L$, while the fundamental of flavor SU(3) in the SM is identified with $\mathbf{1} \oplus \mathbf{2}$ of $\mathrm{SU}(2)_I$.

of pNGBs containing an iso-triplet (the pions), two iso-doublets (the kaons), and an iso-singlet (the SM η).[2] The SM G-parity transformation is $G_{\rm SM} = \mathcal{C}e^{i\pi I_y}$ (where I_y is the second generator of $\mathrm{SU}(2)_I$), which has eigenstates

$$\eta'_{\rm SM} \overset{G_{\rm SM}}{\to} \eta'_{\rm SM}, \qquad \pi_{\rm SM} \overset{G_{\rm SM}}{\to} -\pi_{\rm SM}, \qquad \eta_{\rm SM} \overset{G_{\rm SM}}{\to} \eta_{\rm SM}, \tag{3.4}$$

among the lowest-lying pseudo-scalar mesons. The $G_{\rm SM}$ charge of a more general meson is $(-1)^{I+\ell+s}$, where $I \in \{0,1\}$ is the isospin, ℓ is the orbital angular momentum of the constituent quarks, and s is the total spin of the constituent quarks [167]. SM G-parity is preserved by QCD, which leads to selection rules such as the forbidding of the $\eta_{\rm SM} \to 3\pi^0_{\rm SM}$ decay as a strong process [168]. However, SM G-parity is violated at tree-level by QED. After all, $\eta_{\rm SM} \to 3\pi^0_{\rm SM}$ is one of the principal decay modes of the $\eta_{\rm SM}$. By contrast, G-parity in the dark sector provides much stronger selection rules.

The dark G-parity transformation on dark sector matter content is [5]

$$G = \mathcal{C}e^{i\pi J_y} = \mathcal{C}\mathcal{H}, \tag{3.5}$$

where the isospin rotation in the SM G-parity definition has been replaced by a global $\mathrm{SU}(2)_L$ rotation.[3] Clearly, G and $\mathcal{H}$ are closely related. A key difference is that G maps particles to anti-particles, while $\mathcal{H}$ maps a particle to a different particle in the same electroweak multiplet, up to a sign. In the case of baryons, G maps a baryon to an anti-baryon, so a baryon cannot be G eigenstate even if it can be an $\mathcal{H}$ eigenstate. Mesons, however, have particles and anti-particles *in the same electroweak multiplet*, so they can be eigenstates of G, $\mathcal{H}$, or both.

[2] More precisely, the SM η and η' mass eigenstates are admixtures of the flavor singlet and flavor octet. We comment on mass mixings of dark sector flavor states in Sec. 3.2.3.

[3] G also acts as charge conjugation on the dark gluon field so that the dark $\mathrm{SU}(N_c)$ coupling is G-even [5].

Consider a meson state $|J,\, Q\rangle$ in the $2J+1$-dimensional representation of $\mathrm{SU}(2)_L$ with electric charge Q. That is,

$$J_z|J,\, Q\rangle = Q|J,\, Q\rangle\,, \tag{3.6}$$

$$J^2|J,\, Q\rangle = J(J+1)|J,\, Q\rangle\,, \tag{3.7}$$

where J_z is the third generator of $\mathrm{SU}(2)_L$, and J^2 is the quadratic Casimir operator. Following the SM analogy, the actions of the various $\mathbb{Z}_2$ transformations can be self-consistently written as

$$\mathcal{H}|J,\, Q\rangle = \quad (-1)^{J-Q}|J,\, -Q\rangle\,, \tag{3.8}$$

$$\mathcal{C}|J,\, Q\rangle = (-1)^{Q+s+\ell}|J,\, -Q\rangle\,, \tag{3.9}$$

$$G|J,\, Q\rangle = (-1)^{J+s+\ell}|J,\, Q\rangle\,. \tag{3.10}$$

One can see from these transformation rules that *every meson state in a particular electroweak multiplet is an eigenstate of G-parity.* We focus on the pseudo-scalar pNGBs in this work, so we set $s = \ell = 0$ from now on.

Recall from Eq. (3.3) that the mesons appear in the $\mathbf{1}, \mathbf{3}, \mathbf{5}, \ldots$ representations of $\mathrm{SU}(2)_L$. Therefore, Eq. (3.10) implies that the meson multiplets have alternating G-parity, *i.e.* the singlet, 5-plet, 9-plet, *etc.* are G-even, and the 3-plet, 7-plet, 11-plet, *etc.* are G-odd. To make our meson naming scheme explicit, we denote the G-odd pNGBs as $\hat{\pi}$ and the G-even pNGBs as $\hat{\eta}$. We also specify the $\mathrm{SU}(2)_L$ representations of each meson with subscripts and electric charges with superscripts when necessary. Again, we emphasize that only the neutral components of electroweak multiplets have well-defined $\mathcal{H}$-parity, while entire meson multiplets have well-defined G-parity.

Dark G-parity can be broken by the dimension-5 effective operators [5]

$$B_{\mu\nu}\overline{\mathbf{Q}}\,\sigma^{\mu\nu}\,\mathbf{Q} \overset{G}{\to} B_{\mu\nu}\left(\mathcal{C}\overline{\mathbf{Q}}\,\sigma^{\mu\nu}\,\mathbf{Q}\mathcal{C}\right) = -B_{\mu\nu}\overline{\mathbf{Q}}\,\sigma^{\mu\nu}\,\mathbf{Q}\,, \tag{3.11}$$

$$H^\dagger \tau^a H \, \overline{\mathbf{Q}} \, J^a \, \mathbf{Q} \xrightarrow{G} H^\dagger \tau^a H \, \overline{\mathbf{Q}} \left(e^{-i\pi J_y} J^a e^{i\pi J_y} \right) \mathbf{Q} = H^\dagger \tau^a H \, \overline{\mathbf{Q}} \, (-J^a)^* \, \mathbf{Q}, \tag{3.12}$$

where $B_{\mu\nu}$ is the hypercharge field strength, H is the Higgs doublet, and τ^a is a generator of the fundamental representation of $\mathrm{SU}(2)_L$. However, unlike SM G-parity, there are no gauge-invariant renormalizable operators that violate the dark G-parity.[4] This quasi-stabilizes the lightest G-odd meson, which is the $\hat{\pi}_3^0$. As noted in Refs. [5, 12], if these operators are suppressed by the Planck scale, then the quasi-stable $\hat{\pi}$ mesons produced in the early universe may survive past Big Bang Nucleosynthesis but be too short-lived to be cosmologically safe. By dimensional analysis, we can roughly estimate the scaling of the $\hat{\pi}_3^0$ lifetime τ_3 with the scale of G-parity breaking $\Lambda_{\not{G}}$ as

$$\tau_3 \sim \frac{a^2 \Lambda_{\not{G}}^2}{m_\pi^3}, \tag{3.13}$$

$$\Lambda_{\not{G}} \sim \frac{10^{16}\,\mathrm{GeV}}{a} \sqrt{\left(\frac{m_\pi}{1\,\mathrm{TeV}}\right)^3 \left(\frac{\tau_3}{0.1\,\mathrm{s}}\right)}, \tag{3.14}$$

where $a > 1$ is a dimensionless coefficient encapsulating coupling and phase space factors. To ensure $\tau_3 \lesssim 0.1\,\mathrm{s}$ (so that the decays do not disrupt nucleosynthesis [169, 170]), $\Lambda_{\not{G}}$ should be below $\sim 10^{16}\,\mathrm{GeV}$ when $m_\pi \sim \mathcal{O}(1)\,\mathrm{TeV}$. Therefore, we need some UV completion below the Planck scale to facilitate these decays. It was also noted in Chapter II that a UV completion below the Planck scale is required for many values of N_c and N_f to address sub-Planckian Landau poles of the electroweak coupling, and such a UV completion could also provide the needed G violation. While these G-parity violating decays may themselves have interesting phenomenology and help probe the scale of the UV completion, we do not consider

[4] $\mathcal{H}$-parity is violated at two-loop order by the SM due to its action on the hypercharge field [12]. By contrast, G leaves all SM fields invariant.

them in this work. The lifetime could easily be well beyond the detector scale, and so we treat the $\hat{\pi}_3^0$ as stable in our collider study in Sec. 3.6.

3.2.3 Meson Masses. The chiral effective theory we employ has a regime of validity up to a UV mass scale of $\sim 4\pi f_\pi$. We therefore restrict our discussion to the range of pNGB masses below that scale, but there is some subtlety in the mass spectrum of the different pseudo-scalar species. The pNGBs get their masses from explicit breaking of chiral symmetry, of which there are two sources: quark masses and the gauging of the $\mathrm{SU}(2)_L$ subgroup. The quark masses are degenerate at tree-level, so the pNGB masses are as well. Mass splittings arise due to loops with electroweak bosons of the form



that depend on the meson charge and representation. First, consider the mass splitting between mesons in different electroweak multiplets. The diagram on the left is quadratically divergent, so a meson in the $2J+1$-dimensional representation of $\mathrm{SU}(2)_L$ gets a dominant correction to its mass-squared of $\sim 4\pi\alpha_W J(J+1)f_\pi^2$, where α_W is the $\mathrm{SU}(2)_L$ coupling [5]. Even in the massless quark limit, this prevents m_π from being much smaller than f_π without fine-tuning. Then, the difference in the squared masses of the pNGB multiplets scales like the difference in their quadratic Casimirs, but we cannot precisely compute it in perturbation theory.

Next, consider the mass splitting between mesons with different charges in the same electroweak multiplet. The same kinds of loops contribute, but the splitting is due to electroweak symmetry breaking rather than the cutoff of the

EFT. The calculation is performed in Ref. [67], and the splitting is $\sim 170\,\text{MeV}$ between singly-charged and neutral components of a multiplet for meson masses above $\mathcal{O}(100)\,\text{GeV}$.

The splittings between components of the electroweak multiplets have a strong impact on the $\hat{\pi}$ meson lifetimes, as they are forbidden from decaying directly to the SM by G-parity. Therefore, charged $\hat{\pi}$ mesons decay via cascade, *i.e.* they decay to a lighter species in the same electroweak multiplet by radiating one or two off-shell gauge bosons, and the lighter species (if charged) then decays in the same way. This implies the singly-charged $\hat{\pi}$ mesons can decay as $\hat{\pi}^\pm \to \hat{\pi}^0\ \pi^\pm_{\text{SM}}$, as the far off-shell $W^\pm$ radiated by the $\hat{\pi}^\pm$ effectively mixes with the SM pion. There is additional discussion of this process in Refs. [171, 172], and the resulting decay rate is[5]

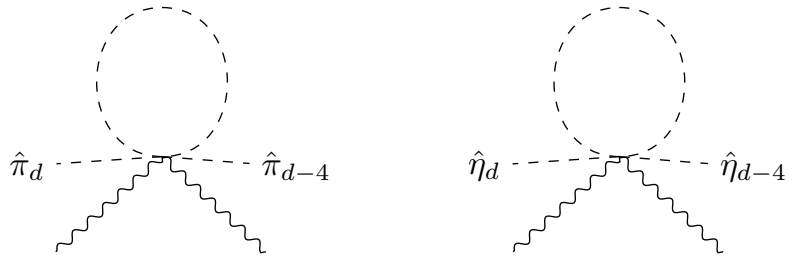
$$\Gamma(\hat{\pi}^\pm \to \hat{\pi}^0\ \pi^\pm_{\text{SM}}) = \pi\,\alpha_W^2\,\frac{f_{\pi,\text{SM}}^2}{m_W^4} J(J+1)\Delta m_{+,0}^2 \sqrt{\Delta m_{+,0}^2 - m_{\pi,\text{SM}}^2}\,, \tag{3.15}$$

where $f_{\pi,\text{SM}} \simeq 92\,\text{MeV}$ is the SM pion decay constant, J indicates the $\hat{\pi}$ meson representation, m_W is the W boson mass, $\Delta m_{+,0}$ is the splitting between the singly-charged and neutral $\hat{\pi}$ mesons, and $m_{\pi,\text{SM}}$ is the SM pion mass.[6] The small phase space for this decay causes the $\hat{\pi}_3^+$ to be long-lived on a collider scale with proper lifetime τ roughly between 4 cm and 6 cm (depending on the mass). We explore the consequences for phenomenology in Sec. 3.6.1.

[5] As discussed in Ref. [171], decays with leptonic final states are suppressed to the extent that the charged state would be collider-stable if the hadronic channel were not open. This is in part due to multi-body phase space suppression.

[6] One can compute the corresponding rate for a higher-charge $\hat{\pi}$ meson to decay to $\hat{\pi}$ meson with one less charge by replacing $J(J+1)$ in Eq. (3.15) with the square of the corresponding element of the $\text{SU}(2)_L$ ladder operator in the appropriate representation.

The mass splittings between different multiplets implies that the higher multiplets can decay by "hopping" down to a lower one. These processes are permitted by loop diagrams of the form [5]



with some dark meson species in the loop. These six-point vertices arise from dimension-6 effective operators in the meson EFT. In this way, mesons in representations larger than the **5** can hop down to a meson in a lower representation with the same G-parity by emitting two electroweak bosons. Since these decays are facilitated by dimension-6 operators, we expect the decay rate to scale with the model parameters as

$$\Gamma_{\text{hop}} \sim \alpha_W^2 \frac{\Delta m_{d,d-4}^5}{(4\pi)^5 f_\pi^4}\,, \tag{3.16}$$

where $\Delta m_{d,d-4}$ is the splitting between the initial and final meson multiplets. While this decay rate is suppressed by a loop factor and multi-body phase space, the mass splitting itself is expected to scale as f_π. Moreover, the divergence of the loop introduces an additional numerical enhancement. Therefore, we expect the higher multiplets to rapidly decay to the $\hat{\pi}_3$ or $\hat{\eta}_5$ in this way.

This work focuses on the limit where the pNGBs are light enough to be accessible at the LHC while the heavier mesons (the $\hat{\eta}'$, vector mesons $\hat{\rho}$, *etc.*) are inaccessible. The reason is to avoid various complications such as the $\hat{\rho}$ mixing with the SM Z boson [10], interactions of the pNGBs with the $\hat{\rho}$, and the tower of other

excited meson states. Indeed, many excited QCD resonances appear within an $\mathcal{O}(1)$ factor of the SM ρ mass [167], so we expect the same to be true in the dark sector. We generically expect these heavier meson masses to be $\sim 4\pi f_\pi$, so we will take $4\pi f_\pi$ to be above some threshold (below which some resonance searches may be sensitive) to safely ignore them. One possible exception, depending on the details of the UV, is the $\hat{\eta}'$, which becomes light in the large-N_c limit [173]. A light $\hat{\eta}'$ would slightly alter phenomenology for reasons that will become clear in Sec. 3.3, but we neglect this possibility in the rest of this work.

To get a rough estimate of the minimum mass where the $\hat{\rho}$ may be visible, we can compare our model to the similar dark sector described in Refs. [9] and [10] with dark vector mesons mixing with SM gauge bosons. There are dilepton resonance searches [174, 175], as well as the search in Ref. [141] for the vector meson in the similar model decaying to pairs of pNGB mesons. These searches probe the vector mass scale up to $\sim 2\,\text{TeV}$ at most, so this serves as a rough lower bound on $4\pi f_\pi$ above which the signals discussed in this work are dominant.

Another possible complication is mixing of mesons in different electroweak multiplets. This is in some sense analogous to SM η-η' mixing, but it is clearly only permitted in the dark sector by electroweak symmetry breaking. Chapter II shows how mixing of baryon multiplets is important to understanding their dark matter phenomenology, but the effect disappears as the relevant mass scales in the dark sector become larger than the electroweak scale. Also, if any of the dark sector mass scales were below the electroweak scale, then the details of the electroweak interactions between individual quarks may significantly alter the meson spectrum, as was the case for baryons in Chapter II. We neglect these effects in this work, as the relevant scales are set by $4\pi f_\pi$.

In summary, the mass splitting between the multiplets is set by the Casimirs and f_π, the splitting between entries within a multiplet is small and leads to long-lived $\hat{\pi}_3^\pm$ states, and the pNGBs are the only mesons we consider in our collider study. We have yet to discuss the decays of the $\hat{\eta}_5$ mesons, for which we need the findings of Sec. 3.3. This will show that each meson multiplet has its own idiosyncrasies with direct impact on experimental signals.

3.3 The 5-plet Anomaly

This section presents the striking result that not only can the $\hat{\eta}_5$ be singly produced and decay via an anomaly with $\mathrm{SU}(2)_L$, but also that it is *unique* among the pNGBs in this way. The gauge-invariant form of the Wess-Zumino-Witten [176–178] operator contains the dimension-5 effective operator [74, 5, 179]

$$\mathcal{L}_{\text{anomaly}} = \frac{g_W^2}{16\pi^2}\frac{N_c}{f_\pi}\hat{\phi}^a \varepsilon^{\mu\nu\alpha\beta} W^i_{\mu\nu} W^j_{\alpha\beta} \mathrm{Tr}\left[T^a J^i J^j\right], \tag{3.17}$$

where $g_W = \sqrt{4\pi\alpha_W}$, $W^i_{\mu\nu}$ is the $\mathrm{SU}(2)_L$ field strength, J^i is a generator of $\mathrm{SU}(2)_L$, the sum over the index a is a sum over all pNGBs $\hat{\phi}$, and T^a is the generator of flavor $\mathrm{SU}(N_f)$ corresponding to the a^{th} pNGB. It has been noticed that this operator vanishes for the $\hat{\pi}_3$ [5, 180, 148], and Refs. [5, 148] remarked that the G-even mesons can decay in this way, but the fact that the $\hat{\eta}_5$ is unique has not appeared in the literature. That is, if N_f is large enough such that an $\hat{\eta}_9, \hat{\eta}_{13}$, *etc.* exist in the spectrum, they do not have an anomaly with $SU(2)_L$, and so they do not decay like the $\hat{\eta}_5$. Recall from Sec. 3.2.1 that the $\hat{\eta}_5$ only exists in the spectrum if the quarks are in larger representations of $\mathrm{SU}(2)_L$ than the fundamental, so studies with constituents in exclusively fundamental representations of their gauge groups would have missed this mechanism.

3.3.1 Review of Standard Model Meson Anomalies. First, we review the basics of the chiral anomalies that appear in QCD, which serve as an

instructive comparison to the dark sector. They arise due to non-conservation of the chiral flavor currents j^5_μ, such as the current corresponding to the axial U(1) mentioned in Sec. 3.2.1. Consider the divergence of j^{5a}_μ due to SM gluons, with a indexing the generators that are broken during confinement:

$$\partial^\mu j^{5a}_\mu \propto G^b_{\rm SM} \widetilde{G}^c_{\rm SM} \mathrm{Tr}\left[T^a\, t^b\, t^c\right], \tag{3.18}$$

where $G^a_{\rm SM}$ is the QCD field strength, and t^a is a generator of $\mathrm{SU}(3)_{\rm color}$. The flavor generator T^a has flavor indices, while t^a has color indices, so the trace factorizes as

$$\mathrm{Tr}\left[T^a\, t^b\, t^c\right] = \mathrm{Tr}\left[T^a\right] \mathrm{Tr}\left[t^b\, t^c\right] = 0, \tag{3.19}$$

since the flavor generator is traceless. However, if we consider the flavor-singlet $\eta'_{\rm SM}$, the "flavor generator" is the identity in flavor space, which is not traceless, and the divergence becomes

$$\partial^\mu j^5_\mu \propto G^a_{\rm SM} \widetilde{G}^b_{\rm SM} \mathrm{Tr}\left[t^a\, t^b\right] = \frac{1}{2} G^a_{\rm SM} \widetilde{G}^a_{\rm SM}. \tag{3.20}$$

The flavor-singlet axial U(1) is therefore not a good symmetry of the UV theory, so the $\eta'_{\rm SM}$ is not a pNGB.

The SM pNGBs do not have an anomaly with QCD, but the neutral pion famously decays via an anomaly with QED. The effective operator governing this decay is

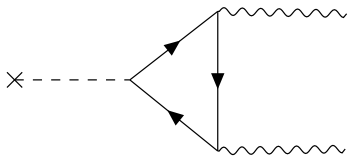
$$\mathcal{L}^{\rm QED}_{\rm anomaly} \propto \pi^0_{\rm SM} F \widetilde{F}\, \mathrm{Tr}\left[T^0\, Q^2\right], \tag{3.21}$$

where F is the QED field strength, and the generators are

$$T^0 = \frac{1}{2} \begin{pmatrix} 1 & & \\ & -1 & \\ & & 0 \end{pmatrix}, \qquad Q = \begin{pmatrix} 2/3 & & \\ & -1/3 & \\ & & -1/3 \end{pmatrix}, \tag{3.22}$$

which both have SU(3) flavor indices. The product $T^0\,Q^2$ is not traceless, so this anomaly is non-vanishing.

We emphasize that the above anomalies are non-vanishing even though QED and QCD are vector-like theories. The flavor currents appearing in triangle diagrams of the form



are global chiral currents, so these global-gauge-gauge anomalies do not contradict the required absence of pure gauge anomalies. Each of these points is useful to keep in mind as we discuss the analogous anomalies in the dark sector.

3.3.2 Uniqueness of the 5-plet Anomaly. In this section, we study the anomalous interaction from Eq. (3.17) in detail. There is a simple argument from gauge invariance that the $\hat{\eta}_5$ is unique among the pNGBs in that it has an anomaly with $\mathrm{SU}(2)_L$. We have an effective operator in Eq. (3.17) of the form $\hat{\pi} W\widetilde{W}$ or $\hat{\eta}\, W\widetilde{W}$. The W operators are in the $\mathbf{3}$ of $\mathrm{SU}(2)_L$, and the $\hat{\pi}$ or $\hat{\eta}$ is in some representation $\mathbf{d}$. The effective operator can only be a gauge singlet if the product

$$\mathbf{3} \otimes \mathbf{3} \otimes \mathbf{d} = (\mathbf{1} \oplus \mathbf{3} \oplus \mathbf{5}) \otimes \mathbf{d} \tag{3.23}$$

contains a $\mathbf{1}$. This only occurs if $\mathbf{d}$ is $\mathbf{1}$, $\mathbf{3}$, or $\mathbf{5}$, so only the $\hat{\eta}'$, $\hat{\pi}_3$, and $\hat{\eta}_5$ could have the anomaly. In light of the discussion in Sec. 3.3.1, it is unsurprising that the $\hat{\eta}'$ has an anomaly with $\mathrm{SU}(2)_L$ in addition to $\mathrm{SU}(N_c)$, but it is not a pNGB. This

leaves only the $\hat{\pi}_3$ and $\hat{\eta}_5$, but the anomaly with the $\hat{\pi}_3$ vanishes for other reasons explained below.[7]

If the term in Eq. (3.17) with the $\hat{\pi}_3$ were non-vanishing, then it would clearly violate G-parity. However, we show here that this term vanishes regardless of G-violation in the UV (which further implies that the anomaly preserves G). Consider how one would determine the flavor generator T^a in Eq. (3.17) corresponding to a particular meson species in a particular multiplet. The flavor generator encodes the meson state as a linear combination of quark/anti-quark flavor states, which should be an eigenstate of the $\mathrm{SU}(2)_L$ quadratic Casimir operator J^2 and the electric charge operator Q. Transformations of the meson state under $\mathrm{SU}(2)_L$ can be written as transformations of T^a using

$$T^a \xrightarrow{J^i} [J^i, T^a], \tag{3.24}$$

where J^i is a generator of the N_f-dimensional representation of $\mathrm{SU}(2)_L$. Then, the charge and Casimir operators act as

$$T^a \xrightarrow{Q} [J_z, T^a], \qquad\qquad T^a \xrightarrow{J^2} [J^i, [J^i, T^a]]\,. \tag{3.25}$$

Therefore, the meson with charge Q in the $2J+1$-dimensional representation of $\mathrm{SU}(2)_L$ corresponds to the flavor generator with

$$T^a \xrightarrow{Q} Q\,T^a, \qquad\qquad T^a \xrightarrow{J^2} J(J+1)\,T^a. \tag{3.26}$$

We provide a recipe to explicitly construct these generators in Sec. 3.4. Suppose a meson's flavor generator is itself a linear combination of the $\mathrm{SU}(2)_L$ generators.

[7] Outside of the context of our model, one could consider a minimal dark matter candidate that is the neutral component of a pseudoscalar $\mathrm{SU}(2)_L$ 5-plet ϕ_5. Using the UV-agnostic framework of Ref. [67], the $\phi_5 W\widetilde{W}$ effective operator (analogous to the anomaly operator in this work) would destabilize this dark matter candidate, and additional model building would be required for the UV completion to forbid this decay channel. This observation builds on the result of Ref. [67] that a *scalar* 5-plet minimal dark matter candidate can also be destabilized at dimension-5.

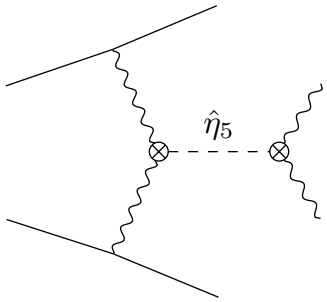


Figure 3. Feynman diagram corresponding to the anomaly-induced resonant production of the $\hat{\eta}_5$. The $\otimes$ symbols denote insertions of the anomaly operator in Eq. (3.29). The $\hat{\eta}_5$ species are the unique pNGBs of dark chiral symmetry breaking with this operator. Observation of this signal provides sensitivity to UV parameters such as N_c and N_f, which set the strength of the coupling (see Eqs. (3.29) and (3.30)). LHC implications are discussed in Sec. 3.6.2.

Then, its transformation under the Casimir operator is found using

$$J^a \xrightarrow{J^2} [J^i, [J^i, J^a]] = \varepsilon^{aij}\varepsilon^{ijk}J^k = 2J^a, \tag{3.27}$$

i.e. the meson is in the $J = 1$ (3-plet) representation. Thus, the flavor generators corresponding to the $\hat{\pi}_3$ multiplet are (unsurprisingly) linear combinations of $\mathrm{SU}(2)_L$ generators. Then, the operator in Eq. (3.17) for the $\hat{\pi}_3$ contains

$$\varepsilon^{\mu\nu\alpha\beta}W^i_{\mu\nu}W^j_{\alpha\beta}\mathrm{Tr}\left[J^aJ^iJ^j\right]. \tag{3.28}$$

Unlike the SM flavor and color generators in Eq. (3.19), the generators in this trace all have the same flavor indices (analogously to Eq. (3.21)), so the trace itself neither factorizes nor vanishes. However, the trace is anti-symmetric in the i and j indices,[8] while $\varepsilon^{\mu\nu\alpha\beta}W^i_{\mu\nu}W^j_{\alpha\beta}$ is symmetric in i and j, so the operator vanishes. Therefore, the $\hat{\pi}_3$ does not have an anomaly with $\mathrm{SU}(2)_L$. The flavor generators for meson multiplets besides the $\hat{\pi}_3$ are *not* linear combinations of $\mathrm{SU}(2)_L$ generators, so the above argument does not forbid the $\hat{\eta}_5$ from having the anomaly.

[8]Equivalently, the totally symmetric invariant tensor d^{abc} of SU(2) vanishes.

In this way, we have shown that the $\hat{\eta}_5$ is the unique pNGB with a global-SU(2)$_L$-SU(2)$_L$ anomaly. One can also see this by finding the generators for the $\hat{\pi}_7, \hat{\eta}_9$, *etc.* and observing that the trace in Eq. (3.17) for these species vanishes identically, unlike the trace in Eq. (3.28). Then, we can expand Eq. (3.17) as

$$\begin{aligned}\mathcal{L}_{\text{anomaly}} = c\,\frac{g_W^2}{16\pi^2}\frac{N_c}{f_\pi}\varepsilon^{\mu\nu\alpha\beta}\Bigg[&\sqrt{\frac{3}{2}}\,\hat{\eta}_5^{++}\,(W^1_{\alpha\beta}+iW^2_{\alpha\beta})(W^1_{\mu\nu}+iW^2_{\mu\nu}) \\ &-\sqrt{6}\,\hat{\eta}_5^{+}\,W^3_{\mu\nu}(W^1_{\alpha\beta}+iW^2_{\alpha\beta}) \\ &+\hat{\eta}_5^{0}\,(2W^3_{\mu\nu}W^3_{\alpha\beta}-W^1_{\mu\nu}W^1_{\alpha\beta}-W^2_{\mu\nu}W^2_{\alpha\beta}) \\ &+\sqrt{6}\,\hat{\eta}_5^{-}\,W^3_{\mu\nu}(W^1_{\alpha\beta}-iW^2_{\alpha\beta}) \\ &+\sqrt{\frac{3}{2}}\,\hat{\eta}_5^{--}\,(W^1_{\alpha\beta}-iW^2_{\alpha\beta})(W^1_{\mu\nu}-iW^2_{\mu\nu})\Bigg],\end{aligned} \tag{3.29}$$

where

$$c = \frac{1}{12\sqrt{10}}\sqrt{\frac{(N_f+2)!}{(N_f-3)!}} \tag{3.30}$$

is an overall coefficient derived in Sec. 3.5. Since c scales as $N_f^{5/2}$, the strength of the anomaly interaction increases rather quickly with N_f. In the electroweak-broken phase, this operator leads to the decay of the $\hat{\eta}_5$ to different combinations of $W^\pm$, γ, and Z boson pairs.[9] In addition, the anomaly also allows the $\hat{\eta}_5$ to be *resonantly produced* in proton-proton collisions via VBF [47],[10] followed by decay to pairs of electroweak bosons, as shown in Fig. 3. The collider phenomenology of this global-gauge-gauge anomalous interaction is discussed in Sec. 3.6.2.

The anomaly is the dominant decay mode of each species in the 5-plet. One may have expected the singly-charged $\hat{\eta}^\pm$ mesons to decay analogously to

[9]Since $W^i_{\mu\nu}$ is the full SU(2)$_L$ non-abelian field strength, these operators also include couplings of the $\hat{\eta}_5$ to three electroweak bosons at higher order in g_W.

[10]See Ref. [181] for another example (in a composite Higgs context) of having a subset of mesons that can be produced through VBF via an anomaly.

Species	$\mathrm{SU}(2)_L$ Rep.	$N_{f,\min}$	G-parity	Dominant decay
$\hat{\pi}_3$	$\mathbf{3}$	2	-1	cascade ($\hat{\pi}_3^\pm$), G-violation ($\hat{\pi}_3^0$)
$\hat{\eta}_5$	$\mathbf{5}$	3	$+1$	anomaly
$\hat{\pi}_7$, $\hat{\pi}_{11}$, $\hat{\pi}_{15}$, ...	$\mathbf{7}, \mathbf{11}, \mathbf{15}, \ldots$	$4, 6, 8, \ldots$	-1	hopping
$\hat{\eta}_9$, $\hat{\eta}_{13}$, $\hat{\eta}_{17}$, ...	$\mathbf{9}, \mathbf{13}, \mathbf{17}, \ldots$	$5, 7, 9, \ldots$	$+1$	

Table 3. Summary of the pNGBs of dark chiral symmetry breaking, including their representation under $\mathrm{SU}(2)_L$, the minimum N_f such that the species exists in the spectrum (Sec. 3.2.1), the charge under the dark G-parity (Sec. 3.2.2), and the dominant decay mode (Secs. 3.2.2 and 3.3.2) for each meson. Decay modes specific to particular components of the $\mathrm{SU}(2)_L$ multiplets are specified. Several species decay via cascade, *i.e.* they decay to lighter meson in the same multiplet by radiating an off-shell gauge boson. The higher multiplets decay by hopping down to a lower multiplet with the same G-parity and emitting two gauge bosons.

the SM pion, *i.e.* via effectively mixing with the W boson. However, the operator $W_\mu^\pm \partial^\mu \pi_{\mathrm{SM}}^\mp$ that leads to this mixing is parity-violating. The couplings of the W to the SM quarks violate parity, so this mixing operator naturally appears in the chiral Lagrangian. By contrast, the dark quarks have vector-like couplings to the W, so operators such as $W_\mu^\pm \partial^\mu \hat{\eta}^\mp$ are forbidden.

The anomaly allows one to probe some details of the UV theory while only measuring a few IR processes. The $\mathrm{SU}(N_f)$ generators T^a and $\mathrm{SU}(2)_L$ generators J^i in Eq. (3.17) depend on N_f, which causes the strength of the anomaly interaction also to have dependence on N_f that is captured by the coefficient c in Eq. (3.30). In an idealized scenario, one could precisely measure the rate for some process involving self-interactions of the pNGBs to extract f_π, as well as the rates for the anomaly-induced processes to extract $c\,N_c/f_\pi$. Then, one may be able to reconstruct the UV parameters N_c and N_f. (Since N_c and N_f are discrete, the product $c\,N_c$ is usually not degenerate between different combinations of N_c and

N_f.) This is analogous to using SM pion decay rates to extract the number of colors in QCD.

We have now explored each pNGB of chiral symmetry breaking and their decays, which are summarized in Table 3. In Sec. 3.6.2, we explore signals of resonant production of the $\hat{\eta}_5$. We only consider production and decay via the anomaly, which allows us to put an experimental bound on $4\pi f_\pi/N_c$ for a particular choice of N_f.

3.4 Obtaining Flavor Generators

Here, we present a method to explicitly construct the flavor generators corresponding to meson species in specific $\mathrm{SU}(2)_L$ multiplets with specific electric charges. One starts with a basis for the diagonal generators $\{D^a\}$ of $\mathrm{SU}(N_f)$. For example,

$$D^1 = \frac{1}{2}\,\mathrm{diag}(1,-1,0,\ldots,0), \tag{3.31}$$

$$D^2 = \frac{1}{2\sqrt{3}}\,\mathrm{diag}(1,1,-2,0,\ldots,0), \tag{3.32}$$

$$\ldots, \tag{3.33}$$

$$D^{N_f-1} = \frac{1}{\sqrt{2N_f(N_f-1)}}\,\mathrm{diag}(1,\ldots,1,1-N_f)\,. \tag{3.34}$$

Then, one can define the matrix

$$M_{ab} = 2\,\mathrm{Tr}\left(D^a[J^i,[J^i,D^b]]\right), \tag{3.35}$$

where J^i is a generator of the N_f-dimensional representation of $\mathrm{SU}(2)_L$. As discussed in Sec. 3.3.2, the matrix M encodes the action of the quadratic Casimir operator of $\mathrm{SU}(2)_L$ on the generators. The eigenvalues of M are $J(J+1)$ with $J \in \{1,2,\ldots,N_f-1\}$, and the eigenvectors provide the linear combinations of the D^a generators corresponding to the neutral mesons in each of the $\mathrm{SU}(2)_L$ representations $\mathbf{3},\mathbf{5},\ldots,\mathbf{2N_f-1}$. They must be the neutral mesons because the

generators are diagonal and therefore commute with the third $\mathrm{SU}(2)_L$ generator J_z. Now that one has the generators for the neutral mesons in each representation, one can construct the remaining flavor generators using the $\mathrm{SU}(2)_L$ ladder operators

$$J^{\pm} = J_x \pm iJ_y, \tag{3.36}$$

$$\langle m_1|J^{\pm}|m_2\rangle = \delta_{m_1,m_2\pm1}\sqrt{\frac{N_f^2-1}{4} - m_2(m_2 \pm 1)}\,, \tag{3.37}$$

where J_x and J_y are the first and second $\mathrm{SU}(2)_L$ generators. If T_J^Q is the flavor generator corresponding to the meson with charge Q in the $2J+1$-dimensional representation of $\mathrm{SU}(2)_L$, then one can raise or lower it to obtain

$$T_J^{Q\pm1} = \frac{1}{\sqrt{J(J+1) - Q(Q\pm1)}}[J^{\pm}, T_J^Q]\,. \tag{3.38}$$

Each multiplet contains a neutral meson, so the iterative application of the ladder operators to the diagonal generators allows one to find the flavor generators for all meson species.

As an explicit example, consider the generators for the meson 5-plet $\hat{\eta}_5$ when $N_f = 3$. A basis for the diagonal generators of SU(3) is

$$D^1 = \frac{1}{2}\begin{pmatrix} 1 & & \\ & -1 & \\ & & 0 \end{pmatrix}, \qquad D^2 = \frac{1}{2\sqrt{3}}\begin{pmatrix} 1 & & \\ & 1 & \\ & & -1 \end{pmatrix}, \tag{3.39}$$

with which one finds

$$M = \begin{pmatrix} 5 & -\sqrt{3} \\ -\sqrt{3} & 3 \end{pmatrix}. \tag{3.40}$$

M has eigenvalues 2 and 6, as we expect from having 3-plet and 5-plet mesons. The eigenvectors of M show that the generator corresponding to the neutral 5-plet

meson is

$$T_2^0 = \frac{\sqrt{3}}{2} D^1 - \frac{1}{2} D^2 = \frac{1}{2\sqrt{3}} \begin{pmatrix} 1 & & \\ & -2 & \\ & & 1 \end{pmatrix} . \tag{3.41}$$

Then, using the ladder operators

$$J^+ = \sqrt{2} \begin{pmatrix} 0 & 1 & 0 \\ 0 & 0 & 1 \\ 0 & 0 & 0 \end{pmatrix} , \qquad J^- = \sqrt{2} \begin{pmatrix} 0 & 0 & 0 \\ 1 & 0 & 0 \\ 0 & 1 & 0 \end{pmatrix} \tag{3.42}$$

in combination with Eq. (3.38), one can construct the remaining 5-plet flavor generators

$$T_2^{++} = \frac{1}{\sqrt{2}} \begin{pmatrix} 0 & 0 & 1 \\ 0 & 0 & 0 \\ 0 & 0 & 0 \end{pmatrix} , \qquad T_2^{+} = \frac{1}{2} \begin{pmatrix} 0 & -1 & 0 \\ 0 & 0 & 1 \\ 0 & 0 & 0 \end{pmatrix} , \tag{3.43}$$

$$T_2^{--} = \frac{1}{\sqrt{2}} \begin{pmatrix} 0 & 0 & 0 \\ 0 & 0 & 0 \\ 1 & 0 & 0 \end{pmatrix} , \qquad T_2^{-} = \frac{1}{2} \begin{pmatrix} 0 & 0 & 0 \\ 1 & 0 & 0 \\ 0 & -1 & 0 \end{pmatrix} . \tag{3.44}$$

This calculation helps establish the relative factors between different terms in the anomaly operator in Eq. (3.29), and the overall factor c is computed in Sec. 3.5.

3.5 Computing the 5-plet Anomaly

The coefficient c in Eq. (3.29) encodes the N_f dependence of the 5-plet anomaly. Here, we compute c for an arbitrary N_f using general properties of the 5-plet generators. To start with a helpful analogy, recall from Sec. 3.3.2 that

the generators corresponding to the 3-plet mesons are linear combinations of the $\mathrm{SU}(2)_L$ generators J^i in the N_f-dimensional representation. This is expected, as J^i transforms as a **3**, so the generators of the **3** do so as well.

We can make a similar argument for the 5-plet by noticing that the **5** of SU(2) is the symmetric traceless combination of two **3**'s. Therefore, the object

$$S^{ij} = \{J^i, J^j\} - \frac{1}{N_f}\,\mathrm{Tr}(\{J^i, J^j\})\mathbb{1}, \tag{3.45}$$

where $\mathbb{1}$ is the identity in flavor space, is a tensor that transforms as a **5**. This means that the generators for the 5-plet mesons are linear combinations of the components of S^{ij}. To fully convince oneself of this, one can explicitly show

$$[J^k, [J^k, S^{ij}]] = 6S^{ij}, \tag{3.46}$$

as required of the 5-plet generators (see Eq. (3.26)), using the identities

$$[J^k, [J^k, \{J^i, J^j\}]] = 6\{J^i, J^j\} - 4\delta^{ij}J^2 = 6\{J^i, J^j\} - (N_f^2 - 1)\delta^{ij}\,\mathbb{1}, \tag{3.47}$$

and

$$\frac{1}{N_f}\,\mathrm{Tr}(\{J^i, J^j\}) = \frac{1}{6}(N_f^2 - 1)\delta^{ij}\,. \tag{3.48}$$

Then, the flavor generators corresponding to each 5-plet species are proportional to the components of S^{ij} in the spherical basis. In particular, the diagonal generator (corresponding to the neutral component of the 5-plet) is [182, 183]

$$\begin{aligned} T_2^0 &\propto \frac{1}{\sqrt{6}}(2S^{33} - S^{11} - S^{22}) \\ &\propto 3J_z^2 - J^2 = 3J_z^2 - \frac{N_f^2 - 1}{4}\,\mathbb{1}\,. \end{aligned} \tag{3.49}$$

To enforce the normalization $\mathrm{Tr}((T_2^0)^2) = 1/2$, we have

$$T_2^0 = \sqrt{10\frac{(N_f - 3)!}{(N_f + 2)!}}\left(3J_z^2 - \frac{N_f^2 - 1}{4}\,\mathbb{1}\right), \tag{3.50}$$

which follows from

$$J_z = \mathrm{diag}((N_f - 1)/2, (N_f - 1)/2 - 1, \ldots, -(N_f - 1)/2)\,. \tag{3.51}$$

Species	Production	Lifetime	Signal
$\hat{\pi}_3^{\pm}$	pairs via DY and VBF	$\mathcal{O}(0.1)$ ns	disappearing tracks
$\hat{\pi}_3^0$		collider-stable	
$\hat{\eta}_5^0$, $\hat{\eta}_5^{\pm}$, $\hat{\eta}_5^{\pm\pm}$	resonances via the anomaly	prompt	diboson decays

Table 4. Summary of the dark mesons we consider in our collider study.

The general form for T_2^0 will help us compute c.

The anomaly operator in Eq. (3.17) contains traces of the form

$$\mathrm{Tr}(T^a J^i J^j)\,. \tag{3.52}$$

The a index picks out a particular meson species, and the i and j indices pick out particular components of the $\mathrm{SU}(2)_L$ field strength $W^i_{\mu\nu}$. If we focus on the term with $i = j = 3$, we have

$$\mathcal{L}_{\text{anomaly}} \supset \frac{g_W^2}{16\pi^2}\frac{N_c}{f_\pi}\varepsilon^{\mu\nu\alpha\beta}W^3_{\mu\nu}W^3_{\alpha\beta}\,\hat{\eta}_5^0\,\mathrm{Tr}(T_2^0 J_z^2)\,. \tag{3.53}$$

The relative factors between the traces over different combinations of generators are fixed by gauge invariance, so it is sufficient to compute only one of them for an arbitrary N_f, and c is an overall factor in the anomaly operator. Thus, we can match Eq. (3.53) onto Eq. (3.29) to conclude

$$\begin{aligned} c &= \frac{1}{2}\mathrm{Tr}(T_2^0 J_z^2) \\ &= \frac{1}{12\sqrt{10}}\sqrt{\frac{(N_f+2)!}{(N_f-3)!}}\,. \end{aligned} \tag{3.54}$$

This tells us how the strength of the anomaly interaction varies with N_f.

3.6 Collider Signals and Constraints

The results of Secs. 3.2 and 3.3 imply striking collider signals of the model's dark mesons. A summary of the properties and signals of the pNGBs of dark chiral symmetry breaking is shown in Table 4. The $\hat{\pi}_3$ and $\hat{\eta}_5$ multiplets have entirely

distinct and complementary signatures, each of which is the subject of several LHC searches. We use these searches to place constraints on the meson masses and the ratio f_π/N_c. For event generation, we use MadGraph5_aMC@NLO [184, 185] with a model we implement in FeynRules [186, 187]. For the LLP study, we use Pythia 8 [188] for showering and Delphes 3 [189] with the default ATLAS card for detector simulation, which includes jet clustering using FastJet [186, 187] with the anti-k_T clustering algorithm [190]. We generate events with zero, one, or two jets in the hard process, which are combined by MadGraph5 with matrix-level matching.

3.6.1 Disappearing Tracks: A 3-plet Signature. The $\hat{\pi}_3^\pm$ decays with a lifetime of $\mathcal{O}(0.1)$ ns to a neutral collider-stable $\hat{\pi}_3^0$ and a soft SM pion, which leads to the same kind of signal as the classic chargino decay to a neutralino in the Minimal Supersymmetric Standard Model when the wino is much lighter than all of the other superpartners. The charged particle leaves a few hits in the inner tracker before it decays, the soft SM pion is not reconstructed, and the result is a track that seems to stop inside the tracker.[11] These disappearing tracks signals are the subjects of recent searches by the ATLAS and CMS collaborations [192, 193], which place strong lower bounds on chargino masses.

The $\hat{\pi}_3$ is produced via DY and VBF in opposite charge, same charge, or charged-plus-neutral pairs, as pictured in Fig. 4. As has been pointed out in the contexts of sleptons and charginos [194, 195], the VBF cross section falls slower than that of DY as a function of mass, thus it can become the dominant process for masses above an $\mathcal{O}(100)$ GeV threshold. This effect is partially due to DY suffering from an s-channel propagator, while the vector bosons facilitating VBF can be light

[11] There has been progress in reconstructing the soft SM pions that have $p_T \gtrsim 500$ MeV, which helps resolve the decay vertex and reject fake tracks that come from random hits [191].

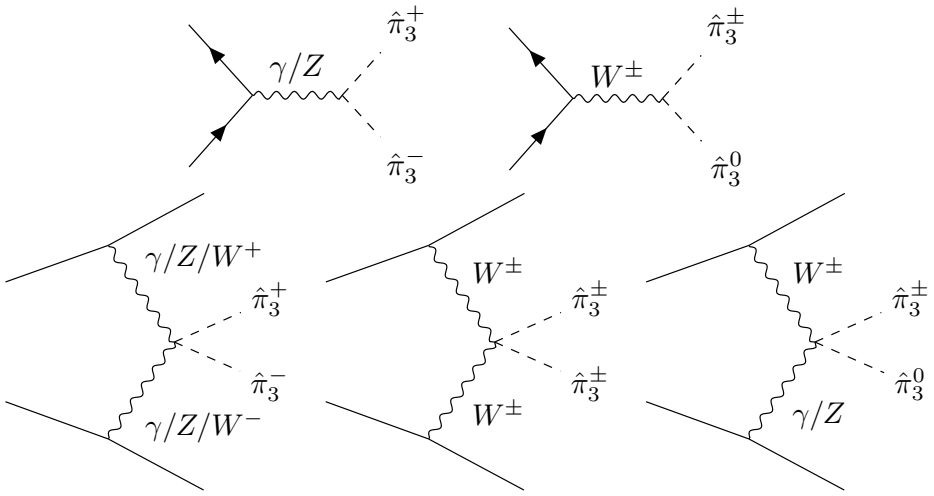


Figure 4. Diagrams representing pair production of the $\hat{\pi}_3$ mesons via Drell-Yan (top) and vector boson fusion (bottom). The VBF processes also get contributions from diagrams with three-point vertices coupling the mesons to vector bosons. Diagrams with production of two neutral mesons via VBF are not pictured, as we do not consider such processes.

and close to on-shell. Another contribution to the enhancement of VBF over DY is that DY requires a sea anti-quark in the initial state, which has a suppressed parton distribution function compared to the quark initial states allowed in VBF. As shown in Fig. 5, we find that VBF dominates DY by a factor of $\mathcal{O}(100)$ for $m_\pi \gtrsim 700\,\text{GeV}$ in our case. This is a stronger enhancement than, for example, that of a selectron, in part due to the combinatorics involved in producing the various states within the $\hat{\pi}_3$ multiplet. The large production cross section allows us to place even stronger constraints on the $\hat{\pi}_3$ mass than existing constraints on chargino masses.

If $N_f \geq 4$, then there is a $\hat{\pi}_7$ in the meson spectrum in addition to the $\hat{\pi}_3$. The decays of the $\hat{\pi}_7$ to the $\hat{\pi}_3^\pm$ may also contribute to the disappearing tracks signal. However, these hopping decays (hopping from heavier to light pions with the same G-parity) are associated with additional SM states due to the emitted

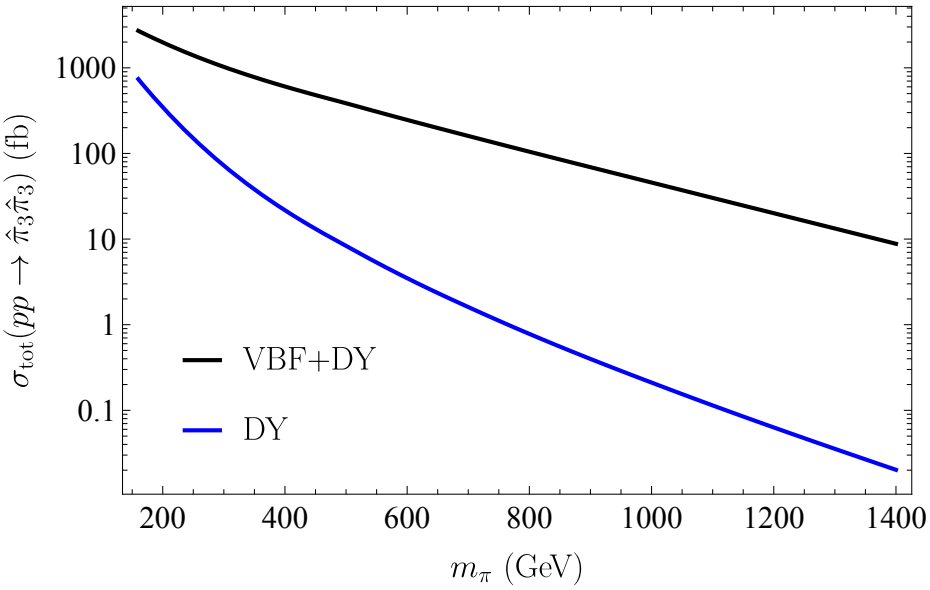


Figure 5. Total LHC production cross sections of the dark meson triplet $\hat{\pi}_3$ pairs we consider. The production rate for exclusively Drell-Yan processes falls much faster as a function of the $\hat{\pi}_3$ mass m_π than the rate of processes that include vector boson fusion.

EW bosons, which complicates the disappearing tracks analysis. Therefore, we do not include the $\hat{\pi}_7$ (or larger multiplets present at higher N_f) in our analysis.

We re-use the methods from Ref. [172] available in the LLP Recasting Repository [197] to re-interpret two Run 2 ATLAS disappearing tracks searches.[12] The reinterpretation package enables us to compute the visible cross section, *i.e.* the product of the total production cross section and the efficiency of identifying a disappearing track. The first search, which the re-interpretation code was built for, used a dataset with an integrated luminosity of 36.1 fb^{-1} and placed a model-independent constraint on the visible cross section of disappearing tracks of 0.22 fb at the 95% confidence level [196]. The second search used an integrated luminosity of 136 fb^{-1} and found a constraint of 0.037 fb [192]. Our use of the

[12]The most recent ATLAS and CMS searches in Refs. [192, 193] derived very similar model-dependent constraints on masses of supersymmetric particles, so we expect the CMS constraints on our model to be closely comparable.

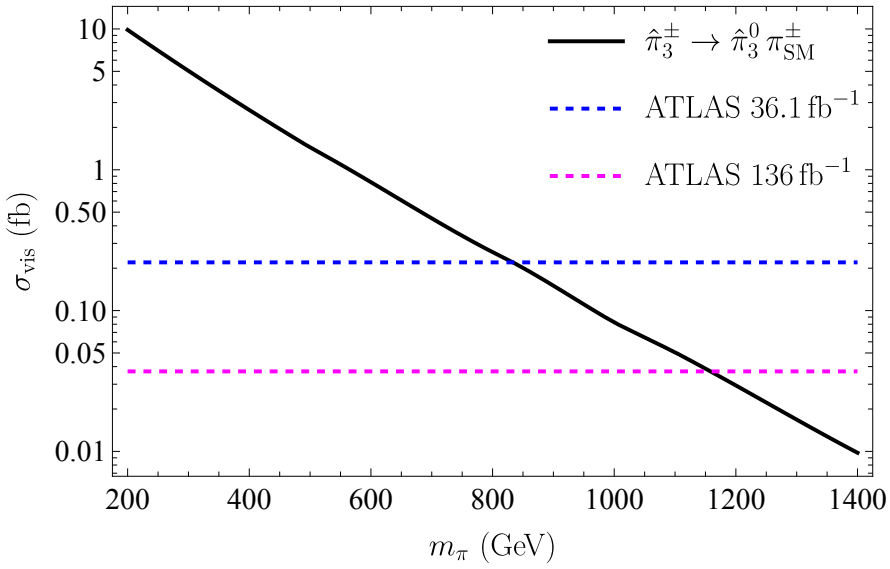


Figure 6. The visible cross section for production of disappearing tracks due to decays of the long-lived $\hat{\pi}_3^\pm$ meson. The dashed lines indicate model-independent upper bounds on this cross section based on the ATLAS searches in Refs. [196, 192] and using the re-interpretation methods provided by Ref. [172]. This shows a strong lower bound on the $\hat{\pi}_3$ meson mass m_π of $\sim 1.2\,\text{TeV}$.

more recent search limit on the visible cross section while taking advantage of the previous search reinterpretation methods provides a rough estimate that assumes the two searches have similar signal efficiencies. In Fig. 6 we show the visible cross section computed in our model as a function of the $\hat{\pi}_3$ mass. The efficiency is $\mathcal{O}(0.1)\%$ across the mass range in the figure. We find that the more recent search constrains the $\hat{\pi}_3$ mass to be $m_\pi \gtrsim 1.2\,\text{TeV}$.

The $\hat{\pi}_3$ production rate is independent of f_π, N_c, and N_f (unlike the resonance signature discussed in the upcoming section). This result therefore imposes a remarkably strong lower bound on the masses of all mesons in the spectrum, particularly since the $\hat{\pi}_3$ is the lightest state. Recall from Sec. 3.2.3 that the relationship between the $\hat{\pi}_3$ mass and the $\hat{\eta}_5$ mass m_η is somewhat uncertain due to its dependence on the UV cutoff of the meson EFT. Therefore, we cannot

directly translate the bound on m_π into a bound on m_η, but we can estimate based on the scaling discussed in Sec. 3.2.3 that $m_\eta - m_\pi$ is roughly within an $\mathcal{O}(1)$ factor of f_π. This places an even larger lower bound on m_η that complements the constraints we show in Sec. 3.6.2.

3.6.2 Anomaly-induced Resonances: A 5-plet Signature. The $\hat{\eta}_5$ mesons can be singly produced through VBF and dominantly decay to pairs of electroweak bosons via the anomaly explained in Sec. 3.3.2 and shown in Fig. 3. Recall that while the $\hat{\pi}_3$ exists in the spectrum for all $N_f \geq 2$, the $\hat{\eta}_5$ is only present for $N_f \geq 3$. As a concrete benchmark, we set $N_f = 4$ in this section, but changing N_f simply modifies cross sections by $\mathcal{O}(1)$ factors explained in Eqs. (3.29) and (3.30). Setting $N_f = 4$ is a motivated choice, since it results in larger production rates than $N_f = 3$, and having $N_f \geq 5$ often leads to nearby Landau poles in the $\mathrm{SU}(2)_L$ running coupling, as discussed in Chapter II.

There are many LHC searches for resonances decaying to two electroweak bosons. Various final states have been exploited, including diphoton [203, 205], ZZ in the fully leptonic channel [199, 206], W^+W^- and/or ZZ in the semileptonic channel [200, 202], $W^\pm Z$ [198, 201], and same sign W pairs [201, 204]. Each of these searches quotes limits on the total production cross sections of a scalar resonantly produced via VBF and decaying to each pair of bosons (except the diphoton searches, which do not specify the production channel).[13]

We show the upper limits on the cross sections from each search in Fig. 7.[14] While the diphoton searches probe the lowest cross sections, the branching ratio of

[13] The diphoton search in Ref. [203] quotes a limit on the fiducial cross section, which is defined in terms of generator-level cuts. These cuts modify our cross sections only by a small $\mathcal{O}(1)$ factor.

[14] The searches in Refs. [207, 208] target the γZ final state, which is a principal decay mode of the $\hat{\eta}_5^0$, but these specialize to the gluon-gluon fusion production channel, so we do not include them.

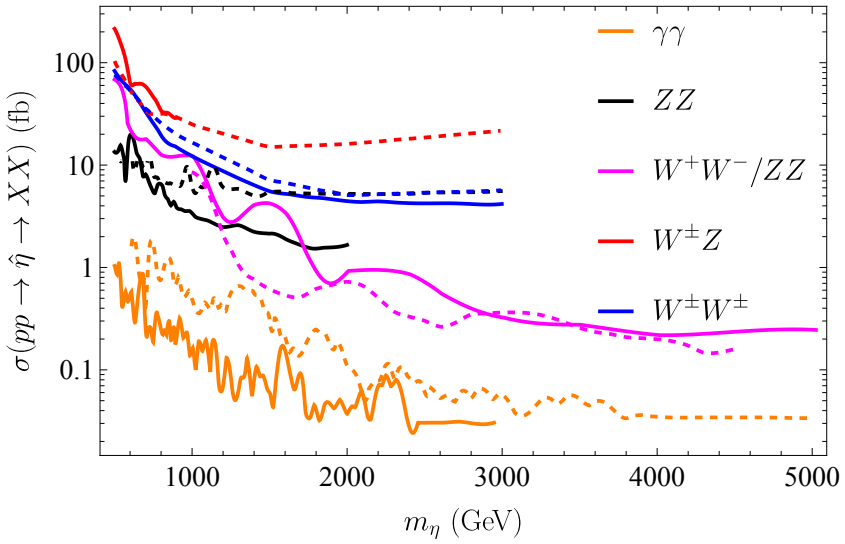


Figure 7. Upper bounds on the cross section to produce various final states from the searches in Refs. [198–206] through resonant production and decay of the scalar $\hat{\eta}$. Solid (dashed) lines correspond to ATLAS (CMS) searches. The ZZ searches used the fully leptonic channel, and the W^+W^-/ZZ searches used the semileptonic channel. In the context of our model, the $\hat{\eta}$ is one of the pNGBs of dark chiral symmetry breaking in the $\mathrm{SU}(2)_L$ 5-plet. Besides the diphoton searches, each of these is specialized to production via VBF. We interpret these upper bounds as lower bounds on $4\pi f_\pi/N_c$ in Fig. 8.

$\hat{\eta}_5^0 \to \gamma\gamma$ is about 4%, and the branching ratios to W^+W^- and ZZ are each roughly 1/3. Likewise, the same sign W searches tend to probe higher cross sections than other final states, but this is the principal decay mode of the $\hat{\eta}_5^{\pm\pm}$. Therefore, it is not obvious *a priori* which search imposes the strongest constraint on the model, and future searches for final states that currently impose weaker bounds may become competitive with searches for other final states if they attain greater signal efficiency.

To get a sense of the $\hat{\eta}_5$ decay widths, we can use the partial width

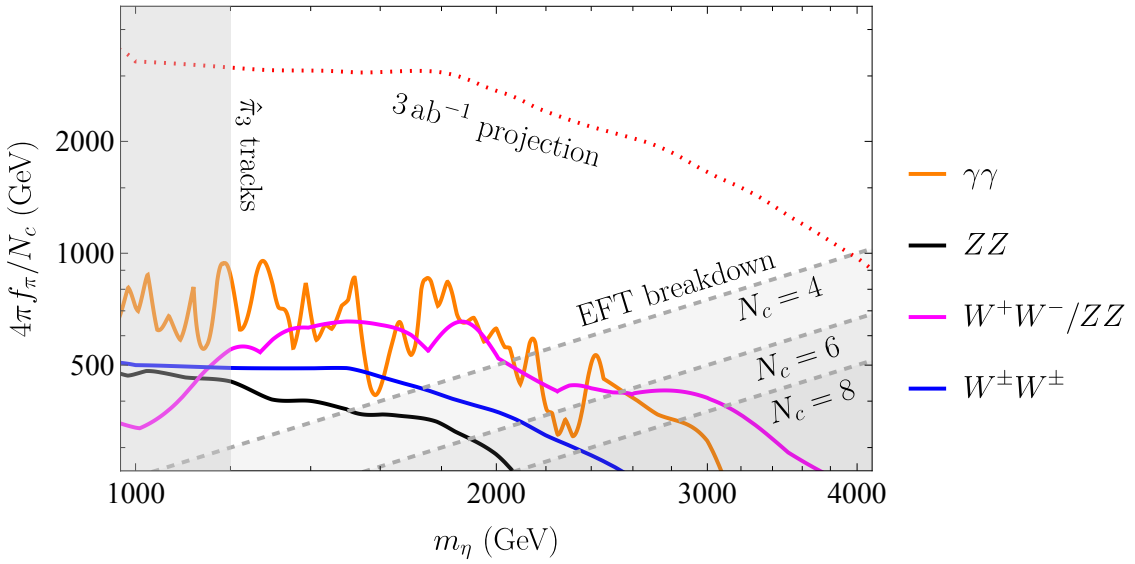


Figure 8. Lower bounds on the ratio $4\pi f_\pi/N_c$ as a function of the $\hat{\eta}_5$ meson mass m_η using the strongest constraints in Fig. 7 for each diboson final state. The gray contours indicate lower bounds on $4\pi f_\pi/N_c$ for a few values of N_c, below which $m_\eta > 4\pi f_\pi$ and the EFT of mesons breaks down. The region with $m_\eta < 1.2\,\text{TeV}$ is excluded by the disappearing tracks analysis in Sec. 3.6.1. The dotted red contour indicates a projection from a naïve luminosity rescaling of the expected limits of the searches with the strongest constraints on our model for a $3\,\text{ab}^{-1}$ dataset.

$$\begin{aligned}\Gamma(\hat{\eta}_5^0 \to \gamma\gamma) &= \frac{2}{\pi}\alpha^2\, m_\eta^3 \left(\frac{N_c}{4\pi f_\pi}\right)^2 \\ &\simeq 0.039\,\text{GeV}\left(\frac{m_\eta}{1\,\text{TeV}}\right)^3 \left(\frac{1\,\text{TeV}}{4\pi f_\pi/N_c}\right)^2,\end{aligned} \tag{3.55}$$

where $\alpha \simeq 1/128$ is the electromagnetic coupling, and $N_f = 4$. Since the branching ratio to diphoton is $\sim$ 4%, the total widths Γ_η are $\mathcal{O}(1)\,\text{GeV}$ when the other relevant mass scales are $\mathcal{O}(1)\,\text{TeV}$. Likewise, the ratio Γ_η/m_η is $\mathcal{O}(10^{-3})$, so the narrow width approximation is valid in this regime.

In Fig. 8, we use the fact that the cross section scales as $(N_c/f_\pi)^2$ to recast the upper bounds on the production cross sections in Fig. 7 as lower bounds on the ratio $4\pi f_\pi/N_c$ as a function of m_η. The searches for diphoton and W^+W^-/ZZ in the semileptonic channel impose very similar constraints, and the same sign W and

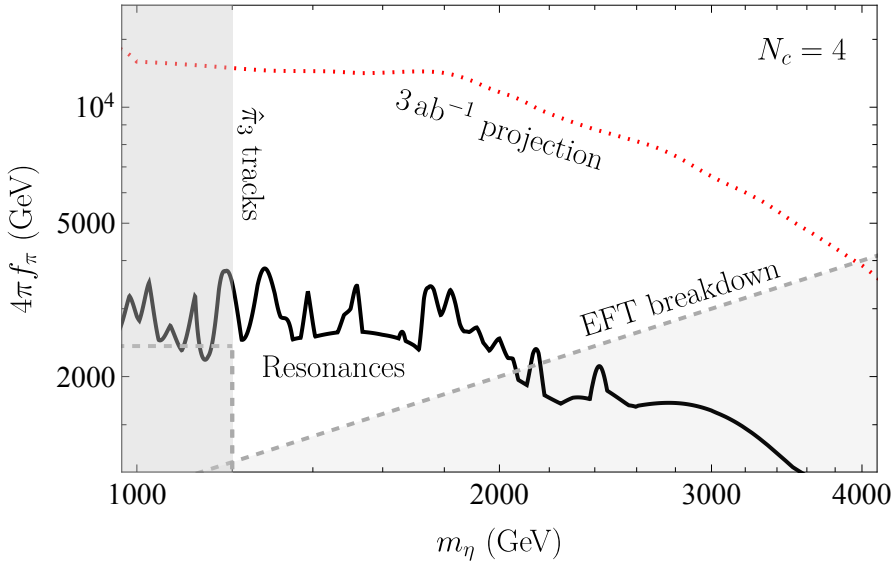


Figure 9. Lower bounds on $4\pi f_\pi$ as a function of the $\hat{\eta}_5$ meson mass m_η in the case of $N_c = 4$. Existing and projected resonance constraints due to the 5-plet anomaly, constraints from disappearing tracks due to the dark meson 3-plet $\hat{\pi}_3$, and the meson EFT breakdown where $m_\eta > 4\pi f_\pi$ are shown as in Fig. 8. The disappearing tracks constraint below $4\pi f_\pi = 2.4\,\text{TeV}$ is indicated by a dashed line, where pair production of $\hat{\pi}_3$ mesons with a mass of 1.2 TeV is outside the EFT regime of validity.

fully leptonic ZZ constraints are only an $\mathcal{O}(1)$ factor below. Constraints due to $W^\pm Z$ searches are not shown, as they are too weak to exclude any valid parameter space.

While we cannot precisely compute $m_\eta - m_\pi$, we know $m_\eta > m_\pi$, so the disappearing tracks analysis in Sec. 3.6.1 excludes the region where $m_\eta \lesssim 1.2\,\text{TeV}$. The figure also shows contours where $m_\eta = 4\pi f_\pi$ for a few values of N_c. For values of f_π/N_c below these contours, one is probing the theory at a scale outside of the EFT's regime of validity, so that range of parameters is not physical. Our comparison of the $\hat{\pi}_3$ constraint with the $\hat{\eta}_5$ constraints presents another possible issue of EFT validity. The $\hat{\pi}_3$ pair production mechanisms we consider occur via marginal operators, so we can always implicitly enforce in Fig. 6 that the EFT

scale $4\pi f_\pi$ is greater than the invariant mass of the $\hat{\pi}_3$ pairs. However, for smaller values of $4\pi f_\pi$ in Fig. 8, *pairs* of $\hat{\pi}_3$ mesons with masses of 1.2 TeV may have a greater invariant mass than the EFT scale, in which case the disappearing tracks constraint does not have a sensible interpretation within the EFT. This issue is most pronounced for smaller values of N_c.

In Fig. 9, we show the anomaly-induced resonance constraints for the choice of $N_c = 4$ and find that the bound on $4\pi f_\pi$ is greater than 2 TeV for the full $\hat{\eta}_5$ mass range within the EFT's regime of validity. Recall from Sec. 3.2.3 that heavier meson resonances may become visible when $4\pi f_\pi \lesssim 2\,\text{TeV}$. The figure shows that the anomaly-induced resonance signatures are at least competitive with those of the vector mesons, and they may be dominant. However, this 2 TeV estimate is predicated on a loose analogy between our model and the dark sector studied in Refs. [9] and [10]. The actual mass threshold where vector resonances gain importance depends strongly on details of the model such as N_c, the $\hat{\rho}/\hat{\pi}$ mass ratio, and the branching ratios of the $\hat{\rho}$ decays to other meson species. A thorough analysis of the vector meson phenomenology is beyond the scope of this work.

The constraints we derived in this section apply to meson mass scales up to multiple TeV and depend on f_π and N_c, while the disappearing tracks constraints in Sec. 3.6.1 apply to mass scales of $\sim$1 TeV and do not depend (at least explicitly) on f_π or N_c. These two strategies are therefore complementary and represent exciting opportunities for future searches.

In Figs. 8 and 9, we also show projected bounds from a naïve luminosity rescaling of the expected limits from the searches with the strongest constraints on $4\pi f_\pi/N_c$. Specifically, we take the expected constraint on the cross section from each search, compute the corresponding constraints on $4\pi f_\pi/N_c$, and re-scale

these constraints by $\sqrt{3\,\text{ab}^{-1}/L}$ with L each search's luminosity. We then take the maximum of these re-scaled constraints for each value of m_η as the projected constraint. This projection demonstrates that if future searches attain similar signal efficiencies to existing searches, and if the High-Luminosity LHC acquires a dataset of $3\,\text{ab}^{-1}$, then such searches could reach a significantly larger region of parameter space.

3.7 Conclusion

This paper studied dark mesons arising in the confined phase of a strongly-coupled sector with vector-like dark quarks. We chose the dark quarks to be in the fundamental representation of a new confining $\text{SU}(N_c)$ and the N_f-dimensional representation of $\text{SU}(2)_L$. Considering the limit where the dark quark mass is much less than the dark confinement scale, we discussed the spectrum of $\text{SU}(2)_L$ representations of these mesons, their masses, and their transformations under various $\mathbb{Z}_2$ symmetries including a dark G-parity. We then studied two exotic collider signatures of the dark mesons in detail:

- The G-odd mesons are long-lived and therefore excellent targets for current and future LLP searches. In particular, the singly charged 3-plet $\hat{\pi}_3^\pm$ give rise to disappearing track signals.

- If $N_f \geq 3$, there is a G-even 5-plet meson $\hat{\eta}_5$ in the spectrum, which we showed is the unique pNGB of the dark sector chiral symmetry breaking that has an anomaly with $\text{SU}(2)_L$. This anomaly enables the $\hat{\eta}_5$ to be resonantly produced through VBF and decay to pairs of electroweak bosons with a rate that depends on N_c and the dark pion decay constant f_π.

We used the reinterpretation framework from Ref. [172] and the disappearing tracks searches in Refs. [196] and [192] to place a strikingly strong lower bound on the $\hat{\pi}_3$ mass m_π of $\sim 1.2\,\text{TeV}$. We also used the searches for scalar resonances decaying to electroweak boson pairs in Refs. [201, 199, 200, 202–206] to derive lower bounds on the ratio $4\pi f_\pi/N_c$ as a function of the $\hat{\eta}_5$ mass m_η. Measuring the rates of the anomaly-induced processes could help reconstruct N_c and N_f, thereby revealing a great deal about the UV theory while only measuring states in the IR. These anomaly-induced resonances therefore remain an exciting target for diboson searches, including those using the unusual same sign W final state.

The model under study is an example of a confining dark sector with $\mathcal{H}$-parity [12]. The baryons in such models may be viable dark matter candidates that are characteristically challenging to probe via direct detection despite having constituents that are electrically charged. This is particularly true in the Noble Dark Matter case defined in Chapter II, where the dark matter candidate is either a total SM singlet or a singlet with a small mixing with other states. As discussed in Ref. [12] and Chapter II, there are various opportunities for further analyzing the early universe dynamics, indirect detection, and astrophysical signatures of these dark matter scenarios. The results of this work show that a broad space of parameters with light 3-plet mesons or collider-scale 5-plet mesons is already ruled out, and future analyses can focus on other cases.

Several natural extensions of this work remain to be explored. While G-parity may stabilize some of the meson species on a detector timescale, the possibility of G violation by Planck-suppressed dimension-5 operators threatens the model's cosmological safety unless G is broken at a sub-Planckian scale that

shortens the lifetime to below the timescale of Big Bang Nucleosynthesis. The lifetime could still be well beyond the detector scale, which is the case we consider in this work, but interesting new signals may emerge if the neutral $\hat{\pi}$ mesons can decay within the detector. For example, the $\hat{\pi}_3^{\pm}$ could leave a track that disappears within the tracker but points to a displaced energy deposit within the calorimeter where the $\hat{\pi}_3^0$ decays later. Measuring this process would probe the scale of G violation, and we leave the analysis of such signals for future work. Likewise, decays of pair-produced mesons in representations larger than the **5** that hop down to lower representations may lead to interesting signals from emission of multiple electroweak bosons, and measuring the rate for such processes would help reconstruct f_π.

We focused on the light quark limit with $4\pi f_\pi \gtrsim 2\,\text{TeV}$ because of the simplicity of the meson EFT. A smaller f_π would result in complications due to having a tower of lighter excited meson states. A natural direction for future studies would be to include consideration of the vector mesons in our model, along the lines of the discussion in Refs. [9] and [10] for a similar dark sector. Our dark $\hat{\rho}$ mesons can mix with the SM W and Z, leading to resonance signals that may be competitive with those discussed in this work when f_π is sufficiently small. The flavor-singlet $\hat{\eta}'$ may also play an important role as an additional anomaly-induced resonance.

Another small modification to our regime is the heavy quark limit (studied in Chapter II in the context of dark baryons). Here, producing dark sector states at a collider would probe the theory at a scale beyond the meson EFT's regime of validity. Instead, one would produce quirks [24], where a quark/anti-quark pair is joined by an unbroken flux tube and non-perturbatively radiates dark glueballs,

photons, *etc.* before annihilating. Such a regime would have distinct signals from those presented here that are also more difficult to model. An advantage of heavy quarks is the ability to compute the hadron mass spectrum in perturbation theory, thereby avoiding ambiguities such as the $\hat{\pi}_3$-$\hat{\eta}_5$ mass splitting discussed above. One can also exploit the squeezeout mechanism in the heavy quark limit for determining the dark matter relic abundance of the dark baryons [88–90]. (In either the heavy- or light-quark limit, a matter/anti-matter asymmetry in the dark sector may be necessary for the dark baryons to have the relic abundance of dark matter [8, 88–90].) The light and heavy quark limits are therefore qualitatively different, and each merits further investigation.

The work presented here shows an example of how dark matter models with $\mathcal{H}$-parity can be (counter-intuitively) more easily discovered at colliders than other experiments searching for dark sectors with electroweak interactions. The 5-plet anomaly also serves as an example of how the rich spectra of confining dark sectors can enable a variety of counter-intuitive search strategies for physics beyond the Standard Model.

REFERENCES CITED

[1] P. Asadi, A. Batz, and G. D. Kribs, "Noble dark matter: Surprising elusiveness of dark baryons," *Phys. Rev. D* **111** (May, 2025) 095025, 2412.14240. https://link.aps.org/doi/10.1103/PhysRevD.111.095025.

[2] P. Asadi, A. Batz, E. Bernreuther, M. Costa, S. Homiller, and G. D. Kribs, "Stopping dark mesons in their tracks with long-lived particle and resonant signatures," *JHEP* **03** (2026) 234, arXiv:2507.13430 [hep-ph].

[3] M. Cirelli, A. Strumia, and J. Zupan, "Dark Matter," arXiv:2406.01705 [hep-ph].

[4] C. Kilic, T. Okui, and R. Sundrum, "Vectorlike Confinement at the LHC," *JHEP* **02** (2010) 018, arXiv:0906.0577 [hep-ph].

[5] Y. Bai and R. J. Hill, "Weakly Interacting Stable Pions," *Phys. Rev. D* **82** (2010) 111701, arXiv:1005.0008 [hep-ph].

[6] O. Antipin, M. Redi, and A. Strumia, "Dynamical generation of the weak and Dark Matter scales from strong interactions," *JHEP* **01** (2015) 157, arXiv:1410.1817 [hep-ph].

[7] T. Appelquist *et al.*, "Stealth Dark Matter: Dark scalar baryons through the Higgs portal," *Phys. Rev. D* **92** no. 7, (2015) 075030, arXiv:1503.04203 [hep-ph].

[8] A. Mitridate, M. Redi, J. Smirnov, and A. Strumia, "Dark Matter as a weakly coupled Dark Baryon," *JHEP* **10** (2017) 210, arXiv:1707.05380 [hep-ph].

[9] G. D. Kribs, A. Martin, and T. Tong, "Effective Theories of Dark Mesons with Custodial Symmetry," *JHEP* **08** (2019) 020, arXiv:1809.10183 [hep-ph].

[10] G. D. Kribs, A. Martin, B. Ostdiek, and T. Tong, "Dark Mesons at the LHC," *JHEP* **07** (2019) 133, arXiv:1809.10184 [hep-ph].

[11] T. Abe, R. Sato, and T. Yamanaka, "Composite Dark Matter with Forbidden Annihilation," arXiv:2404.03963 [hep-ph].

[12] P. Asadi, G. D. Kribs, and C. J. H. Mantel, "Direct detection of dark baryons naturally suppressed by $\mathcal{H}$-parity," *Phys. Rev. D* **111** (May, 2025) 095030, 2410.23631. https://link.aps.org/doi/10.1103/PhysRevD.111.095030.

[13] R. Essig, "Direct Detection of Non-Chiral Dark Matter," *Phys. Rev. D* **78** (2008) 015004, arXiv:0710.1668 [hep-ph].

[14] J. Hisano, K. Ishiwata, and N. Nagata, "A complete calculation for direct detection of Wino dark matter," *Phys. Lett. B* **690** (2010) 311–315, arXiv:1004.4090 [hep-ph].

[15] R. J. Hill and M. P. Solon, "Standard Model anatomy of WIMP dark matter direct detection I: weak-scale matching," *Phys. Rev. D* **91** (2015) 043504, arXiv:1401.3339 [hep-ph].

[16] R. J. Hill and M. P. Solon, "Standard Model anatomy of WIMP dark matter direct detection II: QCD analysis and hadronic matrix elements," *Phys. Rev. D* **91** (2015) 043505, arXiv:1409.8290 [hep-ph].

[17] C.-Y. Chen, R. J. Hill, M. P. Solon, and A. M. Wijangco, "Power Corrections to the Universal Heavy WIMP-Nucleon Cross Section," *Phys. Lett. B* **781** (2018) 473–479, arXiv:1801.08551 [hep-ph].

[18] S. Bottaro, D. Buttazzo, M. Costa, R. Franceschini, P. Panci, D. Redigolo, and L. Vittorio, "Closing the window on WIMP Dark Matter," *Eur. Phys. J. C* **82** no. 1, (2022) 31, arXiv:2107.09688 [hep-ph].

[19] S. Bottaro, D. Buttazzo, M. Costa, R. Franceschini, P. Panci, D. Redigolo, and L. Vittorio, "The last complex WIMPs standing," *Eur. Phys. J. C* **82** no. 11, (2022) 992, arXiv:2205.04486 [hep-ph].

[20] Q. Chen, G.-J. Ding, and R. J. Hill, "General heavy WIMP nucleon elastic scattering," *Phys. Rev. D* **108** no. 11, (2023) 116023, arXiv:2309.02715 [hep-ph].

[21] I. M. Bloch, S. Bottaro, D. Redigolo, and L. Vittorio, "Looking for WIMPs through the neutrino fogs," arXiv:2410.02723 [hep-ph].

[22] M. J. Strassler and K. M. Zurek, "Echoes of a hidden valley at hadron colliders," *Phys. Lett. B* **651** (2007) 374–379, arXiv:hep-ph/0604261.

[23] T. Han, Z. Si, K. M. Zurek, and M. J. Strassler, "Phenomenology of hidden valleys at hadron colliders," *JHEP* **07** (2008) 008, arXiv:0712.2041 [hep-ph].

[24] J. Kang and M. A. Luty, "Macroscopic Strings and 'Quirks' at Colliders," *JHEP* **11** (2009) 065, arXiv:0805.4642 [hep-ph].

[25] J. E. Juknevich, D. Melnikov, and M. J. Strassler, "A Pure-Glue Hidden Valley I. States and Decays," *JHEP* **07** (2009) 055, arXiv:0903.0883 [hep-ph].

[26] G. D. Kribs, T. S. Roy, J. Terning, and K. M. Zurek, "Quirky Composite Dark Matter," *Phys. Rev. D* **81** (2010) 095001, arXiv:0909.2034 [hep-ph].

[27] J. E. Juknevich, "Pure-glue hidden valleys through the Higgs portal," *JHEP* **08** (2010) 121, arXiv:0911.5616 [hep-ph].

[28] R. Harnik, G. D. Kribs, and A. Martin, "Quirks at the Tevatron and Beyond," *Phys. Rev. D* **84** (2011) 035029, arXiv:1106.2569 [hep-ph].

[29] M. Frigerio, A. Pomarol, F. Riva, and A. Urbano, "Composite Scalar Dark Matter," *JHEP* **07** (2012) 015, arXiv:1204.2808 [hep-ph].

[30] P. Schwaller, D. Stolarski, and A. Weiler, "Emerging Jets," *JHEP* **05** (2015) 059, arXiv:1502.05409 [hep-ph].

[31] T. Cohen, M. Lisanti, and H. K. Lou, "Semivisible Jets: Dark Matter Undercover at the LHC," *Phys. Rev. Lett.* **115** no. 17, (2015) 171804, arXiv:1503.00009 [hep-ph].

[32] A. Carmona and M. Chala, "Composite Dark Sectors," *JHEP* **06** (2015) 105, arXiv:1504.00332 [hep-ph].

[33] S. Knapen, S. Pagan Griso, M. Papucci, and D. J. Robinson, "Triggering Soft Bombs at the LHC," *JHEP* **08** (2017) 076, arXiv:1612.00850 [hep-ph].

[34] S. Knapen, H. K. Lou, M. Papucci, and J. Setford, "Tracking down Quirks at the Large Hadron Collider," *Phys. Rev. D* **96** no. 11, (2017) 115015, arXiv:1708.02243 [hep-ph].

[35] J. A. Evans and M. A. Luty, "Stopping Quirks at the LHC," *JHEP* **06** (2019) 090, arXiv:1811.08903 [hep-ph].

[36] E. Bernreuther, F. Kahlhoefer, M. Krämer, and P. Tunney, "Strongly interacting dark sectors in the early Universe and at the LHC through a simplified portal," *JHEP* **01** (2020) 162, arXiv:1907.04346 [hep-ph].

[37] E. Bernreuther, T. Finke, F. Kahlhoefer, M. Krämer, and A. Mück, "Casting a graph net to catch dark showers," *SciPost Phys.* **10** no. 2, (2021) 046, arXiv:2006.08639 [hep-ph].

[38] S. Knapen, J. Shelton, and D. Xu, "Perturbative benchmark models for a dark shower search program," *Phys. Rev. D* **103** no. 11, (2021) 115013, arXiv:2103.01238 [hep-ph].

[39] J. Barron, D. Curtin, G. Kasieczka, T. Plehn, and A. Spourdalakis, "Unsupervised hadronic SUEP at the LHC," *JHEP* **12** (2021) 129, arXiv:2107.12379 [hep-ph].

[40] T. Kuwahara and S.-R. Yuan, "Dark vector mesons at LHC forward detector searches," *JHEP* **06** (2023) 208, arXiv:2303.03736 [hep-ph].

[41] A. Batz, T. Cohen, D. Curtin, C. Gemmell, and G. D. Kribs, "Dark sector glueballs at the LHC," *JHEP* **04** (2024) 070, arXiv:2310.13731 [hep-ph].

[42] J. Bagnasco, M. Dine, and S. D. Thomas, "Detecting technibaryon dark matter," *Phys. Lett. B* **320** (1994) 99–104, arXiv:hep-ph/9310290.

[43] D. S. M. Alves, S. R. Behbahani, P. Schuster, and J. G. Wacker, "Composite Inelastic Dark Matter," *Phys. Lett. B* **692** (2010) 323–326, arXiv:0903.3945 [hep-ph].

[44] D. Spier Moreira Alves, S. R. Behbahani, P. Schuster, and J. G. Wacker, "The Cosmology of Composite Inelastic Dark Matter," *JHEP* **06** (2010) 113, arXiv:1003.4729 [hep-ph].

[45] M. R. Buckley and E. T. Neil, "Thermal dark matter from a confining sector," *Phys. Rev. D* **87** no. 4, (2013) 043510, arXiv:1209.6054 [hep-ph].

[46] S. Bhattacharya, B. Melić, and J. Wudka, "Pionic Dark Matter," *JHEP* **02** (2014) 115, arXiv:1307.2647 [hep-ph].

[47] O. Antipin, M. Redi, A. Strumia, and E. Vigiani, "Accidental Composite Dark Matter," *JHEP* **07** (2015) 039, arXiv:1503.08749 [hep-ph].

[48] E. Hardy, R. Lasenby, J. March-Russell, and S. M. West, "Signatures of Large Composite Dark Matter States," *JHEP* **07** (2015) 133, arXiv:1504.05419 [hep-ph].

[49] V. De Luca, A. Mitridate, M. Redi, J. Smirnov, and A. Strumia, "Colored Dark Matter," *Phys. Rev. D* **97** no. 11, (2018) 115024, arXiv:1801.01135 [hep-ph].

[50] R. Contino, A. Podo, and F. Revello, "Composite Dark Matter from Strongly-Interacting Chiral Dynamics," *JHEP* **02** (2021) 091, arXiv:2008.10607 [hep-ph].

[51] W. Detmold, M. McCullough, and A. Pochinsky, "Dark Nuclei I: Cosmology and Indirect Detection," *Phys. Rev. D* **90** no. 11, (2014) 115013, arXiv:1406.2276 [hep-ph].

[52] A. Soni and Y. Zhang, "Hidden SU(N) Glueball Dark Matter," *Phys. Rev. D* **93** no. 11, (2016) 115025, arXiv:1602.00714 [hep-ph].

[53] R. Mahbubani, M. Redi, and A. Tesi, "Indirect detection of composite asymmetric dark matter," *Phys. Rev. D* **101** no. 10, (2020) 103037, arXiv:1908.00538 [hep-ph].

[54] J. M. Cline, Z. Liu, G. D. Moore, and W. Xue, "Composite strongly interacting dark matter," *Phys. Rev. D* **90** no. 1, (2014) 015023, arXiv:1312.3325 [hep-ph].

[55] K. K. Boddy, J. L. Feng, M. Kaplinghat, and T. M. P. Tait, "Self-Interacting Dark Matter from a Non-Abelian Hidden Sector," *Phys. Rev. D* **89** no. 11, (2014) 115017, arXiv:1402.3629 [hep-ph].

[56] G. Krnjaic and K. Sigurdson, "Big Bang Darkleosynthesis," *Phys. Lett. B* **751** (2015) 464–468, arXiv:1406.1171 [hep-ph].

[57] M. A. Buen-Abad, G. Marques-Tavares, and M. Schmaltz, "Non-Abelian dark matter and dark radiation," *Phys. Rev. D* **92** no. 2, (2015) 023531, arXiv:1505.03542 [hep-ph].

[58] C. Gross, A. Mitridate, M. Redi, J. Smirnov, and A. Strumia, "Cosmological Abundance of Colored Relics," *Phys. Rev. D* **99** no. 1, (2019) 016024, arXiv:1811.08418 [hep-ph].

[59] L. Morrison, S. Profumo, and D. J. Robinson, "Large N-ightmare Dark Matter," *JCAP* **05** (2021) 058, arXiv:2010.03586 [hep-ph].

[60] R. Contino, K. Max, and R. K. Mishra, "Searching for elusive dark sectors with terrestrial and celestial observations," *JHEP* **06** (2021) 127, arXiv:2012.08537 [hep-ph].

[61] R. Garani, M. Redi, and A. Tesi, "Dark QCD matters," *JHEP* **12** (2021) 139, arXiv:2105.03429 [hep-ph].

[62] R. Krall and M. Reece, "Last Electroweak WIMP Standing: Pseudo-Dirac Higgsino Status and Compact Stars as Future Probes," *Chin. Phys. C* **42** no. 4, (2018) 043105, arXiv:1705.04843 [hep-ph].

[63] A. De Rujula, H. Georgi, and S. L. Glashow, "Hadron Masses in a Gauge Theory," *Phys. Rev. D* **12** (1975) 147–162.

[64] A. Manohar and H. Georgi, "Chiral Quarks and the Nonrelativistic Quark Model," *Nucl. Phys. B* **234** (1984) 189–212.

[65] H. Georgi, *Weak Interactions and Modern Particle Theory*. 1984.

[66] M. De Sanctis, "A generalization of the Fermi-Breit equation to non-Coulombic spatial interactions," *Eur. Phys. J. A* **41** (2009) 169–178.

[67] M. Cirelli, N. Fornengo, and A. Strumia, "Minimal dark matter," *Nucl. Phys. B* **753** (2006) 178–194, arXiv:hep-ph/0512090.

[68] D. Djukanovic, J. Gegelia, and U.-G. Meißner, "Triviality of quantum electrodynamics revisited," *Commun. Theor. Phys.* **69** no. 3, (2018) 263, arXiv:1706.10039 [hep-th].

[69] D. S. M. Alves, J. Galloway, J. T. Ruderman, and J. R. Walsh, "Running Electroweak Couplings as a Probe of New Physics," *JHEP* **02** (2015) 007, arXiv:1410.6810 [hep-ph].

[70] V. Berestetskii, E. Lifshitz, and L. Pitaevskii, *Quantum Electrodynamics: Volume 4*. Course of theoretical physics. Elsevier Science, 1982. https://books.google.com/books?id=URL5NKX8vbAC.

[71] J. F. Donoghue, E. Golowich, and B. R. Holstein, *Dynamics of the standard model*, vol. 2. CUP, 2014.

[72] D. J. Griffiths and D. F. Schroeter, *Introduction to Quantum Mechanics*. Cambridge University Press, 3 ed., 2018.

[73] M. D. Schwartz, *Quantum Field Theory and the Standard Model*. Cambridge University Press, 3, 2014.

[74] M. E. Peskin and D. V. Schroeder, *An Introduction to quantum field theory*. Addison-Wesley, Reading, USA, 1995.

[75] G. M. Prosperi, M. Raciti, and C. Simolo, "On the running coupling constant in QCD," *Prog. Part. Nucl. Phys.* **58** (2007) 387–438, arXiv:hep-ph/0607209.

[76] R. Corless, G. Gonnet, D. Hare, D. Jeffrey, and D. Knuth, "On the lambert W function," *Advances in Computational Mathematics* **5** (01, 1996) 329–359.

[77] W. Detmold, M. McCullough, and A. Pochinsky, "Dark nuclei. II. Nuclear spectroscopy in two-color QCD," *Phys. Rev. D* **90** no. 11, (2014) 114506, arXiv:1406.4116 [hep-lat].

[78] **LZ Collaboration** Collaboration, J. Aalbers *et al.*, "Dark Matter Search Results from 4.2 Tonne-Years of Exposure of the LUX-ZEPLIN (LZ) Experiment," arXiv:2410.17036 [hep-ex].

[79] **XENON** Collaboration, E. Aprile *et al.*, "Physics reach of the XENON1T dark matter experiment," *JCAP* **04** (2016) 027, arXiv:1512.07501 [physics.ins-det].

[80] C. Blanco, Y. Kahn, B. Lillard, and S. D. McDermott, "Dark Matter Daily Modulation With Anisotropic Organic Crystals," *Phys. Rev. D* **104** (2021) 036011, arXiv:2103.08601 [hep-ph].

[81] C. Blanco, I. Harris, Y. Kahn, B. Lillard, and J. Pérez-Ríos, "Molecular Migdal effect," *Phys. Rev. D* **106** no. 11, (2022) 115015, arXiv:2208.09002 [hep-ph].

[82] D. Tucker-Smith and N. Weiner, "Inelastic dark matter," *Phys. Rev. D* **64** (2001) 043502, arXiv:hep-ph/0101138.

[83] S. Chang, N. Weiner, and I. Yavin, "Magnetic Inelastic Dark Matter," *Phys. Rev. D* **82** (2010) 125011, arXiv:1007.4200 [hep-ph].

[84] K. Kumar, A. Menon, and T. M. P. Tait, "Magnetic Fluffy Dark Matter," *JHEP* **02** (2012) 131, arXiv:1111.2336 [hep-ph].

[85] J. Eby, P. J. Fox, and G. D. Kribs, "Earth-Catalyzed Detection of Magnetic Inelastic Dark Matter with Photons in Large Underground Detectors," arXiv:2312.08478 [hep-ph].

[86] G. Ovanesyan and L. Vecchi, "Direct detection of dark matter polarizability," *JHEP* **07** (2015) 128, arXiv:1410.0601 [hep-ph].

[87] B. J. Kavanagh, P. Panci, and R. Ziegler, "Faint Light from Dark Matter: Classifying and Constraining Dark Matter-Photon Effective Operators," *JHEP* **04** (2019) 089, arXiv:1810.00033 [hep-ph].

[88] P. Asadi, E. D. Kramer, E. Kuflik, G. W. Ridgway, T. R. Slatyer, and J. Smirnov, "Thermal squeezeout of dark matter," *Phys. Rev. D* **104** no. 9, (2021) 095013, arXiv:2103.09827 [hep-ph].

[89] P. Asadi, E. D. Kramer, E. Kuflik, G. W. Ridgway, T. R. Slatyer, and J. Smirnov, "Accidentally Asymmetric Dark Matter," *Phys. Rev. Lett.* **127** no. 21, (2021) 211101, arXiv:2103.09822 [hep-ph].

[90] P. Asadi, E. D. Kramer, E. Kuflik, T. R. Slatyer, and J. Smirnov, "Glueballs in a thermal squeezeout model," *JHEP* **07** (2022) 006, arXiv:2203.15813 [hep-ph].

[91] B. Svetitsky and L. G. Yaffe, "Critical Behavior at Finite Temperature Confinement Transitions," *Nucl. Phys. B* **210** (1982) 423–447.

[92] C. Alexandrou, A. Borici, A. Feo, P. de Forcrand, A. Galli, F. Jegerlehner, and T. Takaishi, "The Deconfinement phase transition in one flavor QCD," *Phys. Rev. D* **60** (1999) 034504, arXiv:hep-lat/9811028.

[93] O. Kaczmarek, F. Karsch, E. Laermann, and M. Lutgemeier, "Heavy quark potentials in quenched QCD at high temperature," *Phys. Rev. D* **62** (2000) 034021, arXiv:hep-lat/9908010.

[94] B. Lucini, M. Teper, and U. Wenger, "The High temperature phase transition in SU(N) gauge theories," *JHEP* **01** (2004) 061, arXiv:hep-lat/0307017.

[95] B. Lucini, M. Teper, and U. Wenger, "Properties of the deconfining phase transition in SU(N) gauge theories," *JHEP* **02** (2005) 033, arXiv:hep-lat/0502003.

[96] Y. Aoki, G. Endrodi, Z. Fodor, S. D. Katz, and K. K. Szabo, "The Order of the quantum chromodynamics transition predicted by the standard model of particle physics," *Nature* **443** (2006) 675–678, arXiv:hep-lat/0611014.

[97] **WHOT-QCD** Collaboration, H. Saito, S. Ejiri, S. Aoki, T. Hatsuda, K. Kanaya, Y. Maezawa, H. Ohno, and T. Umeda, "Phase structure of finite temperature QCD in the heavy quark region," *Phys. Rev. D* **84** (2011) 054502, arXiv:1106.0974 [hep-lat]. [Erratum: Phys.Rev.D 85, 079902 (2012)].

[98] I. Goldman and S. Nussinov, "Weakly Interacting Massive Particles and Neutron Stars," *Phys. Rev. D* **40** (1989) 3221–3230.

[99] A. Gould, B. T. Draine, R. W. Romani, and S. Nussinov, "Neutron Stars: Graveyard of Charged Dark Matter," *Phys. Lett. B* **238** (1990) 337–343.

[100] C. Kouvaris and P. Tinyakov, "Can Neutron stars constrain Dark Matter?," *Phys. Rev. D* **82** (2010) 063531, arXiv:1004.0586 [astro-ph.GA].

[101] A. de Lavallaz and M. Fairbairn, "Neutron Stars as Dark Matter Probes," *Phys. Rev. D* **81** (2010) 123521, arXiv:1004.0629 [astro-ph.GA].

[102] S. D. McDermott, H.-B. Yu, and K. M. Zurek, "Constraints on Scalar Asymmetric Dark Matter from Black Hole Formation in Neutron Stars," *Phys. Rev. D* **85** (2012) 023519, arXiv:1103.5472 [hep-ph].

[103] C. Kouvaris and P. Tinyakov, "Excluding Light Asymmetric Bosonic Dark Matter," *Phys. Rev. Lett.* **107** (2011) 091301, arXiv:1104.0382 [astro-ph.CO].

[104] T. Güver, A. E. Erkoca, M. Hall Reno, and I. Sarcevic, "On the capture of dark matter by neutron stars," *JCAP* **05** (2014) 013, arXiv:1201.2400 [hep-ph].

[105] C. Kouvaris and P. Tinyakov, "Growth of Black Holes in the interior of Rotating Neutron Stars," *Phys. Rev. D* **90** no. 4, (2014) 043512, arXiv:1312.3764 [astro-ph.SR].

[106] J. Bramante and T. Linden, "Detecting Dark Matter with Imploding Pulsars in the Galactic Center," *Phys. Rev. Lett.* **113** no. 19, (2014) 191301, arXiv:1405.1031 [astro-ph.HE].

[107] J. Bramante, A. Delgado, and A. Martin, "Multiscatter stellar capture of dark matter," *Phys. Rev. D* **96** no. 6, (2017) 063002, arXiv:1703.04043 [hep-ph].

[108] C. Kouvaris, P. Tinyakov, and M. H. G. Tytgat, "NonPrimordial Solar Mass Black Holes," *Phys. Rev. Lett.* **121** no. 22, (2018) 221102, arXiv:1804.06740 [astro-ph.HE].

[109] R. Garani, Y. Genolini, and T. Hambye, "New Analysis of Neutron Star Constraints on Asymmetric Dark Matter," *JCAP* **05** (2019) 035, arXiv:1812.08773 [hep-ph].

[110] S. A. R. Ellis, "Premature black hole death of Population III stars by dark matter," *JCAP* **05** no. 05, (2022) 025, arXiv:2111.02414 [astro-ph.CO].

[111] S. Bhattacharya, B. Dasgupta, R. Laha, and A. Ray, "Can LIGO Detect Nonannihilating Dark Matter?," *Phys. Rev. Lett.* **131** no. 9, (2023) 091401, arXiv:2302.07898 [hep-ph].

[112] N. F. Bell, A. Melatos, and K. Petraki, "Realistic neutron star constraints on bosonic asymmetric dark matter," *Phys. Rev. D* **87** no. 12, (2013) 123507, arXiv:1301.6811 [hep-ph].

[113] J. Bramante, K. Fukushima, and J. Kumar, "Constraints on bosonic dark matter from observation of old neutron stars," *Phys. Rev. D* **87** no. 5, (2013) 055012, arXiv:1301.0036 [hep-ph].

[114] J. Bramante, K. Fukushima, J. Kumar, and E. Stopnitzky, "Bounds on self-interacting fermion dark matter from observations of old neutron stars," *Phys. Rev. D* **89** no. 1, (2014) 015010, arXiv:1310.3509 [hep-ph].

[115] M. I. Gresham and K. M. Zurek, "Asymmetric Dark Stars and Neutron Star Stability," *Phys. Rev. D* **99** no. 8, (2019) 083008, arXiv:1809.08254 [astro-ph.CO].

[116] R. K. Leane, T. Linden, P. Mukhopadhyay, and N. Toro, "Celestial-Body Focused Dark Matter Annihilation Throughout the Galaxy," *Phys. Rev. D* **103** no. 7, (2021) 075030, arXiv:2101.12213 [astro-ph.HE].

[117] **FCC** Collaboration, A. Abada *et al.*, "FCC Physics Opportunities: Future Circular Collider Conceptual Design Report Volume 1," *Eur. Phys. J. C* **79** no. 6, (2019) 474.

[118] **FCC** Collaboration, A. Abada *et al.*, "FCC-ee: The Lepton Collider: Future Circular Collider Conceptual Design Report Volume 2," *Eur. Phys. J. ST* **228** no. 2, (2019) 261–623.

[119] M. Cobal, C. De Dominicis, M. Fabbrichesi, E. Gabrielli, J. Magro, B. Mele, and G. Panizzo, "Z-boson decays into an invisible dark photon at the LHC, HL-LHC and future lepton colliders," *Phys. Rev. D* **102** no. 3, (2020) 035027, arXiv:2006.15945 [hep-ph].

[120] T. Han, Z. Liu, L.-T. Wang, and X. Wang, "WIMPs at High Energy Muon Colliders," *Phys. Rev. D* **103** no. 7, (2021) 075004, arXiv:2009.11287 [hep-ph].

[121] R. Mahbubani, P. Schwaller, and J. Zurita, "Closing the window for compressed Dark Sectors with disappearing charged tracks," *JHEP* **06** (2017) 119, arXiv:1703.05327 [hep-ph]. [Erratum: JHEP 10, 061 (2017)].

[122] H. Fukuda, N. Nagata, H. Otono, and S. Shirai, "Higgsino Dark Matter or Not: Role of Disappearing Track Searches at the LHC and Future Colliders," *Phys. Lett. B* **781** (2018) 306–311, arXiv:1703.09675 [hep-ph].

[123] M. Saito, R. Sawada, K. Terashi, and S. Asai, "Discovery reach for wino and higgsino dark matter with a disappearing track signature at a 100 TeV pp collider," *Eur. Phys. J. C* **79** no. 6, (2019) 469, arXiv:1901.02987 [hep-ph].

[124] R. Capdevilla, F. Meloni, R. Simoniello, and J. Zurita, "Hunting wino and higgsino dark matter at the muon collider with disappearing tracks," *JHEP* **06** (2021) 133, arXiv:2102.11292 [hep-ph].

[125] R. Capdevilla, F. Meloni, and J. Zurita, "Discovering Electroweak Interacting Dark Matter at Muon Colliders Using Soft Tracks," *Phys. Rev. Lett.* **134** no. 18, (2025) 181802, arXiv:2405.08858 [hep-ph].

[126] T. Cohen, M. Lisanti, H. K. Lou, and S. Mishra-Sharma, "LHC Searches for Dark Sector Showers," *JHEP* **11** (2017) 196, arXiv:1707.05326 [hep-ph].

[127] K. R. Dienes, D. Kim, T. T. Leininger, and B. Thomas, "Sequential displaced vertices: Novel collider signature for long-lived particles," *Phys. Rev. D* **106** no. 9, (2022) 095012, arXiv:2108.02204 [hep-ph].

[128] G. D. Kribs and E. T. Neil, "Review of strongly-coupled composite dark matter models and lattice simulations," *Int. J. Mod. Phys. A* **31** no. 22, (2016) 1643004, arXiv:1604.04627 [hep-ph].

[129] L. Lee, C. Ohm, A. Soffer, and T.-T. Yu, "Collider Searches for Long-Lived Particles Beyond the Standard Model," *Prog. Part. Nucl. Phys.* **106** (2019) 210–255, arXiv:1810.12602 [hep-ph]. [Erratum: Prog.Part.Nucl.Phys. 122, 103912 (2022)].

[130] J. Alimena *et al.*, "Searching for long-lived particles beyond the Standard Model at the Large Hadron Collider," *J. Phys. G* **47** no. 9, (2020) 090501, arXiv:1903.04497 [hep-ex].

[131] H. Chen, I. Moult, X. Zhang, and H. X. Zhu, "Rethinking jets with energy correlators: Tracks, resummation, and analytic continuation," *Phys. Rev. D* **102** (Sep, 2020) 054012. https://link.aps.org/doi/10.1103/PhysRevD.102.054012.

[132] K. Lee and I. Moult, "Energy Correlators Taking Charge," arXiv:2308.00746 [hep-ph].

[133] **CMS** Collaboration, A. Hayrapetyan *et al.*, "Measurement of energy correlators inside jets and determination of the strong coupling $\alpha_S(m_Z)$," *Phys. Rev. Lett.* **133** (Aug, 2024) 071903. https://link.aps.org/doi/10.1103/PhysRevLett.133.071903.

[134] M. Baumgart, T. Cohen, I. Moult, N. L. Rodd, T. R. Slatyer, M. P. Solon, I. W. Stewart, and V. Vaidya, "Resummed Photon Spectra for WIMP Annihilation," *JHEP* **03** (2018) 117, arXiv:1712.07656 [hep-ph].

[135] L. Rinchiuso, N. L. Rodd, I. Moult, E. Moulin, M. Baumgart, T. Cohen, T. R. Slatyer, I. W. Stewart, and V. Vaidya, "Hunting for Heavy Winos in the Galactic Center," *Phys. Rev. D* **98** no. 12, (2018) 123014, arXiv:1808.04388 [astro-ph.HE].

[136] M. Baumgart, T. Cohen, E. Moulin, I. Moult, L. Rinchiuso, N. L. Rodd, T. R. Slatyer, I. W. Stewart, and V. Vaidya, "Precision Photon Spectra for Wino Annihilation," *JHEP* **01** (2019) 036, arXiv:1808.08956 [hep-ph].

[137] M. Baumgart, N. L. Rodd, T. R. Slatyer, and V. Vaidya, "The quintuplet annihilation spectrum," *JHEP* **01** (2024) 158, arXiv:2309.11562 [hep-ph].

[138] **CMS** Collaboration, A. Tumasyan *et al.*, "Search for resonant production of strongly coupled dark matter in proton-proton collisions at 13 TeV," *JHEP* **06** (2022) 156, arXiv:2112.11125 [hep-ex].

[139] **ATLAS** Collaboration, G. Aad *et al.*, "Search for non-resonant production of semi-visible jets using Run 2 data in ATLAS," *Phys. Lett. B* **848** (2024) 138324, arXiv:2305.18037 [hep-ex].

[140] **CMS** Collaboration, A. Hayrapetyan *et al.*, "Search for dark QCD with emerging jets in proton-proton collisions at $\sqrt{s} = 13$ TeV," *JHEP* **07** (2024) 142, arXiv:2403.01556 [hep-ex].

[141] **ATLAS** Collaboration, G. Aad *et al.*, "Search for dark mesons decaying to top and bottom quarks in proton-proton collisions at $\sqrt{s} = 13$ TeV with the ATLAS detector," *JHEP* **09** (2024) 005, arXiv:2405.20061 [hep-ex].

[142] **CMS** Collaboration, A. Hayrapetyan *et al.*, "Search for Soft Unclustered Energy Patterns in Proton-Proton Collisions at 13 TeV," *Phys. Rev. Lett.* **133** no. 19, (2024) 191902, arXiv:2403.05311 [hep-ex].

[143] **CMS** Collaboration, "Search for soft unclustered energy patterns in association with a Z boson in proton-proton collisions at 13 TeV," tech. rep., 2025. https://cds.cern.ch/record/2928077.

[144] **CMS** Collaboration, "Search for low-mass hidden valley dark showers with displaced dimuons in proton-proton collisions at $\sqrt{s} = 13$ TeV," tech. rep., 2025. https://cds.cern.ch/record/2930038.

[145] **CMS** Collaboration, "Search for soft unclustered energy patterns in association with a W boson in proton-proton collisions at 13 TeV," tech. rep., 2025. https://cds.cern.ch/record/2927983.

[146] **ATLAS** Collaboration, G. Aad *et al.*, "Search for new physics in final states with semi-visible jets or anomalous signatures using the ATLAS detector," arXiv:2505.01634 [hep-ex].

[147] **ATLAS** Collaboration, G. Aad *et al.*, "Search for emerging jets in pp collisions at $\sqrt{s} = 13.6$ TeV with the ATLAS experiment," arXiv:2505.02429 [hep-ex].

[148] D. Barducci, S. De Curtis, M. Redi, and A. Tesi, "An almost elementary Higgs: Theory and Practice," *JHEP* **08** (2018) 017, arXiv:1805.12578 [hep-ph].

[149] H. Mies, C. Scherb, and P. Schwaller, "Collider constraints on dark mediators," *JHEP* **04** (2021) 049, arXiv:2011.13990 [hep-ph].

[150] J. M. Butterworth, L. Corpe, X. Kong, S. Kulkarni, and M. Thomas, "New sensitivity of LHC measurements to composite dark matter models," *Phys. Rev. D* **105** no. 1, (2022) 015008, arXiv:2105.08494 [hep-ph].

[151] C. Kilic and T. Okui, "The LHC Phenomenology of Vectorlike Confinement," *JHEP* **04** (2010) 128, arXiv:1001.4526 [hep-ph].

[152] O. Buchmueller, A. De Roeck, K. Hahn, M. McCullough, P. Schwaller, K. Sung, and T.-T. Yu, "Simplified Models for Displaced Dark Matter Signatures," *JHEP* **09** (2017) 076, arXiv:1704.06515 [hep-ph].

[153] S. Renner and P. Schwaller, "A flavoured dark sector," *JHEP* **08** (2018) 052, arXiv:1803.08080 [hep-ph].

[154] H.-C. Cheng, L. Li, E. Salvioni, and C. B. Verhaaren, "Light Hidden Mesons through the Z Portal," *JHEP* **11** (2019) 031, arXiv:1906.02198 [hep-ph].

[155] A. Pierce, B. Shakya, Y. Tsai, and Y. Zhao, "Searching for confining hidden valleys at LHCb, ATLAS, and CMS," *Phys. Rev. D* **97** no. 9, (2018) 095033, arXiv:1708.05389 [hep-ph].

[156] H. Beauchesne, E. Bertuzzo, G. Grilli Di Cortona, and Z. Tabrizi, "Collider phenomenology of Hidden Valley mediators of spin 0 or 1/2 with semivisible jets," *JHEP* **08** (2018) 030, arXiv:1712.07160 [hep-ph].

[157] H.-C. Cheng, L. Li, and E. Salvioni, "A theory of dark pions," *JHEP* **01** (2022) 122, arXiv:2110.10691 [hep-ph].

[158] S. Born, R. Karur, S. Knapen, and J. Shelton, "Scouting for dark showers at CMS and LHCb," *Phys. Rev. D* **108** no. 3, (2023) 035034, arXiv:2303.04167 [hep-ph].

[159] G. Albouy *et al.*, "Theory, phenomenology, and experimental avenues for dark showers: a Snowmass 2021 report," *Eur. Phys. J. C* **82** no. 12, (2022) 1132, arXiv:2203.09503 [hep-ph].

[160] A. J. Barr, C. G. Lester, M. A. Parker, B. C. Allanach, and P. Richardson, "Discovering anomaly mediated supersymmetry at the LHC," *JHEP* **03** (2003) 045, arXiv:hep-ph/0208214.

[161] N. E. Bomark, A. Kvellestad, S. Lola, P. Osland, and A. R. Raklev, "Long lived charginos in Natural SUSY?," *JHEP* **05** (2014) 007, arXiv:1310.2788 [hep-ph].

[162] Y. Nakai, R. Sato, and K. Tobioka, "Footprints of New Strong Dynamics via Anomaly and the 750 GeV Diphoton," *Phys. Rev. Lett.* **116** no. 15, (2016) 151802, arXiv:1512.04924 [hep-ph].

[163] Y. Bai, J. Berger, and R. Lu, "750 GeV dark pion: Cousin of a dark G -parity odd WIMP," *Phys. Rev. D* **93** no. 7, (2016) 076009, arXiv:1512.05779 [hep-ph].

[164] G. Elor, H. Liu, T. R. Slatyer, and Y. Soreq, "Complementarity for Dark Sector Bound States," *Phys. Rev. D* **98** no. 3, (2018) 036015, arXiv:1801.07723 [hep-ph].

[165] S. Bottaro, A. Strumia, and N. Vignaroli, "Minimal Dark Matter bound states at future colliders," *JHEP* **06** (2021) 143, arXiv:2103.12766 [hep-ph].

[166] T. D. Lee and C. N. Yang, "Charge conjugation, a new quantum number g, and selection rules concerning a nucleon-antinucleon system," *Il Nuovo Cimento (1955-1965)* **3** no. 4, (1956) 749–753. https://doi.org/10.1007/BF02744530.

[167] **Particle Data Group** Collaboration, S. Navas *et al.*, "Review of particle physics," *Phys. Rev. D* **110** no. 3, (2024) 030001.

[168] B. M. K. Nefkens and J. W. Price, "The Neutral decay modes of the eta meson," *Phys. Scripta T* **99** (2002) 114–122, arXiv:nucl-ex/0202008.

[169] K. Jedamzik, "Big bang nucleosynthesis constraints on hadronically and electromagnetically decaying relic neutral particles," *Phys. Rev. D* **74** (2006) 103509, arXiv:hep-ph/0604251.

[170] M. Kawasaki, K. Kohri, T. Moroi, K. Murai, and H. Murayama, "Big-bang nucleosynthesis with sub-GeV massive decaying particles," *JCAP* **12** (2020) 048, arXiv:2006.14803 [hep-ph].

[171] A. Belyaev, G. Cacciapaglia, I. P. Ivanov, F. Rojas-Abatte, and M. Thomas, "Anatomy of the Inert Two Higgs Doublet Model in the light of the LHC and non-LHC Dark Matter Searches," *Phys. Rev. D* **97** no. 3, (2018) 035011, arXiv:1612.00511 [hep-ph].

[172] A. Belyaev, S. Prestel, F. Rojas-Abbate, and J. Zurita, "Probing dark matter with disappearing tracks at the LHC," *Phys. Rev. D* **103** no. 9, (2021) 095006, arXiv:2008.08581 [hep-ph].

[173] E. Witten, "Large n chiral dynamics," *Annals of Physics* **128** no. 2, (1980) 363–375. https://www.sciencedirect.com/science/article/pii/0003491680903255.

[174] **ATLAS** Collaboration, M. Aaboud *et al.*, "Search for new high-mass phenomena in the dilepton final state using 36 fb^{-1} of proton-proton collision data at $\sqrt{s} = 13$ TeV with the ATLAS detector," *JHEP* **10** (2017) 182, arXiv:1707.02424 [hep-ex].

[175] **CMS** Collaboration, A. M. Sirunyan *et al.*, "Search for high-mass resonances in dilepton final states in proton-proton collisions at $\sqrt{s} = 13$ TeV," *JHEP* **06** (2018) 120, arXiv:1803.06292 [hep-ex].

[176] J. Wess and B. Zumino, "Consequences of anomalous Ward identities," *Phys. Lett. B* **37** (1971) 95–97.

[177] E. Witten, "Global Aspects of Current Algebra," *Nucl. Phys. B* **223** (1983) 422–432.

[178] E. Witten, "Nonabelian Bosonization in Two-Dimensions," *Commun. Math. Phys.* **92** (1984) 455–472.

[179] D. Tong, "Gauge theory."
https://www.damtp.cam.ac.uk/user/tong/gaugetheory.html, 2018.
Lecture notes, University of Cambridge.

[180] K. Howe, S. Knapen, and D. J. Robinson, "Diphotons from electroweak triplet-singlet mixing," *Phys. Rev. D* **94** no. 3, (2016) 035021, arXiv:1603.08932 [hep-ph].

[181] M. J. Dugan, H. Georgi, and D. B. Kaplan, "Anatomy of a Composite Higgs Model," *Nucl. Phys. B* **254** (1985) 299–326.

[182] D. A. Varshalovich, A. N. Moskalev, and V. K. Khersonskii, *Quantum Theory of Angular Momentum: Irreducible Tensors, Spherical Harmonics, Vector Coupling Coefficients, 3nj Symbols*. World Scientific Publishing Company, 1988.

[183] J. J. Sakurai and J. Napolitano, *Modern Quantum Mechanics*. Quantum physics, quantum information and quantum computation. Cambridge University Press, 3 ed., 10, 2020.

[184] J. Alwall, R. Frederix, S. Frixione, V. Hirschi, F. Maltoni, O. Mattelaer, H. S. Shao, T. Stelzer, P. Torrielli, and M. Zaro, "The automated computation of tree-level and next-to-leading order differential cross sections, and their matching to parton shower simulations," *JHEP* **07** (2014) 079, arXiv:1405.0301 [hep-ph].

[185] R. Frederix, S. Frixione, V. Hirschi, D. Pagani, H. S. Shao, and M. Zaro, "The automation of next-to-leading order electroweak calculations," *JHEP* **07** (2018) 185, arXiv:1804.10017 [hep-ph]. [Erratum: JHEP 11, 085 (2021)].

[186] M. Cacciari and G. P. Salam, "Dispelling the N^3 myth for the k_t jet-finder," *Phys. Lett. B* **641** (2006) 57–61, arXiv:hep-ph/0512210.

[187] M. Cacciari, G. P. Salam, and G. Soyez, "FastJet User Manual," *Eur. Phys. J. C* **72** (2012) 1896, arXiv:1111.6097 [hep-ph].

[188] C. Bierlich *et al.*, "A comprehensive guide to the physics and usage of PYTHIA 8.3," *SciPost Phys. Codeb.* **2022** (2022) 8, arXiv:2203.11601 [hep-ph].

[189] **DELPHES 3** Collaboration, J. de Favereau, C. Delaere, P. Demin, A. Giammanco, V. Lemaître, A. Mertens, and M. Selvaggi, "DELPHES 3, A modular framework for fast simulation of a generic collider experiment," *JHEP* **02** (2014) 057, arXiv:1307.6346 [hep-ex].

[190] M. Cacciari, G. P. Salam, and G. Soyez, "The anti-k_t jet clustering algorithm," *JHEP* **04** (2008) 063, arXiv:0802.1189 [hep-ph].

[191] **ATLAS** Collaboration, "Performance of tracking and vertexing techniques for a disappearing track plus soft track signature with the ATLAS detector," tech. rep., 2019. https://cds.cern.ch/record/2669015.

[192] **ATLAS** Collaboration, G. Aad *et al.*, "Search for long-lived charginos based on a disappearing-track signature using 136 fb^{-1} of pp collisions at $\sqrt{s} = 13$ TeV with the ATLAS detector," *Eur. Phys. J. C* **82** no. 7, (2022) 606, arXiv:2201.02472 [hep-ex].

[193] **CMS** Collaboration, A. Hayrapetyan *et al.*, "Search for supersymmetry in final states with disappearing tracks in proton-proton collisions at s=13 TeV," *Phys. Rev. D* **109** no. 7, (2024) 072007, arXiv:2309.16823 [hep-ex].

[194] A. Datta, P. Konar, and B. Mukhopadhyaya, "Invisible charginos and neutralinos from gauge boson fusion: A Way to explore anomaly mediation?," *Phys. Rev. Lett.* **88** (2002) 181802, arXiv:hep-ph/0111012.

[195] D. Choudhury, A. Datta, K. Huitu, P. Konar, S. Moretti, and B. Mukhopadhyaya, "Slepton production from gauge boson fusion," *Phys. Rev. D* **68** (2003) 075007, arXiv:hep-ph/0304192.

[196] **ATLAS** Collaboration, M. Aaboud *et al.*, "Search for long-lived charginos based on a disappearing-track signature in pp collisions at $\sqrt{s} = 13$ TeV with the ATLAS detector," *JHEP* **06** (2018) 022, arXiv:1712.02118 [hep-ex].

[197] G. Cottin, N. Desai, S. Kraml, and A. Lessa, "LLP Recasting Repository." https://github.com/llprecasting/recastingCodes/, 2019.

[198] **ATLAS** Collaboration, M. Aaboud *et al.*, "Search for resonant WZ production in the fully leptonic final state in proton-proton collisions at $\sqrt{s} = 13$ TeV with the ATLAS detector," *Phys. Lett. B* **787** (2018) 68–88, arXiv:1806.01532 [hep-ex].

[199] **ATLAS** Collaboration, G. Aad *et al.*, "Search for heavy resonances decaying into a pair of Z bosons in the $\ell^+\ell^-\ell'^+\ell'^-$ and $\ell^+\ell^-\nu\bar{\nu}$ final states using 139 fb^{-1} of proton–proton collisions at $\sqrt{s} = 13$ TeV with the ATLAS detector," *Eur. Phys. J. C* **81** no. 4, (2021) 332, arXiv:2009.14791 [hep-ex].

[200] **ATLAS** Collaboration, G. Aad *et al.*, "Search for heavy diboson resonances in semileptonic final states in pp collisions at $\sqrt{s} = 13$ TeV with the ATLAS detector," *Eur. Phys. J. C* **80** no. 12, (2020) 1165, arXiv:2004.14636 [hep-ex].

[201] **CMS** Collaboration, A. M. Sirunyan *et al.*, "Search for charged Higgs bosons produced in vector boson fusion processes and decaying into vector boson pairs in proton–proton collisions at $\sqrt{s} = 13\,\text{TeV}$," *Eur. Phys. J. C* **81** no. 8, (2021) 723, arXiv:2104.04762 [hep-ex].

[202] **CMS** Collaboration, A. Tumasyan *et al.*, "Search for heavy resonances decaying to WW, WZ, or WH boson pairs in the lepton plus merged jet final state in proton-proton collisions at $\sqrt{s} = 13$ TeV," *Phys. Rev. D* **105** no. 3, (2022) 032008, arXiv:2109.06055 [hep-ex].

[203] **ATLAS** Collaboration, G. Aad *et al.*, "Search for resonances decaying into photon pairs in 139 fb^{-1} of pp collisions at $\sqrt{s}$=13 TeV with the ATLAS detector," *Phys. Lett. B* **822** (2021) 136651, arXiv:2102.13405 [hep-ex].

[204] **ATLAS** Collaboration, G. Aad *et al.*, "Measurement and interpretation of same-sign W boson pair production in association with two jets in pp collisions at $\sqrt{s} = 13$ TeV with the ATLAS detector," *JHEP* **04** (2024) 026, arXiv:2312.00420 [hep-ex].

[205] **CMS** Collaboration, A. Hayrapetyan *et al.*, "Search for new physics in high-mass diphoton events from proton-proton collisions at $\sqrt{\text{s}} = 13$ TeV," *JHEP* **08** (2024) 215, arXiv:2405.09320 [hep-ex].

[206] **CMS** Collaboration, "Search for heavy scalar resonances decaying to a pair of Z bosons in the 4-lepton final state at 13 TeV," tech. rep., 2024. https://cds.cern.ch/record/2905051.

[207] **ATLAS** Collaboration, M. Aaboud *et al.*, "Search for heavy resonances decaying to a Z boson and a photon in pp collisions at $\sqrt{s} = 13$ TeV with the

ATLAS detector," *Phys. Lett. B* **764** (2017) 11–30, arXiv:1607.06363 [hep-ex].

[208] **CMS** Collaboration, V. Khachatryan *et al.*, "Search for high-mass Zγ resonances in $e^+e^-\gamma$ and $\mu^+\mu^-\gamma$ final states in proton-proton collisions at $\sqrt{s} = 8$ and 13 TeV," *JHEP* **01** (2017) 076, arXiv:1610.02960 [hep-ex].